Mass spectrometric analysis of cell metabolism following parasitic infection

Cumulative Dissertation

by

Nils Holger Anschütz

prepared at the

Institute of Inorganic and Analytical Chemistry

for the Degree of

Doctor rerum naturalium (Dr. rer. nat.)

Justus Liebig University

Giessen, 2023

First referee:

Prof. Dr. Bernhard Spengler

Justus-Liebig-Universität Gießen

Institut für Anorganische und Analytische Chemie

Heinrich-Buff-Ring 17

D-35392 Gießen

Second referee:

Prof. Dr. Anja Taubert

Justus-Liebig-Universität Gießen

Institut für Parasitologie

Schubertstraße 81

35392 Gießen

TABLE OF CONTENTS

LIST OF ABBREVIATIONS

AP-SMALDI	atmospheric-pressure scanning microprobe matrix-assisted laser desorption/ionization
B. besnoiti	*Besnoitia besnoiti*
BUVEC	bovine umbilical vein endothelial cells
C. parvum	*Cryptosporidium parvum*
DHB	2,5-dihydroxybenzoic acid
DMEM	Dulbecco's Modified Eagle's Medium
e.g.	exempli gratia
EGGM	endothelial cell growth medium
ESI	electrospray ionization
FCS	foetal calf serum
FDR	false-discovery-rate
FTICR	Fourier-transform ion cyclotron resonance
FWHM	Full Width at Half Maximum
h.p.i.	hours post infection
HPLC	high performance liquid chromatography
i.e.	id est
IgG	Immunoglobulin G
LC	liquid chromatography
LDI	laser desorption/ionisation
m/z	mass-to-charge-number ratio
MALDI	matrix-assisted laser desorption/ionisation
MARC-145	african green monkey kidney epithelial cells
MS	mass spectrometry
MS/MS	tandem mass spectrometry
MSI	MS imaging
MTBE	2-methoxy-2-methylpropane
N. caninum	*Neospora caninum*
PA	phosphatidic acids
PBS	phosphate-buffered saline

LIST OF ABBREVIATIONS

PC	phosphatidylcholines
PCR	polymerase chain reaction
PE	phosphatidylethanolamine
PI	phosphatidylinositol
ppm	parts per million
PS	phosphatidylserine
rpm	revolutions per minute
RT	room temperature
spp.	species pluralis
T. gondii	*Toxoplasma gondii*
TFA	trifluoro acetic acid
TIC	total ion count
TOF	time-of-flight

LIST OF PUBLICATIONS

1. **Atmospheric-pressure scanning microprobe matrix-assisted laser desorption/ionization mass spectrometry imaging of *Neospora caninum*-infected cell monolayers**

   Anschütz, N.H., Gerbig, S., Peter Ventura, A., Silva, L.M.R., Larrazabal, C., Hermosilla, C., Taubert, A., Spengler, B., Analytical Science Advances 2022, 3, 244–254 https://doi.org/10.1002/ansa.202200016

2. **Mass Spectrometry Imaging of In Vitro *Cryptosporidium parvum*-Infected Cells and Host Tissue**
   Anschütz, N.H.; Gerbig, S.; Ghezellou, P.; Silva, L.M.R.; Vélez, J.D.; Hermosilla, C.R.; Taubert, A.; Spengler, B. Mass Spectrometry Imaging of In Vitro *Cryptosporidium parvum*-Infected Cells and Host Tissue. *Biomolecules* 2023, *13*, 1200. https://doi.org/10.3390/biom13081200

DECLARATION

I declare that I have completed this dissertation single-handedly without the unauthorized help of a second party and only with the assistance acknowledged therein. I have appropriately acknowledged and cited all text passages that are derived verbatim from or are based on the content of published work of others, and all information relating to verbal communications. I consent to the use of an anti-plagiarism software to check my thesis. I have abided by the principles of good scientific conduct laid down in the charter of the Justus Liebig University Giessen „Satzung der Justus-Liebig-Universität Gießen zur Sicherung guter wissenschaftlicher Praxis“ in carrying out the investigations described in the dissertation.

Ort, Datum, Unterschrift

ABSTRACT

Neospora caninum and *Cryptosporidium parvum* belong to the phylum Alveolata (Subphylum Apicomplexa) are two very widespread parasites. Cryptosporidiosis, caused by *C. parvum*, is a zoonosis. This is not the case with neosporosis, which is caused by *N. caninum*. However, there is growing concern that *N. caninum* may eventually become a threat to humans, as clinically manifest neosporosis has also been reported in two rhesus monkeys.[1,2] Affecting more than 1 billion people worldwide, human cryptosporidiosis remains a neglected poverty-related disease (PRD) that can be fatal in already weakened patients, especially young children.[3-5] *N. caninum* has a significant economic impact on the livestock industry as it is a major cause of reproductive disorders not only in cattle but also in other small ruminant species.[6] The spread of both parasites and associated diseases is increasing due to climate change and the global movement of people and transport of goods. Both parasites have a demonstrable negative impact on people's quality of life and should therefore be the focus of scientific research. But there is still a lot of catching up to do, especially in the area of basic research in regard to the biomolecular composition of the two parasites and their influence on the metabolism of their hosts. This deficiency could be counteracted in this work.

The parasites were studied using matrix-assisted laser desorption/ionisation (MALDI) mass spectrometry (MS) combined with high performance liquid chromatography (HPLC). MALDI was used as MS and MS imaging (MSI) method. The MALDI experiments were performed using the SMALDI (scanning microprobe matrix-assisted laser desorption/ionisation) ion source, which operates at atmospheric pressure. It is suitable for the analysis of complex 3D surfaces with a low sample amount requirement. MS instrumentation has improved considerably over recent years, allowing detailed mass analysis to determine compounds from their very precise molecular masses.[7-9] It is possible to annotate and subsequently identify analytes. For the structural verification of the markers, HPLC-MS/MS experiments were combined with database search. Identifying molecular biomarkers of parasite-infected host cells and further elucidating their functions were among the main objectives of this study.

The statistically relevant biomarkers, with the focus on lipids, that were found by MS, annotated by database and identified by HPLC-MS/MS measurements, were also found and visualized with AP-SMALDI MSI in infected monolayers and host tissue. There is an overlap of the identified markers between *N. caninum* and *C. parvum* as well as between the two parasites and other parasites from the literature. PI (36:1) has been identified as a marker of host cell infection by *N. caninum*, *C. parvum*, *T. gondii* and *B. besnoiti*. Phosphatidylinositol is found in cell membranes and is essential for anchoring proteins to the membrane. They play a role in the transition of the parasite (*T. gondii*) between its stages (tachyzoites and bradyzoites).[10] Overall, the present approach provides new metabolic insights into both diseases that have been neglected by science.

ZUSAMMENFASSUNG

Die beiden stark verbreiteten Parasiten *Neospora caninum* und *Cryptosporidium parvum* gehören zum Stamm Alveolata sowie dem dazugehörigen Unterstamm Apicomplexa. Bei der durch *C. parvum* verursachten Kryptosporidiose handelt es sich um eine Zoonose. Die durch *N. Caninum* verursachte Neosporose fällt dagegen nicht in diese Kategorie. Allerdings wächst die Sorge, dass *N. caninum* letztendlich zu einer Bedrohung für den Menschen werden könnte, da auch bei Rhesusaffen über eine klinisch manifeste Neosporose berichtet wurde.[1,2] Weltweit sind mehr als eine Milliarde Menschen von Kryptosporidiose betroffen, welche nach wie vor als eine vernachlässigte und armutsbedingte Krankheit gilt, die bei bereits geschwächten Patienten, insbesondere kleinen Kindern, tödlich sein kann.[3-5] Dagegen hat *N. caninum* erhebliche wirtschaftliche Auswirkungen auf die Viehwirtschaft, da es eine Hauptursache für Fortpflanzungsstörungen bei Rindern sowie anderen kleinen Wiederkäuerarten ist.[6] Die Verbreitung von Parasiten und damit verbundenen Krankheiten nimmt aufgrund des Klimawandels und des globalen Personen- und Güterverkehrs stetig zu. Beide Parasiten haben eine nachweislich negative Auswirkung auf die Lebensqualität der Menschen auf unserer Welt und sollten daher im Fokus der wissenschaftlichen Forschung stehen. Doch insbesondere im Bereich der Grundlagenforschung zur biomolekularen Zusammensetzung der beiden Parasiten und ihrem Einfluss auf den Stoffwechsel ihrer Wirte besteht noch großer Nachholbedarf. Diesem Mangel konnte in dieser Arbeit entgegengewirkt werden.

Die Parasiten wurden mittels Matrix-unterstützter Laser-Desorption/Ionisation (MALDI)-Massenspektrometrie (MS) in Kombination mit Hochleistungsflüssigkeitschromatographie (HPLC) untersucht. MALDI wurde als einfache MS-Methode sowie bildgebend (MSI) verwendet. Für die MALDI-Experimente wurde die SMALDI (scanning microprobe matrix-assisted laser desorption/ionisation) Ionenquelle, welche unter Atmosphärendruck arbeitet, eingesetzt. Sie eignet sich dank ihres Autofokus-Systems für die Analyse komplexer 3D-Oberflächen und benötigt dabei nur geringe Probenmengen. Die instrumentelle Entwicklung im Bereich der Massenspektrometrie hat in den letzten Jahren erhebliche Fortschritte erzielt. Eine detaillierte Massenanalyse zur Bestimmung von Verbindungen anhand ihrer höchst präzisen Molekülmassen ist möglich.[7-9] Analyten können nicht nur annotiert, sondern auch identifiziert werden. Zur eindeutigen strukturellen Verifizierung der Marker wurden HPLC-MS/MS-Experimente mit einer Datenbanksuche kombiniert. Zu den Hauptzielen dieser Studie gehörten die Identifizierung molekularer Biomarker parasiteninfizierter Wirtszellen und die weitere Aufklärung ihrer Funktionen.

Die statistisch relevanten Biomarker mit Schwerpunkt auf Lipiden, wurden mit Hilfe von MS-Experimenten gefunden, durch Datenbanken annotiert, durch HPLC-MS/MS-Messungen identifiziert und schlussendlich mit AP-SMALDI MSI in infizierten Monolagen sowie Wirtsgewebe gefunden und visualisiert. Eine Überschneidung der identifizierten Biomarker von *N. caninum* und *C. parvum* sowie zwischen den beiden Parasiten und anderen Parasiten aus der Literatur wurde aufgezeigt. PI (36:1) wurde als Biomarker für eine Infektion der Wirtszellen mit *N. caninum*, *C. parvum*, *T. gondii* und *B. besnoiti* identifiziert. Phosphatidylinositol kommt in Zellmembranen vor und ist für die Verankerung von Proteinen an der Membran unerlässlich. Weiterhin spielen sie eine Rolle beim Übergang des Parasiten (*T. gondii*) zwischen seinen Stadien (Tachyzoiten und Bradyzoiten).[10] Die vorliegende Forschungsarbeit ist in der Lage, neue metabolische Erkenntnisse zu beiden aus wissenschaftlicher Sicht vernachlässigten Krankheiten zu liefern.

CHAPTER 1

Introduction and Motivation

Parasites are found in every organism of every species on earth. The term parasite has its origins in the royal courts of ancient Greece. This expression referred to pre-tasters who were given food for no apparent consideration. The Greek παράσιτος (*parasitos*) means "one who eats at the table of another". That's exactly what we now call parasitism, because a parasite uses its host for its own benefit, regardless of what happens to the host. However parasitic infection and parasitic disease are two very different situations that have arisen from a single process. That means, that the presence of a parasite is a necessary but not sufficient condition for the onset of a parasitic disease.[11] A large phylum of predominantly parasitic alveolates known to cause a variety of diseases, including malaria and toxoplasmosis, are the so-called Apicomplexa. Most of them have a unique form of organelle, used to invade a host cell, which consists of an apicoplast and an apical complex structure. Apicomplexa are a heterogeneous group that contains organisms such as *Piroplasms*, *Haemogregarines*, *Coccidia*, *Gregarines* and *Plasmodia*.[12] This work focuses on two parasites that pose a serious threat to their unwilling hosts. Both parasites belong to the phylum Alveolata (Subphylum Apicomplexa). These are specifically *Neospora caninum* and *Cryptosporidium parvum*. Cryptosporidiosis, caused by *C. parvum*, is a zoonosis. Human cryptosporidiosis affects more than 1 billion people worldwide and remains a neglected poverty-related disease (PRD). It can be fatal in already weakened patients, especially young children.[3-5] It should be noted, however, that the death of the host is the exception rather than the rule. Unlike cryptosporidiosis, neosporosis, caused by *N. caninum* is not a zoonosis. It mainly affects livestock, especially on large farms. However, as clinically manifest neosporosis has also been reported in two rhesus monkeys, there is growing concern that *N. caninum* may eventually become a risk to humans.[1,2] *N. caninum* is a major cause of reproductive disorders not only in cattle but also in other small ruminant species and has a significant economic impact on the livestock industry. These two parasites should be the focus of scientific research because they have a proven negative impact on the quality of life of people. However, research at the molecular level is particularly lacking. But this is particularly important, for example to identify possible targets for active substances.

In this context, lipids are of particular interest. Lipids are substances of biological origin that are soluble in non-polar solvents. According to IUPAC, these include "saponifiable lipids, such as glycerides (fats and oils) and phospholipids , as well as nonsaponifiable lipids, principally steroids".[13] They are a major class of constituents of both the parasites and their hosts, however, there is limited information on its precise biochemical composition. Lipids are fundamental components of structural and functional categories of cells - among other things through the generation of lipid (bi)layers (see Figure 1). In cell membranes, lipids separate functional domains and are involved in different aspects of signalling.

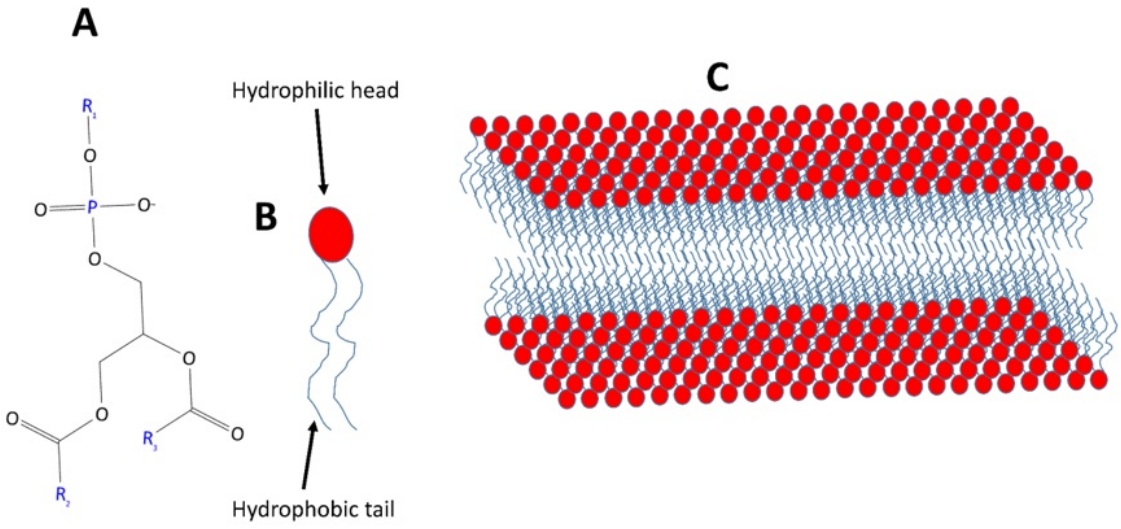

Figure 1: Phospholipids are a group of lipids with a phosphate group and belong to the polar lipids (A). They are composed of a hydrophilic head and two hydrophobic hydrocarbon tails (B). They are involved in building the lipid bilayer of many biomembranes and are therefore found in all animal and plant cells (C).

The spatial distribution and abundance of lipids is therefore of great interest. Mass spectrometry is a tool that enables to fundamentally understand such parasites and thereby offers possibilities to combat these parasites. MS instrumentation has undergone major improvements in recent years, allowing detailed mass analysis of compounds by very precise molecular masses.[7-9] It is possible to annotate and subsequently identify analytes. Analyte distribution in tissues and cells can be visualised using MSI. AP-SMALDI MSI is able to provide high performance, especially with regard to the spatial resolution in the micrometre range and thanks to an autofocus system, it can also handle even the most challenging surfaces. This is also necessary given the small size of the parasites, for example, *N. caninum* tachyzoites are about 6 x 2 µm in size as well as the complex surface of intestinal samples, which are particularly demanding in terms of height differences.

Neospora Caninum and *Cryptosporidium Parvum*

Neospora caninum is an obligate intracellular parasite (phylum Alveaolata and subphylumn Apicomplexa) that infects canids as its definitive host and a broad range of intermediate hosts including goats, bovine, sheep, wild cervids and new world camelids.[14] *N. caninum* is a tissue cyst-forming coccidian, like the closely related parasite *Toxoplasma gondii*.[15] Prior to 1984, *N. caninum* was misidentified as *T. gondii* because of strong similarities in life cycle, morphology, genome and transcriptome.[16-21] Intermediate hosts for *N. caninum* infections can also be canid species [i.e. dogs (*Canis familiaris*), wolves (*Canis lupus*) and coyotes (*Canis latrans*)]. This commitment to canines is also reflected in the name, as *neo* is Latin for "new", *spora* for seed and *canis* for dog. Neosporosis is concentrated in the United States, South America, Central America, Australia and Europe and is considered to be a globally spreading disease. It causes significant economic losses, especially in bovine, goat, sheep and alpaca/llama industries.[22,23] Diagnosis of *N. caninum* infection is serological, using blood tests for either parasite-specific antibodies or antigens, immunohistochemistry or molecular diagnostic tools, are also possible, but underrepresented due to their complexity and

associated costs.[24-27] The offspring of infected bitches can develop severe dermal and neuromuscular symptoms caused by multisystemic lesions based on *N. caninum* infection.[14] There are three stages in the life cycle: rapidly replicating tachyzoites, slowly proliferating bradyzoites within tissue cysts and sporozoites in sporulated oocysts. In intermediate hosts, only two of these stages, tachyzoites and tissue cysts, are found and both show obligate intracellular development.[22] In general, the transmission can take place in a number of different ways. As an example, canids acquire infection by ingestion of infected host tissue or by ingestion of sporulated oocysts from contaminated environments. The other way around, in bovine, transplacental transmission of tachyzoites appears to be the most common route of infection compared with ingestion of oocysts, making vertical transmission the main route for the spread of bovine neosporosis.[27,28] The purchase of infected bovine or the shedding of oocysts by farm dogs is the initial infection of a bovine herd. Depending on the type of host, the symptoms of this disease vary greatly. Infected dogs can become paralysed and debilitated by nerve and organ inflammation.[29] In bovine, *N. caninum* is a major threat to the livestock industry because it can infect the reproductive system of both sexes. One of the most common infectious causes of abortion or mummification of the foetus is due to neosporosis.[6,30,31] In male bovine infected with *N. caninum*, sperm concentration, viability and motility are significantly reduced.[32] The consequences of the spread of bovine neosporosis are having a significant economic impact worldwide, with financial losses running into billions of dollars.[23] Vaccines against *N. caninum* are rare and ineffective in the prevention of abortion in cattle.[33] Clinically manifest neosporosis has also been reported in two rhesus macaques, raising concerns that *N. caninum* may eventually become a threat to humans.[1,2] In addition, there have been reports of the presence of IgG anti-*N. caninum* antibodies in pregnant women and in carriers of the human immunodeficiency virus.[34,35] In addition to the final hosts mentioned above, *N. caninum* has a variety of intermediate hosts. This includes various wild birds as well as the pigeon, which is closely related to humans, domestic chickens and its eggs, farmed red deer or even camels. [36-40] The number of known intermediate hosts is increasing and underlines the potential danger of this parasite.

Like *N. caninum*, *Cryptosporidium parvum* belongs to the phylum Alveolata (Subphylum Apicomplexa) and is the major zoonotic etiology of human cryptosporidiosis. It is an enteropathogenic parasite not only infecting humans, but also a variety of vertebrates, including pets and wildlife.[3] *C. parvum*-thick-walled oocysts are highly resistant exogenous stages in the life cycle and are transmitted orally in two ways. The first option is the uptake by drinking contaminated water or eating food washed with contaminated water.[41] The second option is the ingestion by a new host after the oocysts are released through faeces of infected humans or animals.[41] When ingested, these thick-walled oocysts of *C. parvum* rupture in the gastrointestinal tract of the vertebrate host. In order for the parasite to continue to multiply, free-living sporozoites must infect small intestinal epithelial cells (IEC). A second type of oocyst develops, which is thin-walled and has little resistance to environmental influences. However, these thin-walled oocysts can lead to endogenous autoinfection and are considered to be the main contributor to persistent infection and disease in immunocompromised patients.[3] Another special feature of this species compared to other apicomplexans is the epicytoplasmic intracellular localization of the *C. parvum* sporozoites with their basal adhesion zones (feeding layers). Sporozoites inside the IEC then undergo asexual merogony, giving rise to first-generation merozoites, which then undergo a second merogony, giving rise to second-generation merozoites. Sexual gamogony, resulting in syngamy and final oocyst production, is performed by the second generation of merozoites. The life cycle is then completed by the excretion of resistant, thick-walled oocysts from the host through faecal material.

Affecting more than 1 billion people worldwide, human cryptosporidiosis remains a neglected poverty-related disease (PRD).[4] In low-income countries, the burden of enteric PRD is currently very high.[42] The

most common symptoms of human cryptosporidiosis are abdominal pain, nausea, anorexia, fever, profuse watery diarrhea and severe pediatric diarrhea.[3,5] The disease can be fatal in already weakened patients, especially young children.[3,5] Globally, 9% of child morbidity and mortality is caused by diarrhoeal diseases.[43] Clinically manifest cryptosporidiosis can also affect the growth of children.[42] There is no such thing as truly effective medicine - only preventive medicine is effective, and hygiene is particularly well proven.

Mass Spectrometry

Mass spectrometry (MS) has become an indispensable tool in industry, clinical laboratories and academic research. The development of mass spectrometry began at the end of the 19th century. Wilhelm Wien, investigated the deflection of "canal rays" in electric fields in 1898 and received the Nobel Prize in Physics in 1911 “for his discoveries regarding the laws governing the radiation of heat”.[44] Already in 1906, Joseph John Thomson had received the Nobel Prize in Physics for “in recognition of the great merits of his theoretical and experimental investigations on the conduction of electricity by gases” (1899).[45] More than ten years later, the 1922 Nobel Prize in Chemistry went to Francis William Aston “for his discovery, by means of his mass spectrograph, of isotopes, in a large number of non-radioactive elements, and for his enunciation of the whole-number rule” (1920).[46] The field of MS is characterized by technical developments. William E. Stephens laid the foundation for time-of-flight (TOF) MS around 1946.[47] The development of the double-focusing mass spectrometer by Johnson and Nier in 1953 is another milestone.[48] In 1953, Hans G. Dehmelt and Wolfgang Paul developed the ion trap and received the Nobel Prize in Physics in 1989.[49] The use of MS to characterize organic molecules by J.H. Beynon and the interpretation of the fragmentation of these by Fred W. McLafferty anchored MS in the oil industry.[50] The impetus for new developments in MS over the last few decades have primarily been from the life sciences. These require an ever-increasing mass range with ever-increasing molecular weights and the possibility of examining even more sensitive molecules. John B. Fenn developed electrospray ionization (ESI) in 1984.[51] Matrix Assisted Laser Desorption/Ionization (MALDI) was developed by Karas and Hillenkamp in 1985.[52,53] Two years later Koichi Tanaka developed a similar method called Soft Laser Ionization (SLD).[54] Fenn and Tanaka received the Nobel Prize in Chemistry ”for their development of soft desorption ionisation methods for mass spectrometric analyses of biological macromolecules” in 2002.[55] In the late 1990s, Alexander A. Markarov developed the Orbitrap based on the Kingdon trap (1923). The technology was commercialized in 2005 and has been pioneering ever since.[56] In 1994, Bernhard Spengler expanded MALDI into an imaging method, called MALDI MS imaging.[57] Using the combination of Orbitrap and MALDI MS imaging is the starting point of my research.

The basis of MS is the fact that atoms can be identified by their specific mass defect, which means that atoms have a lower mass than they should have based on the masses of their components. The only exception is by definition ^{12}C. The aim of MS is thus always the identification of a compound from the molecular and atomic masses of its components. The identification of molecules with the help of exact mass determination and the associated database assignments is not the only effective way. Likewise, the identification can also be achieved by carrying out fragmentation experiments and comparing the fragmentation spectra with a reference. In conventional mass spectrometers, the fragmentation step allows ions with very similar m/z values to be identified and separated. It can be understood as an analogue of fingerprint comparison in the justice system. In mass spectrometry, however, these fingerprints must first be generated, and this is done by breaking bonds in the molecule of interest, called precursor ion.

In MS, ions are generated, separated according to their mass to charge number ratio (m/z) and finally detected. For historical reasons, the term mass-to-charge (*m*/*z*) ratio has prevailed. In the mass spectrum, the (relative) signal intensity is plotted against *m*/*z*. The signal intensity is proportional to the concentration, which enables quantification. The ions can be separated by static or dynamic electric or magnetic fields, but also - as in the case of the TOF (time-of-flight) - without a field and with a defined kinetic energy.

Ionization can take place in a variety of ways, including electron impact or photon irradiation. The ionization processes can be subdivided, among other things, according to whether the ionization takes place under soft or hard conditions, or whether the ionization takes place under atmospheric pressure or not. The transfer of ions from condensed phase into the state of isolated ions in the gas phase takes place under atmospheric pressure, whereby the high vacuum of the mass analyzer is gradually reached.[58] Soft ionization methods that work under atmospheric pressure have the advantage that they offer the best possible access to intact biomolecules. Two of the most popular methods, which work under atmospheric pressure and belong to the soft ionization methods, were used in this endeavour. These are ESI and MALDI.

When using ESI (see Figure 2), a liquid solution containing the analyte is pumped through a stainless-steel capillary at a flow rate of several microliters per minute. Between the capillary and the MS inlet, an electrostatic field is applied. At the open end of the capillary, the escaping liquid is exposed to the previously generated electrical field. The electric field leads to charge separation in the electrolyte solution and finally to the deformation of the meniscus towards the so-called Taylor cone. When the surface tension is overcome by the electrostatic forces, a fine jet of liquid begins to emit from the tip in the direction of the counter-electrode. However, this jet of liquid does not last for a long time stable, but breaks up into many small droplets, the so-called electro-spray. There are two model mechanisms for how the droplets ultimately become ions. These are the residue model (CRM) on the one hand and the ion emission model (IEM) on the other. With CRM, the solvent evaporates, charge carriers and analyte remain. IEM assumes that the electrostatic repulsion is so high that ions are ejected from the droplets. CRM applies to large ions and IEM to small ones.

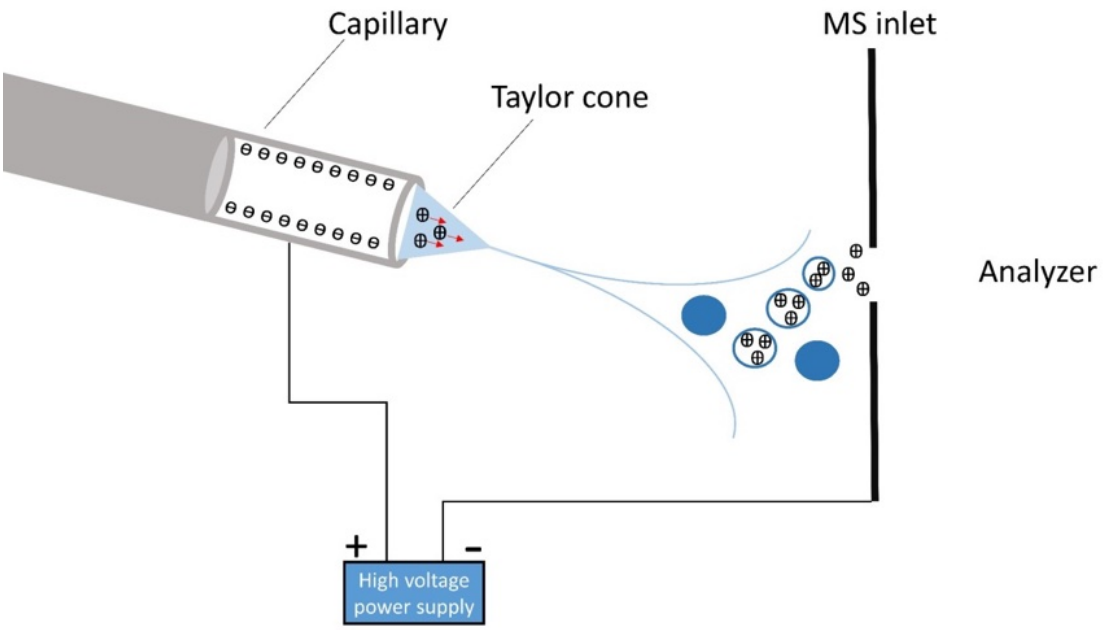

Figure 2: Scheme of ESI in positive ion mode: at high voltage, the Taylor cone emits a jet of liquid droplets.

As a soft ionization method working under atmospheric pressure, ESI is perfectly suited for coupling with chromatographic methods such as HPLC. By linking these two techniques, it is possible to separate complex samples and then ionize and detect them sequentially. HPLC is a common analytical technique for the separation and quantification of constituents in liquid samples. The mobile phase (or first phase) is the solvent used to separate components in a liquid sample. The mobile phase is delivered to a separation column, which contains a packing of small porous particles (the second or stationary phase) at a stable flow rate. The choice of the solvent composition, the column and the flow rate have a decisive influence on the separation of the sample. The stronger the affinity of the analyte with the column, the slower the analyte moves through the column. Conversely, the stronger the affinity of the analyte with the solvents, the faster the analyte moves through the column. The coupling of ESI and chromatographic devices can then be used to perform tandem MS (also MS/MS or MS^2) experiments to identify molecules by their specific fingerprint. Just as two people sit one behind the other in a tandem, two MS steps take place one after the other in tandem MS. The molecules of a certain sample are ionized, and these ions are separated in the first analyzer according to their *m*/*z* value. Ions of a given *m*/*z* value coming from MS1 are selected again and split into smaller fragments, for example through collision-induced dissociation. These fragments are in turn separated and detected based on their *m*/*z* value using the second analyzer (MS2).

With MALDI, a pulsed laser beam instead of a spray is used (see Figure 3). The difference to laser desorption/ionization (LDI) is the combination of the sample with a matrix, strongly absorbing the laser wavelength (typically λ=337nm for N_2 lasers). The matrix consists of crystallised small organic molecules, of which the three most widely used are 2,5-dihydroxybenzoic acid (DHB), α-cyano-4-hydroxycinnamic acid (α-CHCA, alpha-cyano or alpha-matrix) and sinapinic acid.[59] For all analyses and analytes, no single matrix or sample preparation protocol is suitable. The matrix is the factor that makes MALDI a soft ionization method, because it absorbs the energy of the LASER and transmits it more gently to the sample. The matrix must therefore be chosen according to the ion mode, the wavelength of the laser and the analytes to be examined. Isolation, purification, energy uptake, propulsion and ionization are the five key functions of a working matrix. MALDI is used with pulsed mass analyzers such as TOF-MS, Orbitrap™ and Fourier transform ion cyclotron resonance mass spectrometers (FTICR-MS).

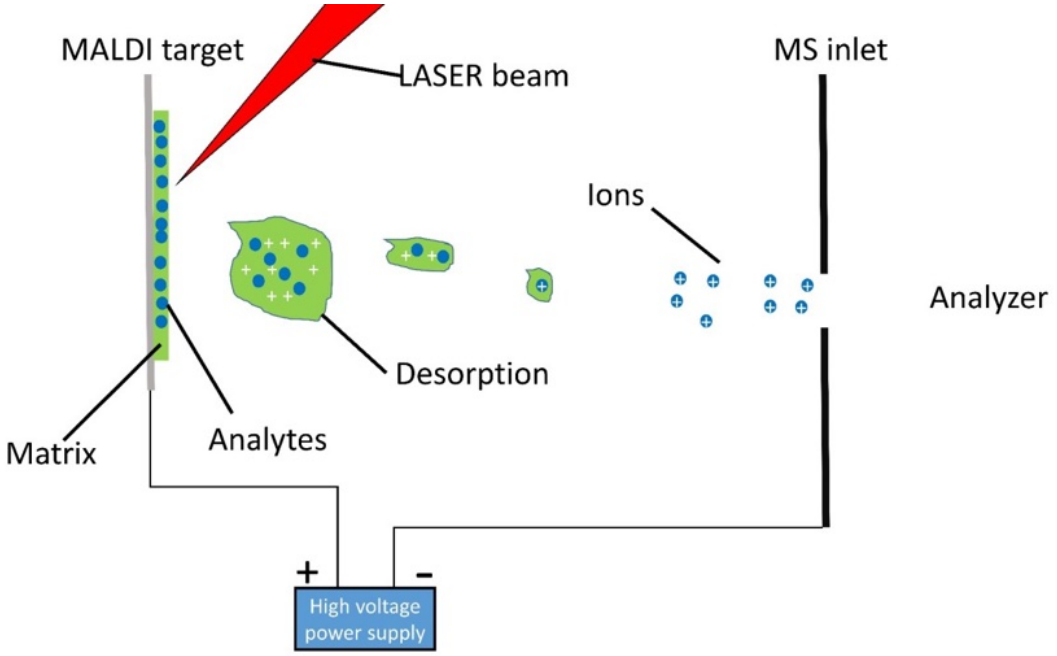

Figure 3: Scheme of the ionisation in the MALDI process (positive ion mode). The LASER shoots at the analytes embedded in the matrix, desorption and ionization occur.

Theoretically, MALDI can be used for quantification, and the number of corresponding publications is increasing. However, the main challenge with quantification using MALDI are matrix and ion suppression effects. They can have an effect on the relationship between the analyte concentration and its corresponding signal.[60]

Mass Spectrometry Imaging

There is a wide range of imaging techniques that are used to study parasites. Light microscopy is strongly represented in all its facets. Intrinsic optical signals are used for polarisation microscopy or quantitative phase imaging (QPI).[61,62] On the other hand, it is possible to use exogenous labelling agents if they do not interfere with the study. However, it is time-consuming and usually requires animal experiments to produce customised, novel antibodies for immunostaining. Bright field microscopy in combination with staining is commonly used to identify and study blood parasites, such as malaria.[63] A very high spatial resolution down to the nanometer range can be achieved with electron microscopy, electron probe X-Ray microanalysis, soft x-ray microscopy or atomic force microscopy. However, none of these methods can provide as good information about the chemical composition and the spatial structure of the sample as mass spectrometry can. MSI is able to rapidly detect a large variety of molecules in a complex sample without labelling. Each individual mass spectrum is linked to location information, allowing the distribution of ions to be visualized. This allows multiple analytes in a single sample to be visualised using different colour channels (RGB being the most meaningful to the human eye).

MALDI-MSI and desorption electrospray ionisation (DESI) are the most commonly used MSI techniques.[64] MALDI and DESI are soft ionization techniques that work under atmospheric pressure and thus also offer access to biomolecules. DESI is the imaging variant of ESI and accordingly also uses a spray, but exclusively with charged solvent particles. As a result, analyte molecules are dissolved and desorbed. The advantage of DESI is that multiple charging is achieved and no matrix needs to be

added.[65] A clear disadvantage is the low lateral resolution, which is typically in the range of 150 to 250 µm.[66] Just like LDI, MALDI can also be used for imaging and is then referred to as MALDI-MSI (see Figure 4). Non-imaging MALDI involves mixing the analyte with an excess of matrix. In the case of imaging, the matrix is sprayed onto the sample in the form of a thin layer. In a MALDI-MSI experiment, the pulsed laser beam is rasterized over the tissue surface. Due to the improvement in MSI instrumentation, lateral resolutions of 1-2 µm became accessible with MALDI, which implies that assembled or even individual cells can be examined by this method.[67] This technique is therefore ideally suited for studying Apicomplexa in cell systems and host tissues. MALDI sources are often combined with TOF instruments. This combination makes it possible to analyze very large molecules such as proteins. This benefit, however, comes at the expense of reduced mass resolution and accuracy, which is essential when studying smaller molecules such as lipids. As already mentioned, this work relies on a unique combination of two leading systems, namely the Q Exactive™ Orbitrap (Thermo Fisher Scientific (Bremen) GmbH, Bremen, Germany) and the AP-SMALDI^5 AF (TransMIT GmbH, Giessen, Germany).

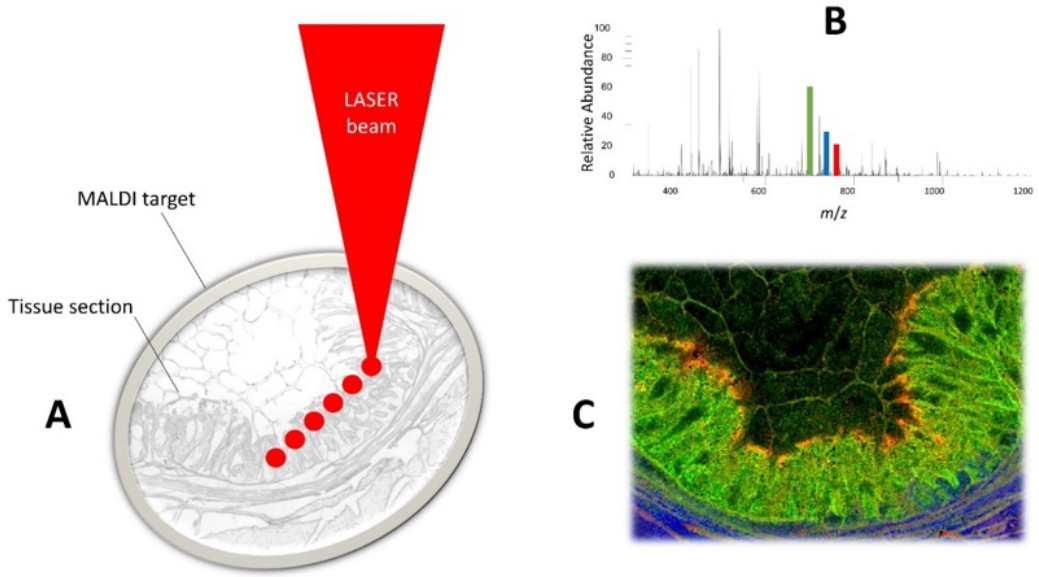

Figure 4: Scheme of MALDI-MSI: A sample is placed on a target and scanned by a LASER (A). The resulting ions enter the mass spectrometer, and a mass spectrum is generated (B). Each individual LASER spot can be linked to an individual mass spectrum, and a distribution image is created (C).

The Q Exactive™ HF is a hybrid quadrupole Orbitrap mass spectrometer. It includes an outer barrel-shaped electrode and a coaxial inner spindle-shaped electrode that traps ions in an orbital motion around the spindle. The real highlight is the so-called c-trap, which directs the ions into the Orbitrap mass analyzer. The mass range is from *m/z* 50-6000. Mass accuracy is 3 ppm when externally calibrated and 1 ppm using an internal standard. The absolute mass resolution is 240,000 (FWHM) at *m/z* = 200.[68]

The AP-SMALDI^5 AF is an atmospheric-pressure ion source with an autofocus system for highest performance under semi-physiological conditions. It can provide high-speed imaging of up to 18 pixels/s (depending on the mass resolution selected) on a Q Exactive™ HF instrument and offers a lateral resolution of 5µm without the risk of oversampling (laser spot size 5 µm). A special mode, which was also used in the case of *C. parvum*, offers improved signal intensities by analyzing the entire sample pixel area.

Results and discussion

MSI of *Neospora caninum*-infected cell monolayers

In order to represent as closely as possible an *in vivo* scenario of rapidly replicating tachyzoites in the vessel endothelium during the acute phase of bovine neosporosis, primary bovine umbilical vein endothelial cells (BUVEC), which are highly immunoreactive, have been used as a model system. Permanent kidney epithelial cells from the African green monkey (MARC-145) were in addition to BUVEC used to provide a system of comparison as well as to promote extensive intracellular replication of the parasite, as a large number of viable tachyzoites were obtained, which were later required for the infection of primary BUVEC. Permanent cell lines provide a consistent sample and reproducible results because they are easy to handle and provide a pure cell population. They are quick to reproduce and never stop growing, guaranteeing an endless supply. Both primary and permanent cells undergo a cycle of cell division, which may have an effect on the metabolism of the cells *in vitro*. However regarding MARC, there are clear disadvantages to these advantages, as permanent cell lines are either genetically engineered or of tumour origin, may not reflect physiological responses as in primary cells, and may therefore give different results.[69] Based on their different cell-derived responses to parasitic infection, the two different cell lines were compared.[70-73] To identify potential markers, consecutive thin sections of *N. caninum*-infected and uninfected host cell pellets were examined. The samples were prepared and stored under identical conditions. All cell pellet measurements were made with a 10µm step size, while monolayers were imaged at 5µm with respect to parasite size (tachyzoites are about 6 x 2 µm in size). A larger step size together with the subsequent defocused laser beam resulted in larger spot sizes. With this procedure, more material is removed by the laser beam and correspondingly ionized. With regard to the cell pellets, three biological and three technical replicates were measured. The measurement of technical replicates is necessary to avoid possible errors in sample preparation or to reduce possible heterogeneities within the cell pellets. To minimise variability in results due to individual differences in the metabolic response of animals to infection, biological replicates are required. In the case of MARC-145, biological replicates cannot be measured as it is a permanent cell line. The Mirion software (TransMIT GmbH, Giessen, Germany) in combination with the Perseus software platform (MPI of Biochemistry, Martinsried, Germany) was used to find potential biomarkers within these cell sections.[74] In Perseus, the data sets were categorised into those that were infected with *N. caninum* and those that were not. Two standardisations followed by multiple-sample tests (ANOVA; permutation-based false-discovery rate, FDR = 0.05, number of randomizations = 250) were the next step. Corresponding values from the previous step were filtered and mismatches rejected. Post-hoc tests were performed on the remaining values in the final step. All subsequent experiments were based on the biomarkers found in these experiments. In positive-ion mode, 582 markers with significantly increased signal intensities were detected in case of infection of BUVEC. 48 signals in positive-ion mode, on the other hand, were significantly reduced in their signal intensity which could indicate that the parasite has metabolized them. In the negative-ion mode, 659 marker signals were significantly increased, respectively 411 significantly reduced. The MARC-145 samples were measured in positive-ion mode only. For MARC-145, only 50 significantly increased signals were found in the positive-ion mode in case of infection. The number of overlaps with BUVEC was 26. This may indicate that these signals are coming directly from the parasite. There were 24 significantly downregulated signals with no overlap to BUVEC. This again supports the assumption that the overlap of significantly upregulated signals originated directly from the parasite. In line with expectations, the results of the two models were very different.[69]

To annotate these specific markers for *N. caninum* infection of BUVEC, the LIPID MAPS® database of computationally-generated "bulk" lipid species was used. This is a virtual database that consists of the most important classes of lipid species.[75] Not every signal recognised as a marker was annotated due to the restriction to lipids (database and subsequent extraction for HPLC-MS/MS). In order to obtain meaningful annotations, the LIPID MAPS search criteria were selected to include appropriate ion adducts with the corresponding polarity. Only species with a single charge were selected. In positive-ion mode, ions of types $[M+H]^+$, $[M+H-H_2O]^+$, $[M+Na]^+$, $[M+NH_4]^+$ and $[M+K]^+$ and in negative-ion mode $[M-H]^-$, $[M+Cl]^-$, $[M+HCOO]^-$, $[M+OAc]^-$ and $[M-CH_3]^-$ were taken into account. In LIPID MAPS, a mass tolerance of *m/z* ±0.05 was chosen. Then, the values with a calculated deviation of more than 5 ppm between the theoretical value and the measured value were discarded. Annotations that differed from the annotation by more than 1 ppm were discarded if several different annotations were found for the same *m/z* value. The results of this procedure can be seen in Figure 5. Because more than one annotation can meet the criteria described above, the number of annotations is greater than the number of *m/z* values. In positive-ion mode, 116 different *m/z* values were significantly upregulated in infected cell pellets, to which 982 annotations could be assigned. In negative-ion mode, the ratio was 357 different *m/z* values to 1654 annotations. 90 annotations (39 different *m/z* values) were determined for the positive-ion mode and 68 (49 different *m/z* values) for the negative-ion mode in the case of significantly downregulated signals.

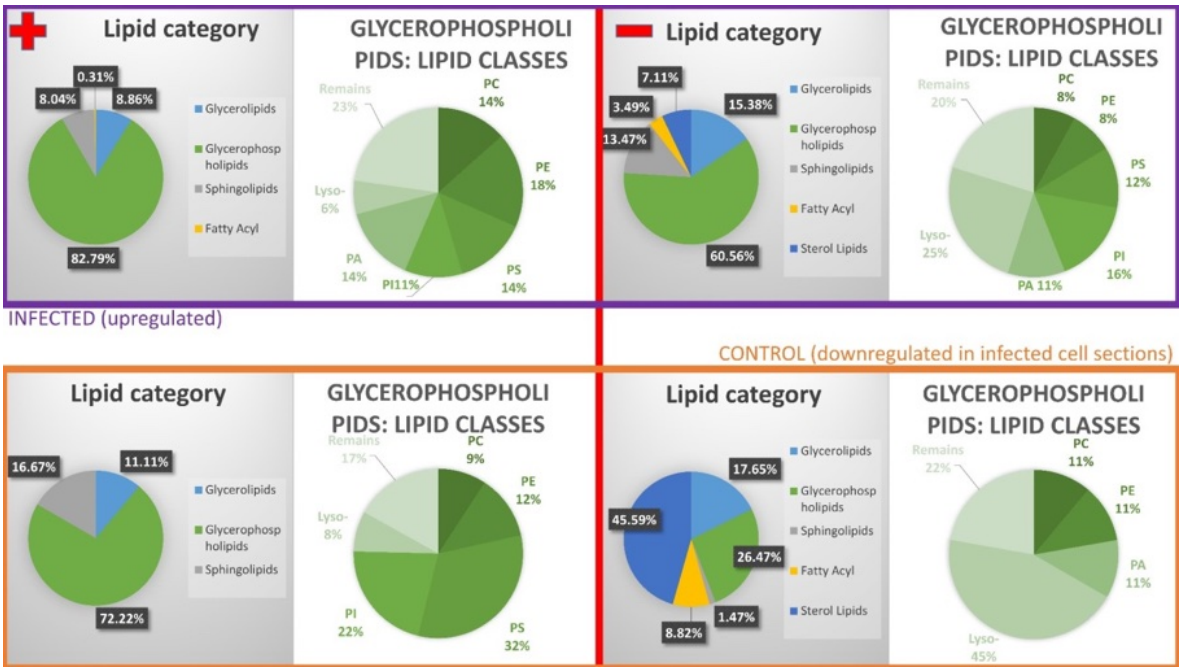

Figure 5: Abundances of categories of detected BUVEC markers (fractions of signal numbers (in [%])). Left: positive-ion mode; Right: negative-ion mode; Upper part: upregulated in infected samples; Lower part: higher signal intensities in control samples – downregulated in infected cells. All annotations can be found in the supplementary information of the corresponding paper.

Additionally, the proportions of signal numbers (in [%]) of all annotated lipid categories are shown in Figure 5. In the positive-ion mode, the *N. caninum* infected samples showed a lower percentage change in phosphatidylserines (PS) and phosphatidylinositols (PI) composition compared to the control samples. It can be seen that the relative phosphatidylserines (PS) and phosphatidylinositols (PI) composition decreases in positive-ion mode in infected samples. In infected samples, increased levels of phosphatidylethanolamine (PE) and especially phosphatidic acids (PA) were found. Sterols are difficult to ionise in positive-ion mode without derivatisation, therefore they were only annotated in

negative-ion mode.[76-79] The absolute number of annotated sterol signals in the samples infected with *N. caninum* was more than three times as high as in the control samples (104 vs. 31). Sterol levels are known to be upregulated in host cells infected with other apicomplexan parasite species.[80] The proportion of lysolipids was almost halved in infected samples with high PI in the negative-ion mode.

Inclusion lists for the HPLC-MS/MS measurements were generated using the annotations obtained from the database searches. In this context, high-resolution full MS and MS/MS spectra were recorded. LipidMatch software (SECIM, Gainesville, USA) in combination with ProteoWizard (MSConvertGUI) and Mzmine were used to identify the molecular markers detected.[81-83] The specific settings can be found in the supplementary information of the corresponding paper. Twelve annotations for upregulated signals in case of *N. caninum*-infected samples were confirmed by MS/MS analysis in positive-ion mode. As observed in infections with other Apicomplexa, the PC lipid class was highly abundant.[84] Three downregulated signals in the positive-ion mode were also identified. MS/MS experiments in negative-ion mode confirmed 28 of the annotations for significantly upregulated signals. Here, the most abundant class of lipids were phosphatidylinositols, which are components of cell membranes. They play a crucial role in trafficking, membrane dynamics and cellular signalling.[85] This is in line with our hypothesis that the markers are a cell response to infection. Almost all of the markers identified contained a short-chain fatty acid, regardless of the ion mode. This observation is also typical for the zoonotic *T. gondii* as described in the literature.[84]

For MSI of monolayers, a lateral resolution of at least 5 µm is required to visualise the small tachyzoites (< 10 µm) within cells. MALDI imaging of *N. caninum*-infected and control monolayers in positive-ion mode can be seen in Figure 6. The infected BUVEC layers are shown on the left-hand side of each panel and the control samples are shown on the right-hand side. The total ion count (TIC) is represented by the green channel. The red channel shows the distribution of different infection markers. The markers were identified by LC-MS/MS with a mass tolerance of ± 5 ppm. As anticipated, only cell layers infected with *N. caninum* showed these signals, or they were significantly more pronounced. Other markers that illustrate the infection in the same way (positive- and negative-ion mode) are visualized in the associated paper. While in Figure 6A the optical image is shown, Figure 6B displays the distribution of an infection-specific signal at *m/z* 468.3087, assigned to LPC(14:0) as $[M + H]^+$ and Figure 6C the distribution of the signal *m/z* 836.5461, which was previously assigned to PS(40:6) as $[M + H]^+$.

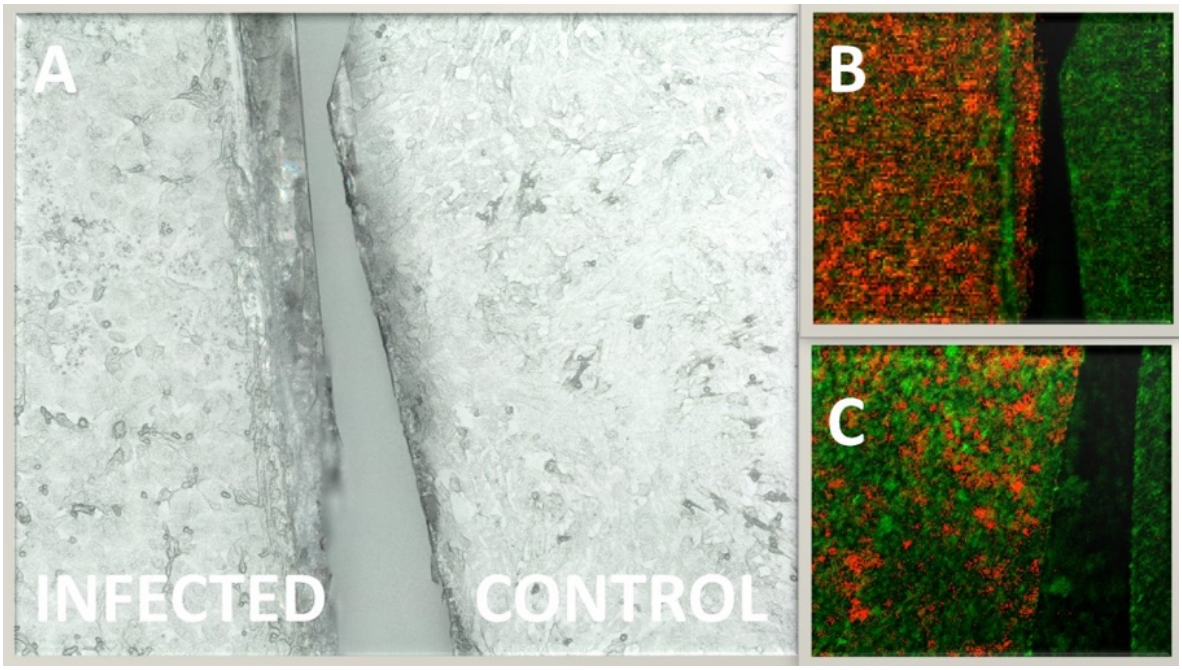

Figure 6: On each panel, the infected monolayer is on the left and the control monolayer on the right. A: Optical image; B&C: MALDI MSI measurements of two BUVEC monolayers measured with 5 µm laser focus diameter and step size in positive-ion mode. B: The green channel represents the TIC. The red channel shows the distribution of an identified infection marker (±5 ppm mass tolerance) at m/z 468.3087, identified as LPC(14:0) as $[M+H]^+$. C: The green channel represents the TIC. The red channel shows the distribution of an identified infection marker (±5 ppm mass tolerance) at m/z 836.5461, identified as PS(40:6) as $[M+H]^+$.

The next step was to examine the correlations between the structures observed in high-resolution light microscopy images and the measured MS images (see Figure 7). Infected and control monolayers are shown on the left and right of each panel, respectively. In Figure 7A, intracellular tachyzoites of *N. caninum*, encircled in yellow, can be seen in infected cell layers as typical 'banana' shaped structures in the microscopic image. The corresponding MS image of the monolayer in positive-ion mode is shown in Figure 7B, the overlay in Figure 7C. The TIC is represented by the green colour channel. The red and blue channels show the distribution of two identified signals, which were significantly upregulated in case of infection, with a mass tolerance of ±5 ppm. The red and the blue colour channel overlap almost perfectly, resulting in pink pixels. The red channel represents an infection marker at *m/z* 692.5225, identified as PC(29:0) as $[M+H]^+$, the blue channel represents an infection marker at *m/z* 704.5225, identified as PC(30:1) as $[M+H]^+$.

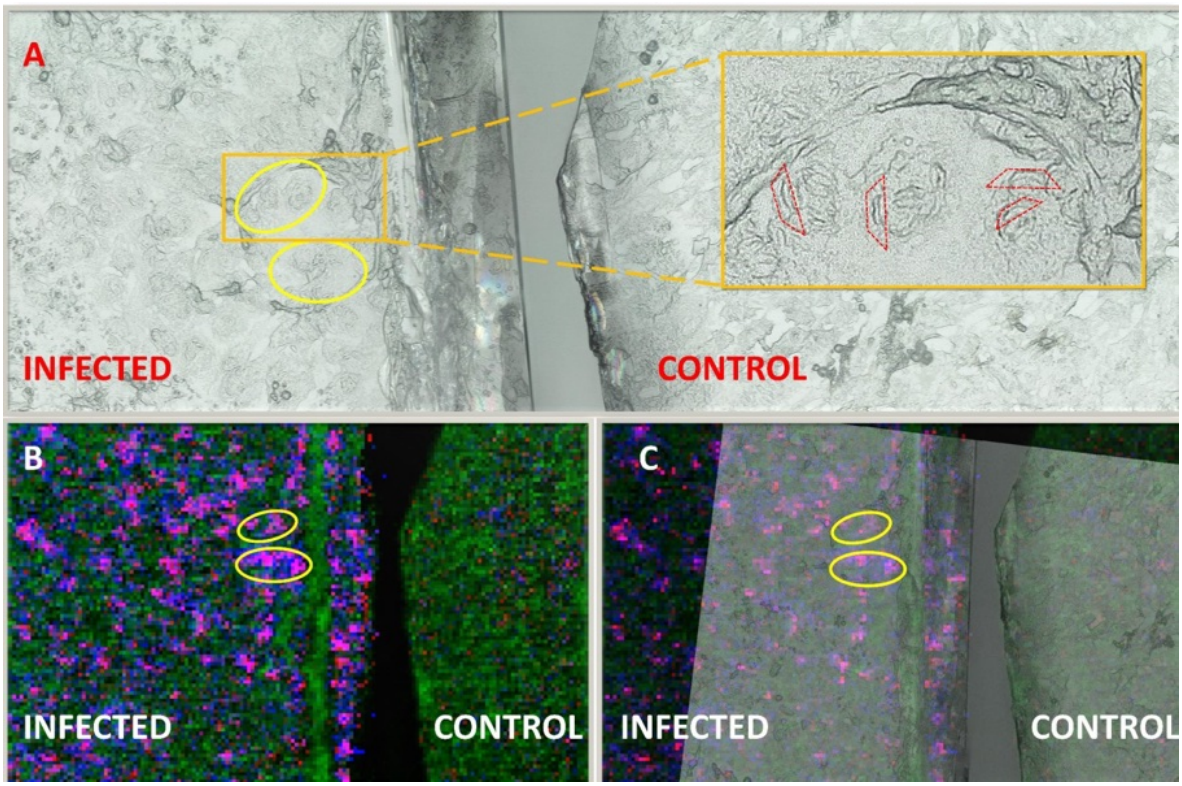

Figure 7: On each panel, the infected monolayer is on the left and the control monolayer on the right. A: Optical image - Intracellular tachyzoites can be recognized as banana-shaped structures (outlined in red) exclusively in the infected monolayer, as part of a rosette-like meront. Two particularly noticeable areas with N. caninum meronts are circled in yellow; B&C: MALDI MSI measurements of two BUVEC monolayers measured with 5 µm laser focus diameter and step size in positive-ion mode. ***B:*** *The green channel represents the TIC. The red and blue channel show the distribution of two identified infection markers (±5 ppm mass tolerance). The two markers overlap to pink pixels. The red channel represents an infection marker at m/z 728.5201, identified as PC(29:0) as $[M+H]^+$ and the blue channel represents an infection marker at m/z 704.5225, identified as PC(30:1) as $[M+H]^+$.* ***C:*** *Overlay of panels A and B. Infection marker signals overlap well with the banana-shaped (tachyzoites) and rosette-like (meronts) structures in the yellow circles.*

MSI of *in vitro Cryptosporidium parvum*-Infected Cells and Host Tissue

As a suitable *in vitro* host cell system, human ileocecal adenocarcinoma cells (HCT-8), in the form of cell pellets and monolayers, were used. It is the most established in vitro system for *C parvum* studies. In addition, artificially and naturally infected bovine neonatal intestinal mucosa was prepared and made accessible for MALDI imaging. Similar to the procedure for *N. caninum*, statistically significant biomarkers were determined using sections from infected and control cell pellets. Three technical replicates were used, no biological ones, since HCT-8, like MARC-145, is a permanent cell line. In contrast to the mass spectrometric investigations of *N. caninum*, however, the normal spot mode, where laser pulses are applied to a single spot in the centre of the pixel, was not sufficient to ensure satisfactory ion signal intensities. For this reason, cell pellet measurements were performed using a signal-enhancing mode of the ion source, the Full Pixel mode, where a larger number of laser pulses is used to ablate the pixel area in a meandering motion leading to more material being removed from the area of the pixel as well as from the depth of the sample (see Figure 8).[86] However, the lateral resolution is lower than in spot mode. However, this is only a limitation with MALDI imaging, but not in this application. In contrast to the cell pellets, monolayers and host tissue were imaged with MALDI-MSI at a lateral resolution of 5 µm in spot mode.

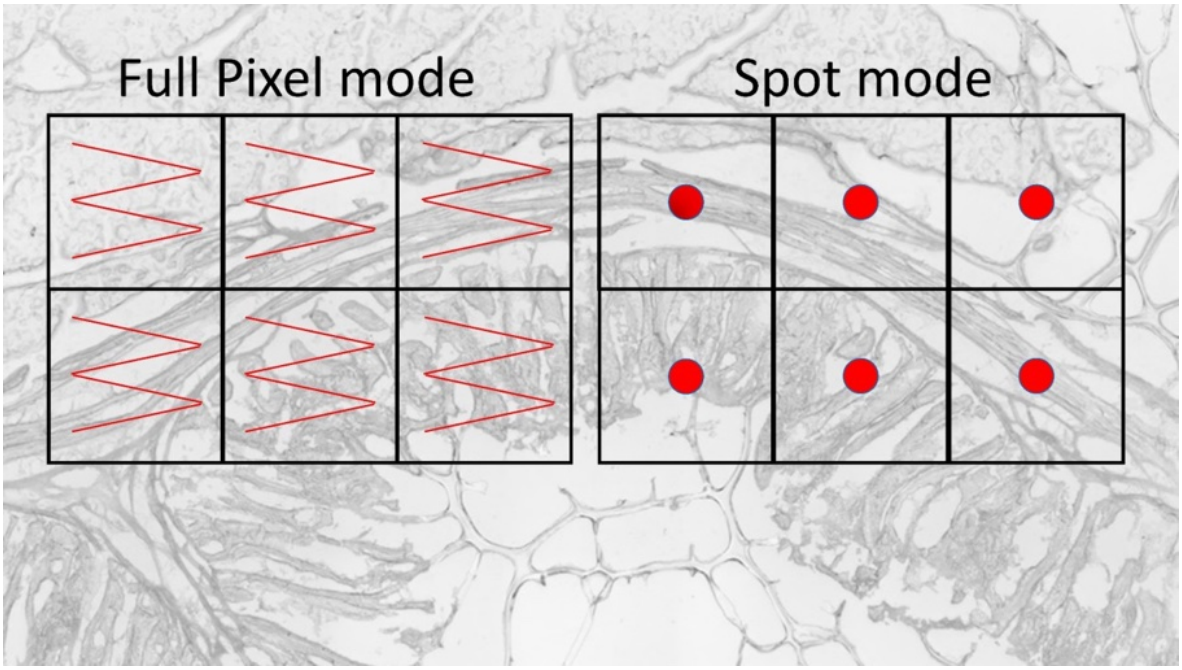

Figure 8: The Full Pixel mode can be seen on the left, the spot mode on the right. The pixel area is outlined in black, and the laser ablation profiles are shown in red. In spot mode, a single laser pulse is applied to the sample in the middle of the pixel. In Full Pixel mode, a larger number of laser pulses within the pixel are applied to the sample in a meandering movement.

As with *N. caninum*, the annotations were made using the LIPID MAPS® database of computationally-generated "bulk" lipid species. The procedure was identical, and the results can be viewed in Figure 9. There was little change in the proportions of lipid categories in infected and control samples in the positive-ion mode.

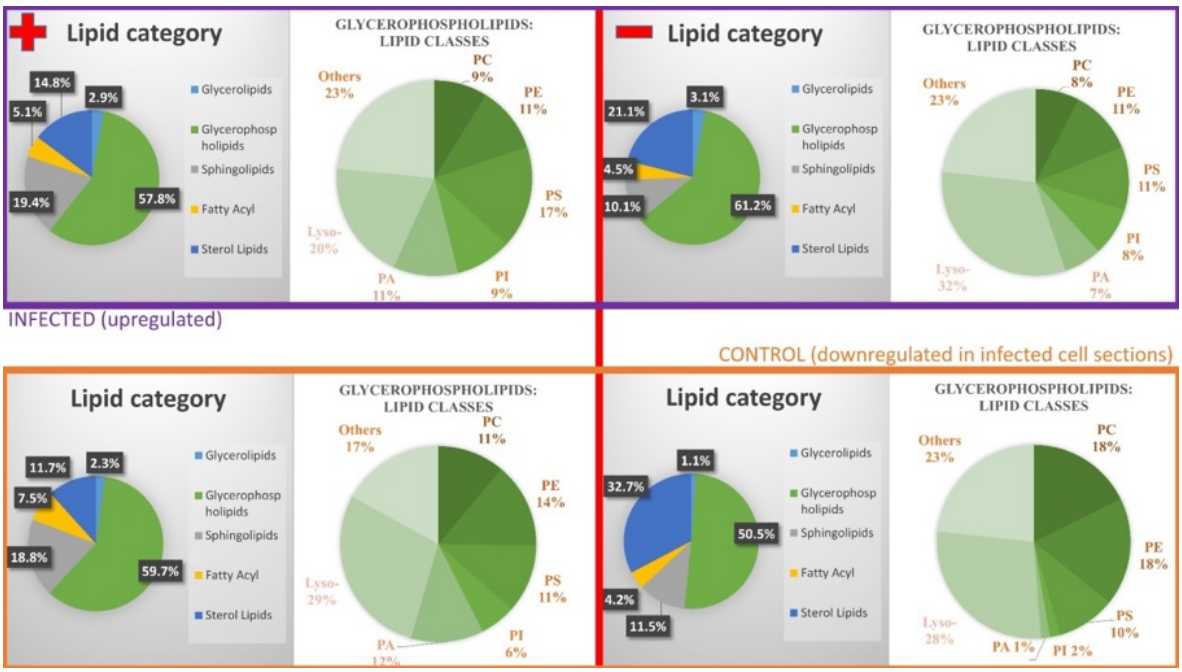

Figure 9: Abundances of categories of detected HCT-8 markers (fractions of signal numbers (in [%])). Left: positive-ion mode; Right: negative-ion mode; Upper part: upregulated in infected samples; Lower part: higher signal intensities in control samples – downregulated in infected cells. All annotations can be found in the supplementary information of the corresponding paper.

In the case of downregulation caused by the parasite invasion, 2333 annotations were determined for 721 different *m*/*z* values in positive-ion mode and 1036 annotations for 380 different *m*/*z* values in negative-ion mode. There was little change in the proportions of lipid categories in infected and control samples in the positive-ion mode. Within the group of glycerophospholipids, the proportions of lipid classes slightly changed. Higher levels of phosphatidylserine (PS) and phosphatidylinositol (PI) were found in the *C. parvum*-infected samples. In contrast to that, the proportion of phosphatidylethanolamines (PE), phosphatidylcholines (PC) and in particular lysolipids (Lyso) was found to be decreased in *C. parvum*-infected samples. The proportions of lipid classes changed significantly in the negative-ion mode. With parasitic infection, the proportion of glycerophospholipids increased. At class level, there was a decrease in the proportions of PC and PE and an increase in the proportions of PI, PA and lysolipids.

The annotated markers were identified in the same way as for *N. caninum*, but LipidMatch software (SECIM, Gainesville, USA) was replaced by LipidMatch Flow (SECIM, Gainesville, USA).[81] All identifications can be found in the supplementary information of the corresponding paper. In summary, 37 of the annotations in positive-ion mode for upregulated lipids in samples infected with *C. parvum* were verified by HPLC-MS/MS experiments. The PC lipid class was highly abundant. PC lipids are a major structural component of membrane bilayers and are known to be the dominant phospholipid class for *C. parvum*.[87] In *T. gondii* and *Plasmodium falciparum*, PC is known to be the most abundant phospholipid class in membranes and is crucial for the replication of both parasite's blood and liver stages.[88-92] In infections with other apicomplexans, PCs are also significantly increased.[84] In positive-ion mode, 15 downregulated lipid annotations were confirmed in infected samples. Using negative-ion mode, 15 of the previously annotated biomarkers were identified for up- and 20 for downregulation. It has also been shown that this apicomplexan infection affects the composition of lysolipids independently of the ion mode. It is known that this lipid species are ubiquitous intermediates in a wide variety of metabolic and signalling pathways in eukaryotic cells.[93] In the case of *P. falciparum*, there is evidence that it utilizes lysolipids already present in the parasitized host for the synthesis of PC.[94] Our observations regarding changes in PC and lysolipid abundances in *C. parvum*-infected host cells and the intestinal mucosa are thus confirmed by the literature.

For MSI of monolayers and host tissue, a lateral resolution of at least 5 µm is required to visualise the small parasites (3-5 µm) attached to the cells. In Figure 10, an MS image shows a *C. parvum*-infected HCT-8 monolayer at the top, and a control sample at the bottom. The green channel represents the TIC. The red and the blue channel show the distribution of two biomarkers obtained by LC-MS/MS analysis (mass tolerance of ±5 ppm) and identified as being upregulated in case of infection. In the *C. parvum*-infected monolayer, these signals were found exclusively or with significantly higher signal intensities, as expected.

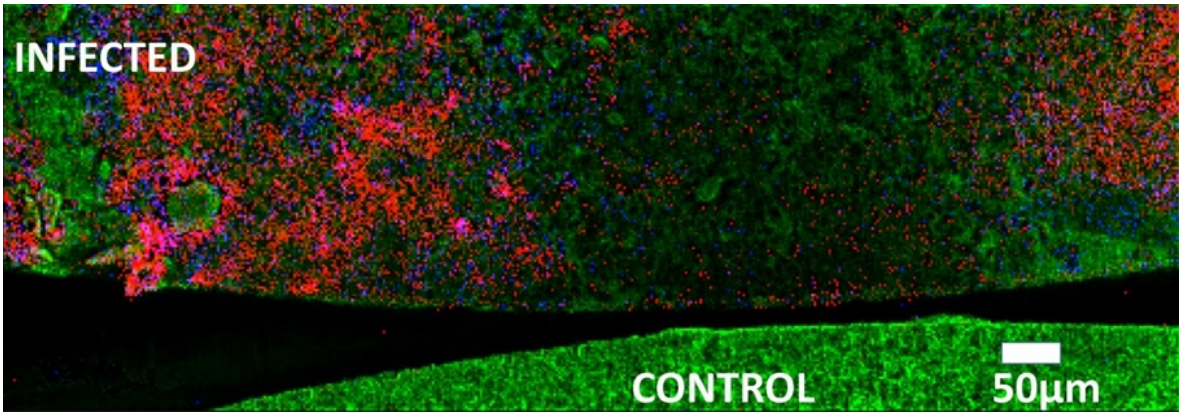

Figure 10: MALDI MSI measurements of monolayers in positive-ion mode, measured with 5 µm laser focus diameter and step size. The green channel represents the TIC, used for visualization purposes only. The red and blue channels show the distribution of two different infection markers (±5 ppm mass tolerance) identified earlier by LC-MS/MS measurements of cell pellets or host tissue. Red: Infection marker signal at m/z 770.6058, identified as plasmanyl-PC(O-36:3) as $[M+H]^+$; Blue: infection marker signal at m/z 811.6687, identified as SM(O_2-42:3) as $[M+H]^+$.

Cryosections of *C. parvum*-infected neonatal bovine intestinal tissue were analysed in addition to cell monolayer measurements. The naturally infected intestinal samples were fixed in formalin (Figure 11A). Small pieces were cut out of these with the help of a scalpel and frozen in blocks of gelatine. These blocks could then be processed in the cryotome. The consistency of these formalin-fixed samples are similar to that of leather, making it possible to produce sections of 20 to 40 µm thickness (see Figure 11B).

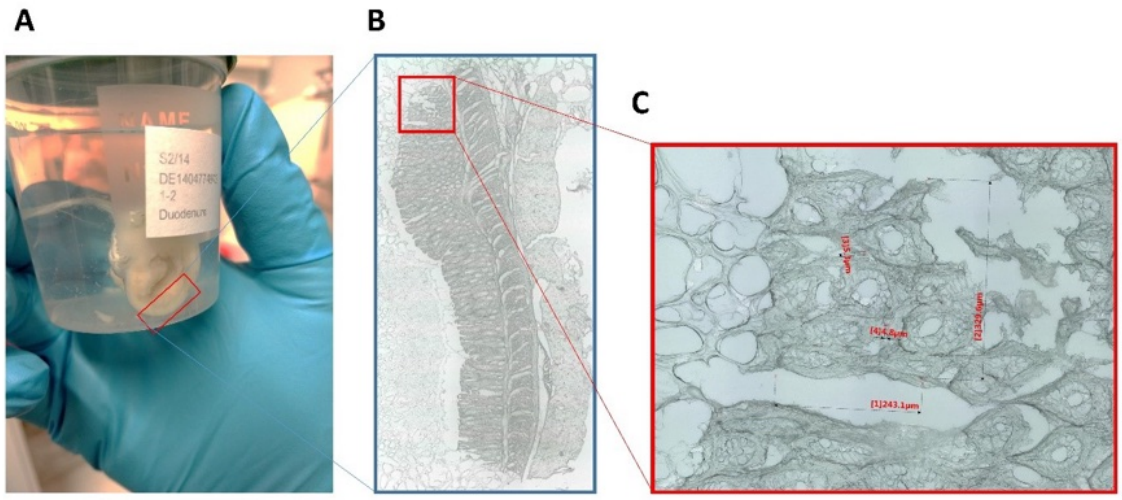

Figure 11: A: Formalin-fixed gut pieces; B: Section of A with a thickness of 20 µm; C: High resolution image of an infected area from B - The parasite is indicated by the red markings.

Figure 12 shows the analysis of a naturally infected intestine. An optical image of the entire intestinal section is shown in Figure 12A. The area of infection (wrinkles and villi) is outlined in red. MS images of this neonatal bovine intestinal section are shown in Figure 12B and C. The green channel in B represents an ion channel at *m/z* 756.5513, which is used for visualization purposes only and shows the entire section of the intestine. In addition, the infection marker signals at *m/z* 536.3711, identified as LPE (22:1) as $[M+H]^+$ and *m/z* 766.5745, identified as plasmanyl PC(O-36:5) as $[M+H]^+$, were

visualized in red and blue. These can also be seen without the green colour channel in Figure 12C. The markers for the infection are upregulated in the inner or luminal area of the small intestine (outlined in white). It is here that *C. parvum* replicates, giving rise to the trophozoite, meront, gamont and oocyst stages.

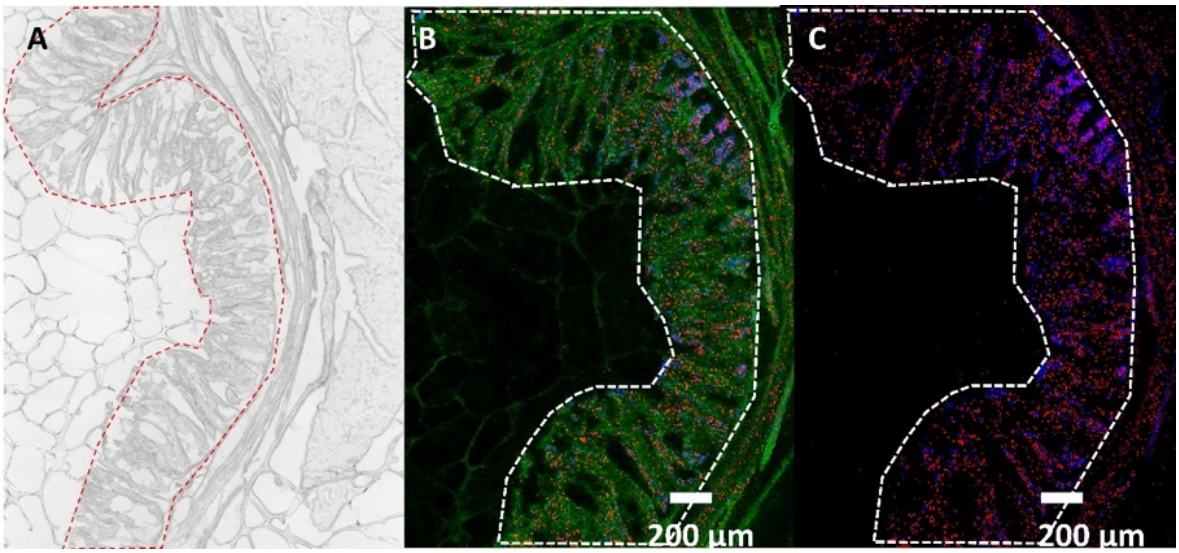

*Figure 12: MALDI MSI measurements of C. parvum-infected neonatal bovine intestine in positive-ion mode, measured with 10 µm laser focus diameter and step size in Full Pixel mode. The red and blue channels show the distribution of two infection markers (±5 ppm mass tolerance) identified earlier by LC-MS/MS measurements of cell pellets or host tissue. (**A**) Optical image of the whole intestine section. The area of infection (wrinkles and villi) is outlined in red (**B**) The green channel represents an ion signal at m/z 756.5513, used for visualization purposes only. Infection marker signal at m/z 536.3711, identified as LPE (22:1) as $[M+H]^+$ in red, and m/z 766.5745, identified as plasmanyl-PC(O-36:5) as $[M+H]^+$in blue. (**C**) Infection marker signal at m/z 536.3711, identified as LPE (22:1) as $[M+H]^+$ in red, and m/z 766.5745, identified as plasmanyl-PC(O-36:5) as $[M+H]^+$in blue.*

Subsequently, MSI was used to study intestinal samples from experimentally infected neonatal calves. The cryosections were made in such a way that the inner part of the intestine, where the infection is most prevalent, is located exclusively on the right-hand side (see Figure 13). In Figure 13 an optical image of the whole intestine section can be seen. The corresponding MS image is shown in Figure 13B, the red channel shows the distribution of an infection marker (±5 ppm mass tolerance) at *m/z* 504.3057, identified as LPE (20:3) as $[M+H]^+$. The fact that the marker is actually upregulated exclusively in that area which is assigned to the infection, can be seen in Figure 13C in the form of an overlay.

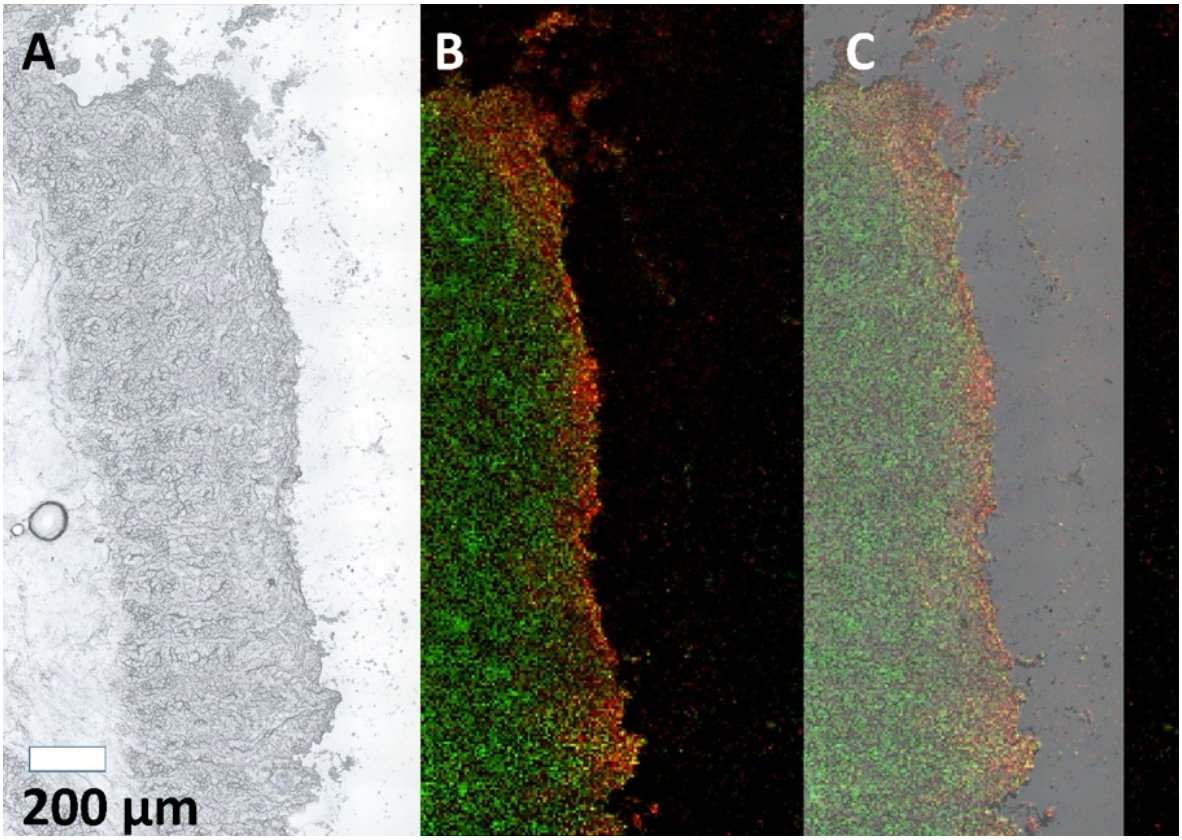

Figure 13: MALDI MSI measurements of bovine intestine in positive-ion mode, infected with C. parvum and measured with 12 µm laser focus diameter and step size. The green channel represents an ion signal at m/z 726.5603, used for visualization purposes only. ***A*** *optical image of the whole intestine section;* ***B*** *The red channel shows the distribution of an infection marker (±5 ppm mass tolerance) at m/z 504.3057, identified as LPE (20:3) as* $[M+H]^+$*;* ***C*** *Overlay of the optical image (A) and the MS image (B); Further MS images can be found in the associated paper.*

Conclusions and Future Perspectives

As Apicomplexa progress through their life cycle, they undergo a cascade of developmental changes. Appropriate stages can then be used to infect cells or host tissue. *N. caninum*- and *C. parvum* -infected cell systems and corresponding host tissues were studied in this work.

The *N. caninum* infection markers identified were compared with previously published *Toxoplasma gondii* and *Besnoitia besnoiti* markers.[95] 25% of the markers that were upregulated during *N. caninum* infection were also identified as markers for *T. gondii* and *B. besnoiti* endothelial host cell infections. A comparison can be found in the supplementary information of the corresponding paper. Phosphatidylinositols were about 80% of these commonly identified markers. As noted above, these molecules play critical roles in cellular signalling, membrane dynamics and trafficking, supporting the hypothesis that these markers are a common response of infected host cells to apicomplexan infection.[85] The *C. parvum* biomarkers were compared with the same data sets as already *N. caninum*. All four parasites belong to the taxonomic subphylum Apicomplexa. However, only one biomarker common to all four parasites, namely PI (36:1) as $[M-H]^-$, was found.

As already described, both MALDI and ESI are soft ionization methods that work under atmospheric pressure. Both therefore offer good access to biomolecules. Nevertheless, both are different ionization techniques in which not all molecules are ionized equally well. This means that it is not possible from

the outset to subsequently identify all markers found with MALDI using ESI. This is certainly a topic for future work.

For high-resolution 3D-surface AP-SMALDI MSI experiments, cell layers infected with both parasites as well as natural and experimentally *C. parvum*-infected host intestinal tissues were analyzed and found markers were imaged. In this way, infected cells or intestinal tissue of the host could be distinguished from uninfected cells and healthy tissue. This allowed to visualize the parasitic infections with a lateral resolution of 5 to 12 µm.

Theoretically, there is the possibility that the biomarkers found for infection with *N. caninum* and *C. parvum* can be used to detect such parasites or at least they could provide strong evidence of infection. In recent years, small mass spectrometers, some of which are portable, have been developed.[96-98] An application directly on site would be conceivable. In the case of *C. parvum* and the resulting cryptosporidiosis, however, this is rather unlikely because it is a poverty-related disease and there is therefore a clear lack of financial resources.

This type of research is of a fundamental nature. With the help of the presented research and the novel lipid data, it might be possible to identify alternative metabolic pathways for novel drug targets. These could then be used not only against *N. caninum* and *C. parvum*, but also against other apicomplexan parasites of veterinary and health relevance.

References

1. Barr BC, Conrad PA, Sverlow KW, Tarantal AF, Hendrickx AG. EXPERIMENTAL FETAL AND TRANSPLACENTAL NEOSPORA INFECTION IN THE NONHUMAN PRIMATE. Laboratory Investigation 1994;71(2):236-242.
2. Robayo-Sanchez L, Gomez-Marin J, Cortes-Vecino J. Neospora caninum: Biological Relationship with Toxoplasma gondii and its Potential as Zoonosis. Revista Mvz Cordoba 2017;22(3):6355-6365. (Review) (In English). DOI: 10.21897/rmvz.1139.
3. Gerace E, Lo Presti VD, Biondo C. Cryptosporidium Infection: Epidemiology, Pathogenesis, and Differential Diagnosis. European Journal of Microbiology and Immunology 2019;9(4):119-123. DOI: 10.1556/1886.2019.00019.
4. Ren Minghui WHO. *Ending the neglect to attain the Sustainable Development Goals: a road map for neglected tropical diseases 2021–2030*. World Health Organization (https://www.who.int/publications/i/item/9789240010352).
5. Kotloff KL, Nataro JP, Blackwelder WC, et al. Burden and aetiology of diarrhoeal disease in infants and young children in developing countries (the Global Enteric Multicenter Study, GEMS): a prospective, case-control study. Lancet 2013;382(9888):209-222. DOI: 10.1016/s0140-6736(13)60844-2.
6. Dubey JP, Lindsay DS. A review of Neospora caninum and neosporosis. Veterinary Parasitology 1996;67(1-2):1-59. DOI: 10.1016/s0304-4017(96)01035-7.
7. Spengler B. De novo sequencing, peptide composition analysis, and composition-based sequencing: A new strategy employing accurate mass determination by Fourier transform ion cyclotron resonance mass spectrometry. Journal of the American Society for Mass Spectrometry 2004;15(5):703-714. DOI: 10.1016/j.jasms.2004.01.007.
8. Spengler B. Accurate mass as a bioinformatic parameter in data-to-knowledge conversion: Fourier transform ion cyclotron resonance mass spectrometry for peptide de novo sequencing. European Journal of Mass Spectrometry 2007;13(1):83-87. DOI: 10.1255/ejms.840.

9. Spengler B, Hester A. Mass-Based Classification (MBC) of Peptides: Highly Accurate Precursor Ion Mass Values Can Be Used to Directly Recognize Peptide Phosphorylation. Journal of the American Society for Mass Spectrometry 2008;19(12):1808-1812. DOI: 10.1016/j.jasms.2008.08.005.
10. Seron K, Dzierszinski F, Tomavo S. Molecular cloning, functional complementation in Saccharomyces cerevisiae and enzymatic properties of phosphatidylinositol synthase from the protozoan parasite Toxoplasma gondii. European Journal of Biochemistry 2000;267(22):6571-6579. DOI: 10.1046/j.1432-1327.2000.01749.x.
11. Araujo A, Jansen AM, Bouchet F, Reinhard K, Ferreira LF. Parasitism, the diversity of life, and paleoparasitology. Memorias Do Instituto Oswaldo Cruz 2003;98:5-11. DOI: 10.1590/s0074-02762003000900003.
12. Morrison DA. Evolution of the Apicomplexa: where are we now? Trends in Parasitology 2009;25(8):375-382. DOI: 10.1016/j.pt.2009.05.010.
13. Moss GP, Smith PAS, Tavernier D. GLOSSARY OF CLASS NAMES OF ORGANIC-COMPOUNDS AND REACTIVE INTERMEDIATES BASED ON STRUCTURE. Pure and Applied Chemistry 1995;67(8-9):1307-1375. DOI: 10.1351/pac199567081307.
14. Villagra-Blanco R, Angelova L, Conze T, et al. Seroprevalence of Neospora caninum-specific antibodies in German breeding bitches. Parasites & Vectors 2018;11. DOI: 10.1186/s13071-018-2683-1.
15. Dubey JP, Carpenter JL, Speer CA, Topper MJ, Uggla A. NEWLY RECOGNIZED FATAL PROTOZOAN DISEASE OF DOGS. Journal of the American Veterinary Medical Association 1988;192(9):1269-1285.
16. Lindsay DS, Upton SJ, Dubey JP. A structural study of the Neospora caninum oocyst. International Journal for Parasitology 1999;29(10):1521-1523. DOI: 10.1016/s0020-7519(99)00121-6.
17. McAllister MM, Dubey JP, Lindsay DS, Jolley WR, Wills RA, McGuire AM. Dogs are definitive hosts of Neospora caninum. International Journal for Parasitology 1998;28(9):1473-1478. DOI: 10.1016/s0020-7519(98)00138-6.
18. Speer CA, Dubey JP, McAllister MM, Blixt JA. Comparative ultrastructure of tachyzoites, bradyzoites, and tissue cysts of Neospora caninum and Toxoplasma gondii. International Journal for Parasitology 1999;29(10):1509-1519. DOI: 10.1016/s0020-7519(99)00132-0.
19. Ramaprasad A, Mourier T, Naeem R, et al. Comprehensive Evaluation of Toxoplasma gondii VEG and Neospora caninum LIV Genomes with Tachyzoite Stage Transcriptome and Proteome Defines Novel Transcript Features. Plos One 2015;10(4). DOI: 10.1371/journal.pone.0124473.
20. Reid AJ, Vermont SJ, Cotton JA, et al. Comparative Genomics of the Apicomplexan Parasites Toxoplasma gondii and Neospora caninum: Coccidia Differing in Host Range and Transmission Strategy. Plos Pathogens 2012;8(3). DOI: 10.1371/journal.ppat.1002567.
21. Dubey JP, Barr BC, Barta JR, et al. Redescription of Neospora caninum and its differentiation from related coccidia. International Journal for Parasitology 2002;32(8):929-946. DOI: 10.1016/s0020-7519(02)00094-2.
22. Dubey JP, Schares G, Ortega-Mora LM. Epidemiology and control of neosporosis and Neospora caninum. Clinical Microbiology Reviews 2007;20(2):323-+. DOI: 10.1128/cmr.00031-06.
23. Reichel MP, Ayanegui-Alcerreca MA, Gondim LFP, Ellis JT. What is the global economic impact of Neospora caninum in cattle - The billion dollar question. International Journal for Parasitology 2013;43(2):133-142. (Review) (In English). DOI: 10.1016/j.ijpara.2012.10.022.
24. Romand S, Thulliez P, Dubey JP. Direct agglutination test for serologic diagnosis of Neospora caninum infection. Parasitology Research 1998;84(1):50-53. (Article) (In English).
25. Bjorkman C, Holmdahl OJM, Uggla A. An indirect enzyme-linked immunoassay (ELISA) for demonstration of antibodies to Neospora caninum in serum and milk of cattle. Veterinary Parasitology 1997;68(3):251-260. DOI: 10.1016/s0304-4017(96)01076-x.

26. Bjorkman C, Lunden A, Holmdahl J, Barber J, Trees AJ, Uggla A. NEOSPORA-CANINUM IN DOGS - DETECTION OF ANTIBODIES BY ELISA USING AN ISCOM ANTIGEN. Parasite Immunology 1994;16(12):643-648. DOI: 10.1111/j.1365-3024.1994.tb00320.x.
27. Trees AJ, Williams DJL. Endogenousand exogenous transplacental infection in Neospora caninum and Toxoplasma gondii. Trends in Parasitology 2005;21(12):558-561. DOI: 10.1016/j.pt.2005.09.005.
28. Davison HC, Otter A, Trees AJ. Estimation of vertical and horizontal transmission parameters of Neospora caninum infections in dairy cattle. International Journal for Parasitology 1999;29(10):1683-1689. DOI: 10.1016/s0020-7519(99)00129-0.
29. Silva RC, Machado GP. Canine neosporosis: perspectives on pathogenesis and management. Veterinary Medicine-Research and Reports 2016;7:59-70. (Review) (In English). DOI: 10.2147/vmrr.s76969.
30. Klauck V, Machado G, Pazinato R, et al. Relation between Neospora caninum and abortion in dairy cows: Risk factors and pathogenesis of disease. Microbial Pathogenesis 2016;92:46-49. DOI: 10.1016/j.micpath.2015.12.015.
31. Wilson DJ, Orsel K, Waddington J, et al. Neospora caninum is the leading cause of bovine fetal loss in British Columbia, Canada. Veterinary Parasitology 2016;218:46-51. DOI: 10.1016/j.vetpar.2016.01.006.
32. Bahrami S, Hamidinejat H, Fatemi-Tabatabaei SR, Sardarifar S. Effect of natural neosporosis on bull sperm quality. Tropical Animal Health and Production 2018;50(1):85-89. (Article) (In English). DOI: 10.1007/s11250-017-1403-8.
33. Weston JF, Heuer C, Williamson NB. Efficacy of a Neospora caninum killed tachyzoite vaccine in preventing abortion and vertical transmission in dairy cattle. Preventive Veterinary Medicine 2012;103(2-3):136-144. DOI: 10.1016/j.prevetmed.2011.08.010.
34. Oshiro LM, Motta-Castro ARC, Freitas SZ, et al. Neospora caninum and Toxoplasma gondii serodiagnosis in human immunodeficiency virus carriers. Revista Da Sociedade Brasileira De Medicina Tropical 2015;48(5):568-572. DOI: 10.1590/0037-8682-0151-2015.
35. Duarte PO, Oshiro LM, Zimmermann NP, et al. Serological and molecular detection of Neospora caninum and Toxoplasma gondii in human umbilical cord blood and placental tissue samples. Scientific Reports 2020;10(1). DOI: 10.1038/s41598-020-65991-1.
36. Darwich L, Cabezon O, Echeverria I, et al. Presence of Toxoplasma gondii and Neospora caninum DNA in the brain of wild birds. Veterinary Parasitology 2012;183(3-4):377-381. DOI: 10.1016/j.vetpar.2011.07.024.
37. Barimani S, Rassouli M, Chashmi SHE. Molecular detection of Neospora caninum in chicken meat and eggs in Iran. Veterinary Parasitology- Regional Studies and Reports 2023;40. DOI: 10.1016/j.vprsr.2023.100862.
38. Qian YX, Jiang YQ, Hong HR, et al. Pathological characteristics and congenital immunological responses of pigeons-infected with Neospora caninum. Microbial Pathogenesis 2023;182. DOI: 10.1016/j.micpath.2023.106224.
39. Amdouni Y, Abedennebi I, Amairia S, Abdelkader A, Chandoul W, Gharbi M. First molecular detection of Neospora caninum from naturally infected slaughtered camels in Tunisia. Veterinary Medicine and Science 2022;8(5):2241-2247. DOI: 10.1002/vms3.901.
40. Soler JP, More G, Urtizbiria F, et al. Epidemic abortions due to Neospora caninum infection in farmed red deer (Cervus elaphus). Parasitology Research 2022;121(5):1475-1485. DOI: 10.1007/s00436-022-07488-6.
41. Tzipori S, Ward H. Cryptosporidiosis: biology, pathogenesis and disease. Microbes and Infection 2002;4(10):1047-1058. DOI: 10.1016/s1286-4579(02)01629-5.
42. Khalil IA, Troeger C, Rao PC, et al. Morbidity, mortality, and long-term consequences associated with diarrhoea from Cryptosporidium infection in children younger than 5 years: a meta-analyses study. Lancet Global Health 2018;6(7):E758-E768. DOI: 10.1016/s2214-109x(18)30283-3.

43. Liu L, Oza S, Hogan D, et al. Global, regional, and national causes of under-5 mortality in 2000-15: an updated systematic analysis with implications for the Sustainable Development Goals. Lancet 2016;388(10063):3027-3035. DOI: 10.1016/s0140-6736(16)31593-8.
44. The Nobel Prize in Physics 1911.
45. The Nobel Prize in Physics 1906.
46. The Nobel Prize in Chemistry 1922.
47. Proceedings of the American Physical Society.69(11-12):674-674.
48. Johnson EG, Nier AO. ANGULAR ABERRATIONS IN SECTOR SHAPED ELECTROMAGNETIC LENSES FOR FOCUSING BEAMS OF CHARGED PARTICLES. Physical Review 1953;91(1):10-17. DOI: 10.1103/PhysRev.91.10.
49. The Nobel Prize in Physics 1989.
50. Beynon JH. New Mass Spectrometer in Production. Chemical & Engineering News 1962;40:64-71.
51. Yamashita M, Fenn JB. ELECTROSPRAY ION-SOURCE - ANOTHER VARIATION ON THE FREE-JET THEME. Journal of Physical Chemistry 1984;88(20):4451-4459. DOI: 10.1021/j150664a002.
52. Karas M, Bachmann D, Bahr U, Hillenkamp F. MATRIX-ASSISTED ULTRAVIOLET-LASER DESORPTION OF NONVOLATILE COMPOUNDS. International Journal of Mass Spectrometry and Ion Processes 1987;78:53-68. DOI: 10.1016/0168-1176(87)87041-6.
53. Karas M, Hillenkamp F. LASER DESORPTION IONIZATION OF PROTEINS WITH MOLECULAR MASSES EXCEEDING 10000 DALTONS. Analytical Chemistry 1988;60(20):2299-2301. DOI: 10.1021/ac00171a028.
54. Tanaka K, Waki H, Ido Y, et al. Rapid Communications in Mass Spectrometry 1988;2(8):151-153.
55. The Nobel Prize in Chemistry 2002.
56. Hu QZ, Noll RJ, Li HY, Makarov A, Hardman M, Cooks RG. The Orbitrap: a new mass spectrometer. Journal of Mass Spectrometry 2005;40(4):430-443. DOI: 10.1002/jms.856.
57. Spengler B, Hubert M, Kaufmann R. MALDI ion imaging and biological ion imaging with a new scanning UV-laser microprobe. In Proceedings of the 42nd ASMS Conference on Mass Spectrometry and Allied Topics 1994:1041.
58. Fenn JB, Mann M, Meng CK, Wong SF, Whitehouse CM. ELECTROSPRAY IONIZATION-PRINCIPLES AND PRACTICE. Mass Spectrometry Reviews 1990;9(1):37-70. DOI: 10.1002/mas.1280090103.
59. Chughtai K, Heeren RMA. Mass Spectrometric Imaging for Biomedical Tissue Analysis. Chemical Reviews 2010;110(5):3237-3277. DOI: 10.1021/cr100012c.
60. Rzagalinski I, Volmer DA. Quantification of low molecular weight compounds by MALDI imaging mass spectrometry - A tutorial review. Biochimica Et Biophysica Acta-Proteins and Proteomics 2017;1865(7):726-739. DOI: 10.1016/j.bbapap.2016.12.011.
61. McIntosh MT, Vaid A, Hosgood HD, et al. Traffic to the malaria parasite food vacuole - A novel pathway involving a phosphatidylinositol 3-phosphate-binding protein. Journal of Biological Chemistry 2007;282(15):11499-11508. (Article) (In English). DOI: 10.1074/jbc.M610974200.
62. Park YK, Diez-Silva M, Popescu G, et al. Refractive index maps and membrane dynamics of human red blood cells parasitized by Plasmodium falciparum. Proceedings of the National Academy of Sciences of the United States of America 2008;105(37):13730-13735. (Article) (In English). DOI: 10.1073/pnas.0806100105.
63. Cho S, Kim S, Kim Y, Park Y. Optical imaging techniques for the study of malaria. Trends in Biotechnology 2012;30(2):71-79. (Review) (In English). DOI: 10.1016/j.tibtech.2011.08.004.
64. van Hove ERA, Smith DF, Heeren RMA. A concise review of mass spectrometry imaging. Journal of Chromatography A 2010;1217(25):3946-3954. DOI: 10.1016/j.chroma.2010.01.033.

65. Takats Z, Wiseman JM, Gologan B, Cooks RG. Mass spectrometry sampling under ambient conditions with desorption electrospray ionization. Science 2004;306(5695):471-473. DOI: 10.1126/science.1104404.
66. Maciel LIL, Bernardo RA, Martins RO, et al. Desorption electrospray ionization and matrix-assisted laser desorption/ionization as imaging approaches for biological samples analysis. Analytical and Bioanalytical Chemistry 2023;415(18):4125-4145. DOI: 10.1007/s00216-023-04783-8.
67. Kompauer M, Heiles S, Spengler B. Atmospheric pressure MALDI mass spectrometry imaging of tissues and cells at 1.4-mu m lateral resolution. Nature Methods 2017;14(1):90-96. DOI: 10.1038/nmeth.4071.
68. Thermo Scientific Q Exactive HF Orbitrap LC-MS/MS System. Waltham: Thermo Fisher Scientific; 2016.
69. Kaur G, Dufour JM. Cell lines Valuable tools or useless artifacts. Spermatogenesis 2012;2:1–5. (In eng). DOI: 10.4161/spmg.19885.
70. Taubert A, Wimmers K, Ponsuksili S, Jimenez CA, Zahner H, Hermosilla C. Microarray-based transcriptional profiling of Eimeria bovis-infected bovine endothelial host cells. Veterinary Research 2010;41(5):18. (Article) (In English). DOI: 10.1051/vetres/2010041.
71. Taubert A, Krull M, Zahner H, Hermosilla C. Toxoplasma gondii and Neospora caninum infections of bovine endothelial cells induce endothelial adhesion molecule gene transcription and subsequent PMN adhesion. Veterinary Immunology and Immunopathology 2006;112(3-4):272-283. (Article) (In English). DOI: 10.1016/j.vetinn.2006.03.017.
72. Hermosilla C, Ruiz A, Taubert A. Eimeria bovis: An update on parasite-host cell interactions. International Journal of Medical Microbiology 2012;302(4-5):210-215. (Review) (In English). DOI: 10.1016/j.ijmm.2012.07.002.
73. Hermosilla C, Barbisch B, Heise A, Kowalik S, Zahner H. Development of Eimeria bovis in vitro: suitability of several bovine, human and porcine endothelial cell lines, bovine fetal gastrointestinal, Madin-Darby bovine kidney (MDBK) and African green monkey kidney (VERO) cells. Parasitology Research 2002;88(4):301-307. DOI: 10.1007/s00436-001-0531-1.
74. Tyanova S, Temu T, Sinitcyn P, et al. The Perseus computational platform for comprehensive analysis of (prote)omics data. Nature Methods 2016;13(9):731-740. DOI: 10.1038/nmeth.3901.
75. The LIPID MAPS® Lipidomics Gateway. (https://www.lipidmaps.org/).
76. Liu S, Sjovall J, Griffiths WJ. Analysis of oxosteroids by nano-electrospray mass spectrometry of their oximes. Rapid Communications in Mass Spectrometry 2000;14(6):390-400. DOI: 10.1002/(sici)1097-0231(20000331)14:6<390::aid-rcm882>3.0.co;2-7.
77. Jiang XT, Ory DS, Han XL. Characterization of oxysterols by electrospray ionization tandem mass spectrometry after one-step derivatization with dimethylglycine. Rapid Communications in Mass Spectrometry 2007;21(2):141-152. DOI: 10.1002/rcm.2820.
78. Honda A, Yamashita K, Hara T, et al. Highly sensitive quantification of key regulatory oxysterols in biological samples by LC-ESI-MS/MS. Journal of Lipid Research 2009;50(2):350-357. DOI: 10.1194/jlr.D800040-JLR200.
79. Sidhu R, Jiang H, Farhat NY, et al. A validated LC-MS/MS assay for quantification of 24(S)-hydroxycholesterol in plasma and cerebrospinal fluid. Journal of Lipid Research 2015;56(6):1222-1233. DOI: 10.1194/jlr.D058487.
80. Taubert A, Silva LMR, Velasquez ZD, Larrazabal C, Lutjohann D, Hermosilla C. Modulation of cholesterol-related sterols during Eimeria bovis macromeront formation and impact of selected oxysterols on parasite development. Molecular and Biochemical Parasitology 2018;223:1-12. (Article) (In English). DOI: 10.1016/j.molbiopara.2018.06.002.
81. Koelmel JP, Kroeger NM, Ulmer CZ, et al. LipidMatch: an automated workflow for rule-based lipid identification using untargeted high-resolution tandem mass spectrometry data. Bmc Bioinformatics 2017;18. DOI: 10.1186/s12859-017-1744-3.

82. Kessner D, Chambers M, Burke R, Agusand D, Mallick P. ProteoWizard: open source software for rapid proteomics tools development. Bioinformatics 2008;24(21):2534-2536. (Article) (In English). DOI: 10.1093/bioinformatics/btn323.
83. Pluskal T, Castillo S, Villar-Briones A, Oresic M. MZmine 2: Modular framework for processing, visualizing, and analyzing mass spectrometry-based molecular profile data. Bmc Bioinformatics 2010;11:11. (Article) (In English). DOI: 10.1186/1471-2105-11-395.
84. Besteiro S, Bertrand-Michel J, Lebrun M, Vial H, Dubremetz JF. Lipidomic analysis of Toxoplasma gondii tachyzoites rhoptries: further insights into the role of cholesterol. Biochemical Journal 2008;415:87-96. DOI: 10.1042/bj20080795.
85. Maffucci T, Falasca M. Analysis, Regulation, and Roles of Endosomal Phosphoinositides. Endosome Signaling, Pt B 2014;535:75-91. DOI: 10.1016/b978-0-12-397925-4.00005-5.
86. Muller MA, Kompauer M, Strupat K, Heiles S, Spengler B. Implementation of a High-Repetition-Rate Laser in an AP-SMALDI MSI System for Enhanced Measurement Performance. Journal of the American Society for Mass Spectrometry 2021;32(2):465-472. (Article) (In English). DOI: 10.1021/jasms.0c00368.
87. Mitschler RR, Welti R, Upton SJ. A COMPARATIVE-STUDY OF LIPID COMPOSITIONS OF CRYPTOSPORIDIUM-PARVUM (APICOMPLEXA) AND MADIN-DARBY BOVINE KIDNEY-CELLS. Journal of Eukaryotic Microbiology 1994;41(1):8-12. DOI: 10.1111/j.1550-7408.1994.tb05927.x.
88. Welti R, Mui E, Sparks A, et al. Lipidomic analysis of Toxoplasma gondii reveals unusual polar lipids. Biochemistry 2007;46(48):13882-13890. DOI: 10.1021/bi7011993.
89. Botte CY, Yamaryo-Botte Y, Rupasinghe TWT, et al. Atypical lipid composition in the purified relict plastid (apicoplast) of malaria parasites. Proceedings of the National Academy of Sciences of the United States of America 2013;110(18):7506-7511. DOI: 10.1073/pnas.1301251110.
90. Gupta N, Zahn MM, Coppens I, Joiner KA, Voelker DR. Selective disruption of phosphatidylcholine metabolism of the intracellular parasite Toxoplasma gondii arrests its growth. Journal of Biological Chemistry 2005;280(16):16345-16353. DOI: 10.1074/jbc.M501523200.
91. Caldarelli SA, Duckert JF, Wein S, et al. Synthesis and Evaluation of Bis-Thiazolium Salts as Potential Antimalarial Drugs. Chemmedchem 2010;5(7):1102-1109. DOI: 10.1002/cmdc.201000097.
92. Itoe MA, Sampaio JL, Cabal GG, et al. Host Cell Phosphatidylcholine Is a Key Mediator of Malaria Parasite Survival during Liver Stage Infection. Cell Host & Microbe 2014;16(6):778-786. DOI: 10.1016/j.chom.2014.11.006.
93. Richmond GS, Smith TK. The role and characterization of phospholipase A(1) in mediating lysophosphatidylcholine synthesis in Trypanosoma brucei. Biochemical Journal 2007;405:319-329. DOI: 10.1042/bj20070193.
94. Sheokand PK, Narwal M, Thakur V, Mohmmed A. GlmS mediated knock-down of a phospholipase expedite alternate pathway to generate phosphocholine required for phosphatidylcholine synthesis in Plasmodium falciparum. Biochemical Journal 2021;478(18):3429-3444. DOI: 10.1042/bcj20200549.
95. Kadesch P, Hollubarsch T, Gerbig S, et al. Intracellular Parasites Toxoplasma gondii and Besnoitia besnoiti, Unveiled in Single Host Cells Using AP-SMALDI MS Imaging. Journal of the American Society for Mass Spectrometry 2020;31(9):1815-1824. (Article) (In English). DOI: 10.1021/jasms.0c00043.
96. Wang J, Pursell ME, Devor A, Awoyemi O, Valentine SJ, Li P. Portable mass spectrometry system: instrumentation, applications, and path to 'omics analysis. Proteomics 2022;22(23-24). DOI: 10.1002/pmic.202200112.
97. Hemida M, Ghiasvand A, Macka M, Gupta V, Haddad PR, Paull B. Recent advances in miniaturization of portable liquid chromatography with emphasis on detection. Journal of Separation Science 2023;46(15). DOI: 10.1002/jssc.202300283.

98. Zhai YB, Fu XY, Xu W. Miniature mass spectrometers and their potential for clinical point-of-care analysis. Mass Spectrometry Reviews 2023. DOI: 10.1002/mas.21867.

CHAPTER 2 – Publication 1

Atmospheric-pressure scanning microprobe matrix-assisted laser desorption/ionization mass spectrometry imaging of *Neospora caninum*-infected cell monolayers

Anschütz, N.H., Gerbig, S., Peter Ventura, A., Silva, L.M.R., Larrazabal, C., Hermosilla, C., Taubert, A., Spengler, B., Analytical Science Advances 2022, 3, 244–254; https://doi.org/10.1002/ansa.202200016

1 Analytical Science Advances | Research Article doi.org/10.1002/ansa.202200016 | Chemistry Europe European Chemical Societies Publishing

Received: 12 May 2022

Revised: 4 August 2022

Accepted: 6 August 2022

Atmospheric-pressure scanning microprobe matrix-assisted laser desorption/ionization mass spectrometry imaging of *Neospora caninum*-infected cell monolayers

Nils H. Anschütz[1] | Stefanie Gerbig[1] | Alejandra M. Peter Ventura[1] | Liliana M. R. Silva[2] | Camilo Larrazabal[2] | Carlos Hermosilla[2] | Anja Taubert[2] | Bernhard Spengler[1]

[1]Institute of Inorganic and Analytical Chemistry, Justus Liebig University Giessen, Giessen, Germany

[2]Institute of Parasitology, Justus Liebig University Giessen, Giessen, Germany

Correspondence
Bernhard Spengler, Institute of Inorganic and Analytical Chemistry, Justus Liebig University Giessen, Giessen, Germany.
Email: bernhard.spengler@anorg.chemie.uni-giessen.de

Funding information
German Research Foundation [Deutsche Forschungsgemeinschaft (DFG), Grant/Award Numbers: Sp314/13-1, Sp314/23-1, INST 162/500-1 FUGG; Federal State of Hesse LOEWE Center DRUID (Novel Drug Targets against Poverty-Related and Neglected Tropical Diseases)

Abstract

Neospora caninum is an obligate intracellular protozoan parasite of the phylum Alveolata (subphylum Apicomplexa) which has not been studied extensively in a biochemical context. *N. caninum* is a primary cause of reproductive disorders causing mummification and abortion not only in cattle but also in other small ruminant species resulting in a substantial economic impact on the livestock industry. In canids, which are the final hosts of *N. caninum*, clinical disease includes neuromuscular symptoms, ataxia, and ascending paralysis. Fatal outcomes of neosporosis have also been reported depending on the host species, age and immune status, however, its zoonotic potential is still uncertain. Therefore, *N. caninum* should be thoroughly investigated. Matrix-assisted laser desorption/ionisation (MALDI) mass spectrometry (MS) and MS imaging (MSI) were used, combined with high-performance liquid chromatography (HPLC) to investigate these intracellular parasites. The aim of this study was to identify molecular biomarkers for *N. caninum* tachyzoite-infected host cells and to further clarify their functions. By atmospheric-pressure scanning microprobe MALDI MS(I), sections of *N. caninum*-infected and non-infected host cell pellets were examined in order to determine potential markers. In vivo, *N. caninum* infects different types of nucleated cells, such as endothelial cells which represent a highly immunoreactive cell type. Therefore, primary bovine umbilical vein endothelial cells were here used as a suitable infection system. For comparison, the permanent MARC-145 cell line was used as an additional, simplified in vitro cell culture model. HPLC-tandem MS (HPLC-MS/MS) experiments

Abbreviations: AP SMALDI, atmospheric-pressure scanning microprobe matrix-assisted laser desorption/ionization; *B. besnoiti*, *Besnoitia besnoiti*; BUVEC, bovine umbilical vein endothelial cells; DHB, 2,5 dihydroxybenzoic acid; DMEM, Dulbecco's Modified Eagle's Medium; e. g., *exempli gratia*; EGGM, endothelial cell growth medium; ESI, electrospray ionization; FCS, foetal calf serum; FDR, false-discovery-rate; h p. i., hours post infection; HPLC, high performance liquid chromatography; i. e., *id est*; IgG, Immunoglobulin G; LC, liquid chromatography; *m/z*, mass-to-charge ratio; MALDI, matrix-assisted laser desorption/ionisation; MARC-145, african green monkey kidney epithelial cells; MS, mass spectrometry; MS/MS, tandem mass spectrometry; MSI, MS imaging; MTBE, 2-methoxy-2-methylpropane; *N. caninum*, *Neospora caninum*; PA, phosphatidic acids; PBS, phosphate-buffered saline; PC, phosphatidylcholines; PCR, polymerase chain reaction; PE, phosphatidylethanolamine; PI, phosphatidylinositol; ppm, parts per million; PS, phosphatidylserine; rpm, revolutions per minute; RT, room temperature; spp., *species pluralis*; *T. gondii*, *Toxoplasma gondii*; TFA, trifluoroacetic acid; TIC, total ion count.

2 Analytical Science Advances | Research Article doi.org/10.1002/ansa.202200016 | Chemistry Europe European Chemical Societies Publishing

combined with database search were employed for structural verification of markers. The statistically relevant biomarkers found by MS and identified by HPLC-MS/MS measurements were partly also found in infected monolayers. Marker signals were imaged in cell layers of *N. caninum*-infected and non-infected host cells at 5 µm lateral resolution.

1 | INTRODUCTION

Neospora caninum is an obligate intracellular parasite (phylum Alveaolata and subphylum Apicomplexa) involving canids as definitive hosts and a wide range of intermediate hosts including cattle, sheep, goats, wild cervids and new world camelids.[1] Like the closely related parasite *Toxoplasma gondii*, *N. caninum* is considered as tissue-cyst forming coccidia.[2] As such, both parasites show strong similarities in their life cycles, morphology, genome and transcriptome.[3–7] These common features led to *N. caninum* being misidentified as *T. gondii* before 1984.[8] Canid species [i.e. dogs (*Canis familiaris*), wolves (*Canis lupus*) and coyotes (*Canis latrans*)] can as well act as intermediate hosts for *N. caninum* infections. In ruminant intermediate host species, neosporosis is considered a major cause of reproductive disorders thereby causing significant economic losses mainly in the cattle, goat, sheep and alpaca/llama industry. Neosporosis is considered a globally spreading disease with a focus on the United States, South America, Central America, Australia and Europe.[9,10] In most cases, diagnosis of *N. caninum* infection is carried out serologically using blood tests for either parasite-specific antibodies or antigens.[11–13] Detection can also be performed by immunohistochemistry or by molecular diagnostic tools, such as polymerase chain reaction, both options being more complex and expensive.[14] As stated above, neosporosis is an infectious disease, especially detrimental for canids and cattle. In canids, *N. caninum* is responsible for multisystemic lesions resulting in severe dermal and neuromuscular symptoms in offspring of infected bitches.[1] Within the life cycle, three different stages are known: fast replicating tachyzoites, slowly proliferating bradyzoites within tissue cysts and sporozoites present in sporulated oocysts. Only two of these stages - tachyzoites and tissue cysts - occur in intermediate hosts, and they show obligate intracellular development.[9] In general, transmission can take place in several ways, for example, canids can acquire infection by ingesting infected host tissue containing cysts with thousands of bradyzoites, congenitally by transfer of tachyzoite stages or via ingestion of sporulated oocysts from contaminated environments. Conversely, in cattle transplacental transmission via tachyzoites seems to be the most common route of infection when compared to oocyst ingestion,[15] thus vertical transmission is the major route involved in the spread of bovine neosporosis.[16] Initial infection of a cattle herd is driven by purchasing infected cattle or by oocyst-excreting farm dogs.[17] The symptoms of this disease strongly depend on the host type. In bovines, *N. caninum* can infect the reproductive system of male and female hosts, which implies a major threat to the cattle industry. In bulls, the sperm concentration, viability and motility are significantly lower if infected with *N. caninum*.[18] In pregnant cows, neosporosis often leads to foetus mummification and/or abortion, and therefore is considered one of the most common infectious causes of abortion worldwide.[19–21] The spread of bovine neosporosis and its consequences lead to significant economic impact with financial losses in the multi-billion dollar range.[10] Vaccines against *N. caninum* are rare and inefficient in preventing abortion in cattle.[22] Since clinically manifested neosporosis has also been reported in two rhesus monkeys,[23] concerns are rising that *N. caninum* might eventually become a threat to humans.[24] Moreover, there are reports on the presence of IgG anti-*N. caninum* antibodies in pregnant women[25] and in human immunodeficiency virus carriers.[26] Therefore, this parasite and the disease should be thoroughly investigated.

A comprehensive investigation of *N. caninum*-infected host cells in a biochemical context has not yet been carried out. Therefore, no lipidomic or metabolomic data of *N. caninum* at a molecular level is available. Available studies are mostly focusing on proteome- or genome-based comparisons to *T. gondii*.[7,27] In this context, mass spectrometry (MS) was used in a supportive or independent manner to identify molecules or to validate results obtained with other methods. Since the beginning of the millennium, MS instrumentation has improved considerably, allowing a detailed mass analysis that can be used to calculate elemental formulae of compounds on the basis of highly accurate molecular mass values.[28–30] MS imaging (MSI) provides the visualization of analyte distribution in tissues and cells, and parasites can be visualized by MSI if specific markers are determined. Tachyzoites are approximately 6 × 2 µm in size.[9] Due to the improvement in MSI instrumentation, lateral resolutions of 1–2 µm became accessible, which implies that assembled or even individual cells can be examined by this method.[31]

In this work, high-performance liquid chromatography (HPLC) and matrix-assisted laser desorption/ionisation (MALDI), coupled with MS and MSI[32] were used to investigate the cellular metabolism of parasites in infected host cells. Model systems for cattle were used with tachyzoites as the corresponding stages. Characteristic m/z signals for the infection of host cells with *N. caninum* were identified using the combination of MSI, HPLC-MS and statistical data analysis.

2 | EXPERIMENTAL SECTION

2.1 | Parasites

N. caninum (strain Nc1) tachyzoites were maintained by serial passages *in Mycoplasma* spp.-free primary bovine umbilical vein endothelial cells

Research Article
doi.org/10.1002/ansa.202200016
Chemistry Europe
European Chemical Societies Publishing

(BUVEC) or permanent African green monkey kidney epithelial cells (MARC-145). Vital *N. caninum* tachyzoites were collected from supernatants of infected host cell monolayers, filtered through 5 µm sterile syringe filters (Sartorius, Goettingen, Germany) to remove cell debris, pelleted (400 × *g*, 12 min), resuspended in cell culture medium, counted (Neubauer haemocyte chamber using the inverted microscope IX81, Olympus, Shinjuku City, Tokyo, Japan) and used for infection of BUVEC. For pure parasite pellets, freshly released tachyzoites were collected from cell culture supernatants, filtered with a 5 µm syringe filter (Sartorius), pelleted (400 × *g*, 12 min), and washed twice with sterile phosphate-buffered saline (PBS) 1X (Sigma-Aldrich, Steinheim, Germany). After fixation with 2.5% glutaraldehyde (Merck, Darmstadt, Germany) for 10 min at room temperature (RT), fixed pellets were immediately frozen in liquid nitrogen and stored at −80°C until further use.[33]

2.2 | Cell culture

MARC-145 cell layers were maintained in Dulbecco's Modified Eagle Medium (Sigma-Aldrich) cell culture medium supplemented with 1% penicillin (500 U/ml; Sigma-Aldrich), streptomycin (500 mg/ml; Sigma-Aldrich) and 5% foetal calf serum (FCS; Gibco, part of Thermo Fisher Scientific, Dreieich, Germany) and incubated at 37°C and 5% CO_2 until confluency. Primary BUVEC were maintained in modified ECGM [endothelial cell growth medium (PromoCell, Heidelberg, Germany); 30% (v/v) ECMG and 70% (v/v) M199, supplemented with 1% penicillin and streptomycin and 5% FCS] at 37°C in 5% CO_2 atmosphere until confluency.[34]

2.3 | Preparation of cell pellets and cell monolayers

For cell pellet preparation, confluent (n = 3) cell layers of BUVEC or MARC cultured in 75 cm^2 flasks were infected with freshly released *N. caninum* tachyzoites at a multiplicity of infection (MOI) = 5:1. At 24 h post-infection, infected and non-infected host cell monolayers were washed with sterile PBS 1X (Sigma-Aldrich) prior to fixation with 2.5% glutaraldehyde (10 min, RT). Monolayers were detached from flasks using cell scrapers (Greiner Bio-One, Kremsmünster, Austria) and flasks were washed with sterile PBS 1X (Sigma-Aldrich) for cell collection. After centrifugation (400 × *g*, 10 min), cell pellets were transferred to microcentrifuge tubes (1.5 ml, Eppendorf, Hamburg, Germany) and washed twice with sterile PBS 1X to remove any traces of fixative (1150 × *g*, 5 min). Fixed pellets were immediately frozen in liquid nitrogen and stored at −80°C until further use.[33] Also, BUVEC were seeded on glass coverslips (15 mm; Thermo Fisher Scientific) and allowed to grow until confluency. Then, cell layers were infected as described above. Following fixation (2.5% glutaraldehyde; 10 min, RT), cell layers were washed carefully twice with PBS 1X (Sigma-Aldrich) and were allowed to dry before being stored at −80°C until further use.

2.4 | Preparation of cryo-sections

To produce comparable samples for MALDI-MS, three technical replicates of sections were prepared from each cell pellet of each cell type. In total, three different biological replicates were used for primary bovine endothelial cells. In all cases, sections with a thickness of 30 µm were cut by a microcryotome (Microm HM 525, Microm International GmbH, part of Thermo Fisher Scientific, Walldorf, Germany) at −25°C with a cutting angle of 11° using a Microm Sec35p® blade.

2.5 | MALDI-MS sample preparation

Note that, 2,5-Dihydroxybenzoic acid (DHB, Merck, Darmstadt, Germany) was used as a matrix for MALDI measurements in positive-ion mode. The matrix solution was prepared by dissolving DHB (30 mg/ml) in 1:1 acetone–water, adding 0.1% of trifluoroacetic acid (Sigma Aldrich). The cell pellet-derived sections and the sections of the host tissue were covered by spraying 100 µl of the matrix solution at a constant flow rate of 10 µl/min using a dedicated pneumatic sprayer (SMALDIPrep; TransMIT GmbH, Giessen, Germany). For cell layer samples, the volume of the matrix solution was increased by 10 µl to reduce the reflectivity of the sample surface during autofocusing operation.

2.6 | Metabolite extraction

Metabolite extraction was performed following literature.[35] The metabolite yield is strongly dependent on the completeness of disruption of assessed cells during extraction. The sample and 25 µl of 0.1% ammonium acetate (Honeywell, Riedel-de Haen, LC-MS Chromasolv) were transferred to a potter homogenizer for cell lysis. To this lysate, 100 µl methanol (Sigma Aldrich) and 400 µl 2-methoxy-2-methylpropane (MTBE, Sigma Aldrich) were added. The mixture was incubated at 4°C and 900 rpm for 1 h. Afterwards, 200 µl of ice-cold MS-grade water was added in order to initiate phase separation. The sample was centrifuged for 10 min at 1000 g. The upper organic phase was removed, and the lower aqueous phase was reextracted. For this purpose, 200 µl MTBE/methanol/water (4:1.2:1; v/v/v) were added. After incubation at 4°C and 900 rpm for 1 h and centrifugation for 10 min at 1000 g, the organic phase was again removed. The two organic phases were combined and dried under nitrogen gas flow. The sample was resuspended in 500 µl acetonitrile/water (60:40; v/v).

2.7 | UHPLC-MS/MS analysis

Liquid chromatographic separation was performed on a Dionex UltiMate 3000 RSLC-System (Thermo Fisher Scientific), using a 2.6 µm C18 (100 × 2.1 mm) UHPLC column (Kinetex Phenomenex), coupled online to a Q Exactive HF-X (Thermo Fisher Scientific, Dreieich, Germany) orbital trapping mass spectrometer. The binary gradient was modified

from the literature.[36] The solvent systems used were as follows: solvent A (60:40 acetonitrile: water, 0.1% formic acid, 10 mM ammonium formate [Sigma Aldrich]) and solvent B (90:8:2 isopropanol: acetonitrile: water, 0.1% formic acid, 10 mM ammonium formate [Sigma Aldrich, Germany]). The elution was performed with a gradient over 32 min. Starting condition was 32% of solvent B for 1.5 min. Until 4 min, solvent B was increased to 45%. From 4 to 5 min, solvent B was increased to 52%, from 5 to 8 min to 58%, from 8 to 11 min to 66%, from 11 to 14 min to 70%, from 14 to 18 min to 75% and from 18 to 21 min to 97%. From 21 to 25 min, the gradient was held constant. By the 26th minute, solvent B was reduced to 32% again. Subsequently, the gradient was kept unchanged for 7 min. The flow rate was kept constant at 260 µl/min throughout the whole measurement.

2.8 | MALDI-mass spectrometry (I)

MALDI-MS and MALDI-MSI experiments were carried out using an AP-SMALDI5 AF (TransMIT GmbH) imaging system (pixel size: ≥ 5 µm) coupled to a Q Exactive HF (Thermo Fisher Scientific) orbital trapping mass spectrometer (mass resolution R = 240000 @ *m/z* 200). In order to achieve the best possible signal intensities and to ensure optimal comparability of the different measurements, the non-flat monolayers were measured with the help of the pixelwise autofocus (3D-surface imaging) system. Due to the small size of the parasites, the highest possible lateral resolution of 5 µm was chosen. In the case of the cell pellet sections, a pattern of 50 × 50 pixels was measured with a lateral resolution (step size) of 10 µm and a slightly defocused laser beam. Due to the larger (defocused) laser spot area at 10 µm, higher signal intensities were obtained. This approach with its constant number of 2500 spectra for each sample led to consistently reliable data. The major advantage here lies in the higher signal intensities due to the larger sampled area compared to the monolayers.

2.9 | Data processing

To find potential biomarkers within the cell pellets, the software Mirion (TransMIT GmbH) in combination with the Perseus software platform (MPI of Biochemistry, Martinsried, Germany) was used.[37] The employed procedure was based on published literature.[33] With the help of Mirion, all MALDI measurements were stitched together. A list of all *m/z* values with an image coverage above or equal to 0.5% was exported. The corresponding deviations (±5 ppm) were calculated, and this new list was applied to all the single cell-section measurements. The results were then imported into Perseus. With Perseus, the data sets were categorized into infected and non-infected host cells. In the second and third steps, a normalization was carried out, first by dividing the intensity values by their sum, then by using the Z-score (median). In the fourth step, multiple-sample tests were carried out (ANOVA; permutation-based false-discovery-rate, FDR = 0.05, number of randomizations = 250). In the fifth step, the corresponding values from step four were filtered. In the sixth step, post hoc tests were performed with the remaining values (visualized using hierarchical clusters). Afterwards, data were prepared for HPLC-MS/MS. Lipid Maps was used to generate annotations from the *m/z* values found by Perseus. A mass list was then generated with these exact masses and their deviations (±5 ppm). For identification of the detected molecular markers, the software LipidMatch (SECIM, Gainesville, USA) in collaboration with ProteoWizard (MSConvertGUI) and MZmine were used.[38–40]

3 | RESULTS AND DISCUSSION

3.1 | Detection of infection markers in cell pellets and subsequent assessment of statistical relevance

BUVEC was used as a model system in order to enable the best possible representation of an in vivo scenario on fast replicating tachyzoites in vessel endothelium during the acute phase of bovine neosporosis. For comparative reasons, MARC-145 cells were also used. This permanent cell line was mainly used to promote massive intracellular *N. caninum* replication, since large numbers of viable tachyzoites were obtained, which were later needed to infect primary BUVEC. Permanent cell lines are easy to handle and offer a pure cell population, thus enabling a consistent sample and reproducible results. Due to their fast and endless proliferation, a practically unlimited supply of material is provided. Nonetheless, since permanent cell lines are either genetically manipulated or of tumorous origin, they may not reflect physiological reactions like in primary cells and therefore may provide deviant results.[41] Primary, as well as permanent cells, include a cycle of cell division which might affect cellular metabolism in vitro. In this paper, the two different cell lines were compared based on their different cell-derived reactions after parasitic infection.[42–45] However, the focus of this work was on the more realistic primary host cell, namely highly immunoreactive endothelial cells.[34,42] In order to obtain a homogeneous sample pattern for the MALDI-MS experiments, cell pellets were cut into consecutive thin sections. This methodology facilitates statistical evaluability. Figure 1 illustrates the chosen experimental approach. Different BUVEC ($n = 3$) cell sections were measured (Figure 1A–C) and the signal at *m/z* 728.5164 as a statistically relevant marker for the infection was visualized using the red colour channel. Figure 1A shows two measurements with 50 × 50 pixels. All measurements of the cell pellets were conducted with a step size of 10 µm. The larger step size, combined with a corresponding defocusing of the laser beam, led to larger spot size, resulting in more material being removed and ionized by the laser beam.

The left part of Figure 1A illustrates an infected section, and the right part the corresponding control sample. The two samples were placed next to each other on one sample holder, sprayed with matrix and measured subsequently thereby applying identical experimental conditions. After that, another two infected and control pairs of the same biological sample were measured in order to obtain triplicate measurements (Figure 1B). Technical replicas were measured to exclude potential errors in sample preparation (e.g. sectioning) or possible heterogeneities within the cell pellets. This procedure was

5 Analytical Science Advances | Research Article doi.org/10.1002/ansa.202200016 | Chemistry Europe European Chemical Societies Publishing

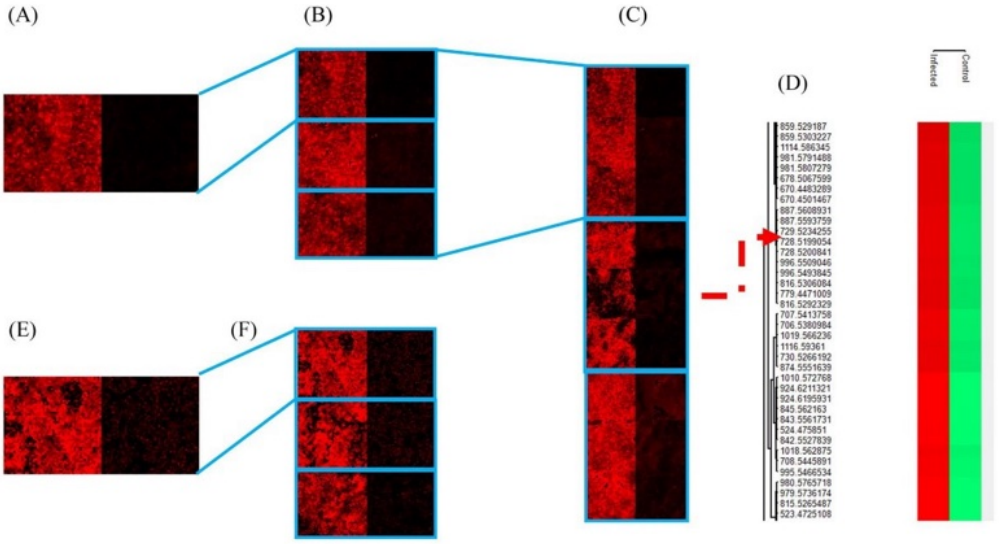

FIGURE 1 Detection of molecular markers in cell pellet sections of N. caninum-infected cells. (A–C) bovine umbilical vein endothelial cells (BUVEC): phosphatidylcholines (PC) (14:0_16:0) as $[M+Na]^+$, *m/z* 728.5164 ± 5 ppm; (D) Segment of a heat map generated with Perseus; (E,F) MARC: PC (30:0) as $[M+H]^+$, *m/z* 678.5034 ± 5 ppm

repeated for two other biological replicates. Figure 1C shows the resulting images of the three biological replicates with three technical replicates. Biological replicates are needed to minimize variations of results due to varying individual metabolic responses of animals to infection. Preparation of samples and their previous storage were all carried out under the same conditions. Figure 1E and F show measurements of MARC-145 cell pellet sections. Figure 1E is the equivalent to Figure 1A in this context. The signal *m/z* 678.5034, visualized in the red colour channel, is a statistically relevant marker for infection. Figure 1F shows the corresponding triplicates. Since MARC-145 is a permanent cell line, biological replicates cannot be measured. To find potential biomarkers within those cell pellet sections, the software Mirion in combination with the Perseus software platform was used.[37] The biomarkers found in these experiments were set as a basis for all subsequent experiments. With Perseus, the data sets were categorized into *N. caninum*-infected and non-infected ones. In the next step, two standardizations were carried out, followed by multiple-sample tests (ANOVA; permutation-based false-discovery-rate, FDR = 0.05, number of randomizations = 250). The corresponding values from the preceding step were filtered and non-fitting values were rejected. In the last step, post hoc tests were performed with the remaining values (visualized using hierarchical clustering, see Figure 1D). For the BUVEC model system, 582 marker signals were found for infection in positive-ion mode (Table S1) and 659 marker signals for infection in negative-ion mode (Table S2). In the control samples, 48 (Table S3) and 411 marker signals (Table S4) were detected, respectively.

3.2 | Annotation of markers

The LIPID MAPS database of computationally-generated "bulk" lipid species, a virtual database composed of major classes of lipid species, was used to annotate previously determined markers.[46] Lipids are basic components for structural and functional categories of cells. In cell membranes, lipids divide the functional areas and are involved in accomplishing various aspects of signal transmission. In the case of MALDI measurements of cell pellets and the following statistical evaluation, all *m/z* signals were taken into account. Subsequently, the focus was exclusively on lipids. Due to the restriction to lipids (database and subsequent extraction for HPLC-MS/MS), not every signal recognized as a marker was annotated. In order to obtain reasonable annotations, expedient ion adducts with the respective polarity were selected as LIPID MAPS search criteria. Only single charged species were selected. In positive-ion mode, ions of types $[M+H]^+$, $[M+H\text{-}H_2O]^+$, $[M+Na]^+$, $[M+NH_4]^+$ and $[M+K]^+$ and in negative-ion mode $[M-H]^-$, $[M+Cl]^-$, $[M+HCOO]^-$, $[M+Oac]^-$ and $[M\text{-}CH_3]^-$ were taken into account. In LIPID MAPS, a mass tolerance of *m/z* ± 0.05 was chosen and afterwards, values with a calculated deviation of more than 5 ppm between obtained and measured values were discarded. If several different annotations for the same *m/z* value were found, annotations which deviated by more than 1 ppm from the annotation with the smallest deviation were discarded. The corresponding results are illustrated in Figure 2. The number of annotations is higher than the number of *m/z* values since more than just one annotation can meet the criteria

6 Analytical Science Advances | Research Article doi.org/10.1002/ansa.202200016 | Chemistry Europe European Chemical Societies Publishing

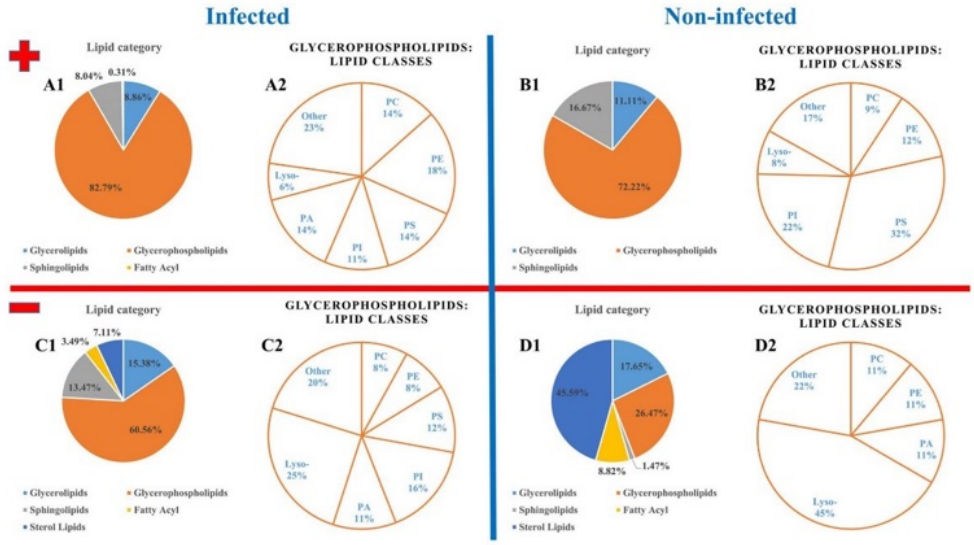

FIGURE 2 Abundances of categories of detected bovine umbilical vein endothelial cells (BUVEC) markers (fractions of signal numbers in [%]). (A,B) positive-ion mode; (C,D) negative-ion mode; (A,C) infected samples; (B,D) control samples; 1: lipid categories, 2: Detected lipid classes in the glycerophospholipids category

described above. In the BUVEC model system, 982 annotations were determined for the positive- (for 116 different *m/z* values, Table S5) and 1654 annotations for the negative-ion mode (for 357 different *m/z* values, Table S6). For control samples, 90 annotations (39 different *m/z* values, Table S8) were determined for the positive- and 68(49 different *m/z* values) annotations for the negative-ion mode (Table S9). Figure 2 shows the fractions of signal numbers (in [%]) of all annotated lipid categories (A1, B1, C1 and D1) as well as the different lipid classes of the particularly prominent lipid category of glycerophospholipids (A2, B2, C2 and D2). While A and B show the results for the positive-ion mode, C and D represent the negative-ion mode. In positive-ion mode, the *N. caninum*-infected samples had a low percentage in the number of phosphatidylserines (PS) and phosphatidylinositols (PI) compared to the control samples. The proportion of phosphatidylethanolamine and especially phosphatidic acids (PA) was found to be increased in infected samples. Sterols were annotated as marker molecules in negative- but not in positive-ion mode. Due to the lack of acidic and basic groups, sterols are difficult to ionize especially in a positive-ion mode without derivatization.[47–50] In positive-ion mode, $[M+H-H_2O]^+$ is the most abundant ion, in the negative-ion mode, it is the deprotonated species $[M-H]^-$. Their percentage was particularly high in the control samples in negative-ion mode. The absolute number of sterol signals in *N. caninum*-infected samples was still more than three times as high (104 vs. 31). It is well-known that sterol levels are increased in host cells infected with other apicomplexan parasite species.[51] In the negative-ion mode, the proportion of lyso-lipids in infected samples was almost halved, with a high PI proportion. However, one has to take into account

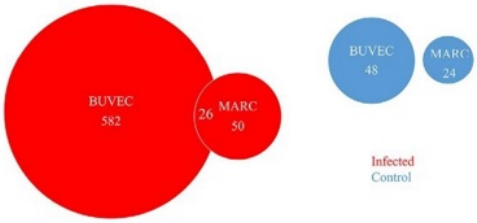

FIGURE 3 Venn diagram of markers found in the positive-ion mode for Neospora caninum-infected and non-infected bovine umbilical vein endothelial cells (BUVEC) and MARC cells. For infected cells, 582 markers were found in BUVEC and 50 markers in MARC-125. 26 of these markers (52% of the MARC-125 markers) were found in both cell models. For the control samples, only 48 (BUVEC) and 24 (MARC) markers were found, with no overlap

that the presented annotations are solely based on accurate mass at this level and that there are often several annotations for a single *m/z* value. For the MALDI MS data, direct identification via on-tissue MS/MS was not possible due to low signal intensities.

In Figure 3, the BUVEC- and the MARC-145-based models are compared in positive-ion mode. As expected, the two models led to highly varying results.[41] The primary bovine host endothelial cells, that is, BUVEC, revealed significantly more markers, thus underlining the in vivo replication site of *N. caninum* tachyzoites and highlighting the importance to indeed analyse primary cell models to be close to the in

7 Analytical Science Advances | Research Article doi.org/10.1002/ansa.202200016 | Chemistry Europe European Chemical Societies Publishing

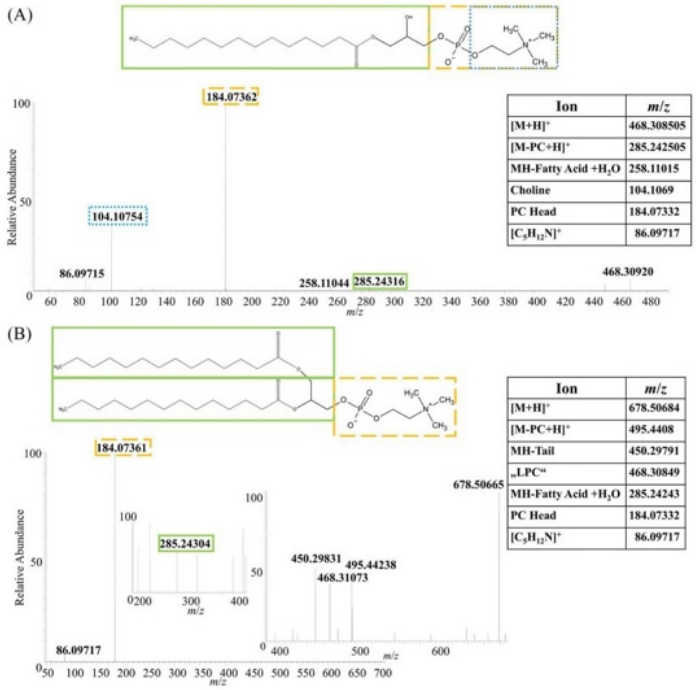

FIGURE 4 Liquid chromatography-electrospray ionization tandem mass spectrometry (LC-ESI-MS/MS) measurements of two selected infection markers. The resulting fragment ion signals were identified by comparison to a database. (A) (LPC 14:0) as $[M+H]^+$; (B) (PC 14:0_14:0) as $[M+H]^+$

vivo situation. Thus, in total 582 markers were found for *N. caninum*-infected BUVEC and only 50 for infected MARC-145. 26 of these markers were found in both cell line systems, suggesting that these markers originated from the parasites. Fewer markers were found in each of the control samples (BUVEC: 48; MARC-145: 24), and there was no overlap between the markers of the two model systems here used.

3.3 | LC-MS/MS-based identification of annotated markers

The annotations obtained from LIPID MAPS were used to create inclusion lists for HPLC-MS/MS measurements. High-resolution full MS and MS/MS spectra were recorded. For identification of the detected molecular markers, the software LipidMatch (SECIM, Gainesville, USA) in combination with ProteoWizard (MSConvertGUI) and Mzmine were used.[38–40] The settings made in LipidMatch can be found in Table S7, and two examples are shown in Figure 4.

In total, 28 annotations were confirmed by MS/MS experiments (Table S10) in negative-ion mode. Phosphatidylinositols, as components of cellular membranes, were the most abundant class of lipids. They play a critical role in membrane dynamics, trafficking, and cellular signalling, which agrees well with our hypothesis that the markers are a cell response to infection.[52] In positive-ion mode, 12 annotations were confirmed by MS/MS analysis (Table S11). The phosphatidylcholines (PC) lipid class was highly abundant, which has already been observed for infections with other Apicomplexa.[53] For corresponding control samples, three annotations were confirmed by MS/MS analysis (Table S12). Remarkably, almost all identified markers, regardless of the ion mode, contained a short-chain fatty acid. In the literature, this finding is also described to be typical for the zoonotic *T. gondii*.[53]

3.4 | MSI of cell layers at a high lateral resolution

In total, 40 biomarkers characteristic for *N. caninum* infection and three biomarkers for control samples were identified in BUVEC layers (Table S10–S12). Visualization of the small tachyzoites (<10 µm)[8] within cells, requires a lateral resolution of at least 5 µm for MSI of monolayers. In each panel of Figure 5, *N. caninum*-infected BUVEC layers are illustrated on the left side, and control samples on the right side. The green

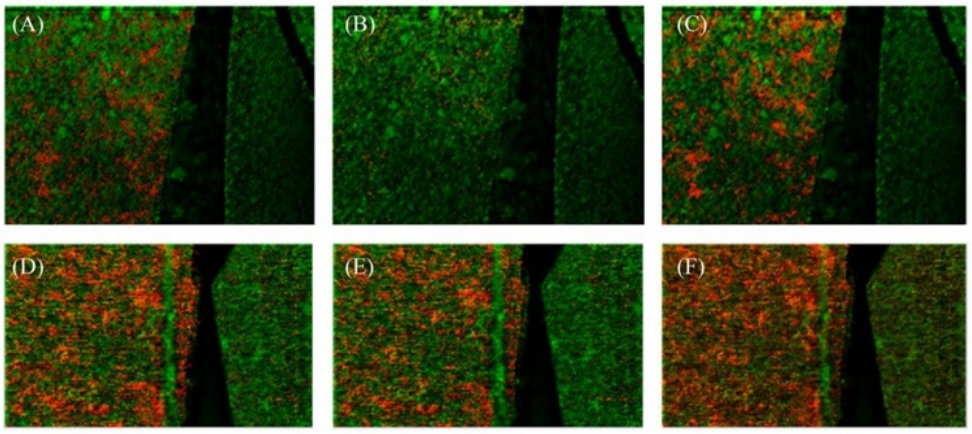

FIGURE 5 Matrix-assisted laser desorption/ionisation mass spectrometry imaging (MALDI MSI) measurements of bovine umbilical vein endothelial cells (BUVEC) cell monolayers, infected with N. caninum and measured with 5 µm laser focus diameter and step size. The green channel represents the total ion count (TIC). The red channel shows the distribution of various infection markers (±5 ppm mass tolerance) identified earlier by liquid chromatography-tandem mass spectrometry (LC-MS/MS) measurements of cell pellets. Each frame A to F contains an infected monolayer on the left and a control monolayer on the right, separated by a blank area. (A–C) Measurements in negative-ion mode: (A) infection marker signal at *m/z* 645.4501 (red), identified as both, PA (14:0_18:1) as $[M-H]^-$ and PA (16:0_16:1) as $[M-H]^-$, (B) infection marker signal at m/z 781.4873 (red), identified as PI (14:0_16:0) as $[M-H]^-$, (C) infection marker signal at m/z 836.5447, identified as PS(18:0_22:5) as $[M-H]^-$; (D–F) Measurements in positive-ion mode: (D) infection marker signal at *m/z* 728.5201, identified as phosphatidylcholines (PC) (14:0_16:0) as $[M+Na]^+$, E: infection marker signal at *m/z* 704.5225, identified as both, PC (14:0_16:1) as $[M+H]^+$and PC (12:0_18:1) as $[M+H]^+$, F: infection marker signal at *m/z* 678.5068, identified as both, PC (14:0_14:0) as $[M+H]^+$ and PC (12:0_16:0) as $[M+H]^+$

channel represents the total ion count (TIC). The red channel shows the distribution of different, LC-MS/MS measurements with a mass tolerance of ±5 ppm identified infection markers. As expected, these signals were found exclusively or significantly more pronounced in *N. caninum*-infected cell layers (left side of each panel). Figure 5A–C shows the measurement in negative-ion mode. In Figure 5A, the distribution of an infection-specific signal at *m/z* 645.4501 is shown in red, assigned to PA (32:1). Since PA are the precursors for the biosynthesis of many other lipids, an increase in this species can be interpreted as the response of host cells to the tachyzoite replication. Figure 5B shows the distribution of the signal *m/z* 781.4873, which was previously assigned to PI (30:0) as $[M-H]^-$ by LC-MS/MS of the cell pellets. As mentioned above, PI plays a critical role in membrane dynamics, trafficking, and cellular signalling, therefore an increase in the abundance of this species would correspond well to an infection-driven reaction.[52] Figure 5C shows in red the distribution of the signal at *m/z* 836.5447, which was previously assigned to PS (18:0–22:5) as $[M-H]^-$. PC are a major component of biological membranes. In line, PS are also well-known components of cell membranes and play a major role in programmed cell apoptosis,[54] which suggests that *N. caninum* intracellular replication might have led to cell death. Figure 5D–F shows MS images of monolayers in positive-ion mode. While in Figure 5D the distribution of an infection-specific signal at *m/z* 728.5201, assigned to PC (30:0) as $[M+Na]^+$, is shown, Figure 5E displays the distribution of the signal *m/z* 704.5225, which was previously assigned to PC (30:1) as $[M+H]^+$. Figure 5F shows the distribution of the signal *m/z* 678.5068, which was previously assigned to PC (28:0) as $[M+H]^+$.

Next, we examined correlations of MS images with structures observed in highly resolved optical microscopic images (Figure 6). In line with previous measurements, an *N. caninum*-infected monolayer was placed on the left, the control sample on the right of the sample holder to ensure identical experimental conditions. Intracellular tachyzoites of *N. caninum* can be recognized in infected cell layers as typical 'banana'-shaped structures in the microscopic image (Figure 6A, encircled in yellow). Figure 6B shows the corresponding MS image of the cell layer in positive-ion mode (green channel: TIC, red and blue channel: two identified infection markers; ±5 ppm mass tolerance). The red channel represents an infection marker at *m/z* 692.5225, identified as PC (29:0) as $[M+H]^+$, the blue channel represents an infection marker at *m/z* 704.5225, identified as PC (30:1) as $[M+H]^+$. The two markers widely overlap, resulting in pink pixels. Both ion signals were also found in controls, but with a much lower signal intensity compared to *N. caninum*-infected cell layers.

4 | Comparison of data with other apicomplexan infections on MS/MS level

The identified markers found for *N. caninum* were compared to markers of *Toxoplasma gondii* and *Besnoitia besnoiti*, as previously published.[33]

9 Analytical Science Advances | Research Article doi.org/10.1002/ansa.202200016 | Chemistry Europe European Chemical Societies Publishing

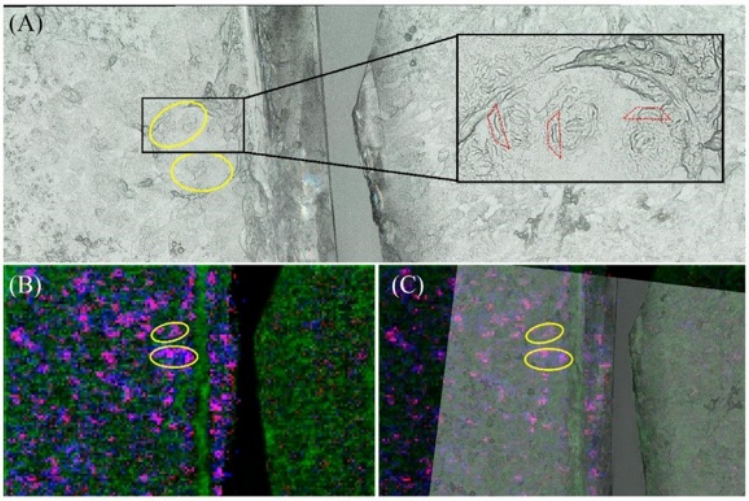

FIGURE 6 Matrix-assisted laser desorption/ionisation mass spectrometry imaging (MALDI MSI) measurements of a bovine umbilical vein endothelial cells (BUVEC) layer, infected with N. caninum and measured with 5 µm laser focus diameter and step size. On each panel, the infected monolayer is on the left and a control monolayer is on the right, separated by a blank area. (A) Microscopic image of the two monolayers. Intracellular tachyzoites can be recognized as banana-shaped structures (outlined in red) exclusively in the infected monolayer, as part of a rosette-like meront. Two particularly noticeable areas with N. caninum meronts are circled in yellow. (B) MS-Image of the monolayers in positive-ion mode. The green channel represents the total ion count (TIC). The red and blue channels show the distribution of two identified infection markers (±5 ppm mass tolerance). The two markers overlap with pink pixels. The red channel represents an infection marker at *m/z* 728.5201, identified as phosphatidylcholines (PC) (29:0) as $[M+H]^+$ and the blue channel represents an infection marker at *m/z* 704.5225, identified as PC (30:1) as $[M+H]^+$. (C) Overlay of panels A and B. Infection marker signals overlap well with the banana-shaped (tachyzoites) and rosette-like (meronts) structures in the yellow circles.

Ten of identified 40 markers for an *N. caninum* infection were also identified as markers for *T. gondii* and *B. besnoiti* infections of endothelial host cells. A comparison is shown in Table S13. About 80% of these commonly identified markers were PI. As already stated, these molecules play critical roles in membrane dynamics, trafficking and cellular signalling, supporting the hypothesis that these markers are a common response of infected host cells to apicomplexan infections.[52]

5 | CONCLUSION

To the best of our knowledge, this is the first study examining *N. caninum*-infected host cells at the molecular level. AP-SMALDI MS and MSI were used to find lipid biomarkers for infection with the obligate intracellular protozoan parasite *N. caninum*, which belongs to the phylum Apicomplexa, by comparing technical and biological triplicates of infected and non-infected sections of cell pellet samples. In this context, permanent (MARC-145) and primary (BUVEC) cell lines were also compared, clearly showing the superiority of the primary cell system. The measurements were carried out in positive- and negative-ion modes and evaluated with statistical software. With this detailed method, 1241 significant markers for infection were found. MS/MS experiments combined with database search were successful in structural verification of 40 markers, while the others could not be unambiguously identified. The obtained data were compared with already published data in the neglected field of apicomplexan parasites (*T. gondii* and *B. besnoiti*). Ten of the 40 identified markers for *N. caninum* infection were also identified as markers for respective infections with *T. gondii* or *B. besnoiti*. Here, 80% of the matching markers were PI. They are assumed to be part of a response of infected host cells to apicomplexan invasion and further replication. For MSI experiments, cell layers were analysed and previously found markers were imaged. This allowed us to display and compare marker compounds in parasite-infected single host cells and non-infected controls at 5 µm lateral resolution. The presented work will be the basis for future detailed investigations on fast replicating *N. caninum* tachyzoites and their impact on host cell lipid metabolism. Overall, current data on lipid biomarkers of single *N. caninum*-infected host endothelial cells unveil lipid sources as essential components for fast replicating tachyzoites. These novel lipid data might help to identify alternative metabolic pathways for novel drug targets not only against *N. caninum* but also against other apicomplexan parasites of veterinary and public health importance.

ACKNOWLEDGEMENTS

Financial support by the German Research Foundation [Deutsche Forschungsgemeinschaft (DFG) under grants Sp314/13-1, Sp314/23-1 and INST 162/500-1 FUGG] and by the Federal State of Hesse LOEWE Center DRUID (Novel Drug Targets against Poverty-Related and Neglected Tropical Diseases), is gratefully acknowledged. We would like to thank the Hans-Böckler-Stiftung for granting Nils Anschütz a scholarship. Instrumental support by TransMIT GmbH and Thermo Fisher Scientific is gratefully acknowledged.

Open access funding enabled and organized by Projekt DEAL.

CONFLICT OF INTEREST

Bernhard Spengler is a consultant and Nils H. Anschütz is a part-time employee of TransMIT GmbH, Giessen, Germany. The other authors declare no conflict of interest.

REFERENCES

1. Villagra-Blanco R, Angelova L, Conze T, et al. Seroprevalence of Neospora caninum-specific antibodies in German breeding bitches. *Parasites Vectors*. 2018;11:96. doi:10.1186/s13071-018-2683-1
2. Dubey JP, Carpenter JL, Speer CA, Topper MJ, Uggla A. Newly recognized fatal protozoan disease of dogs. *J Am Vet Med Assoc*. 1988;192(9):1269-1285.
3. Lindsay DS, Upton SJ, Dubey JP. A structural study of the Neospora caninum oocyst. *Int J Parasitol*. 1999;29(10):1521-1523. doi:10.1016/s0020-7519(99)00121-6
4. McAllister MM, Dubey JP, Lindsay DS, Jolley WR, Wills RA, McGuire AM. Dogs are definitive hosts of Neospora caninum. *Int J Parasitol*. 1998;28(9):1473-1478. doi:10.1016/s0020-7519(98)00138-6
5. Speer CA, Dubey JP, McAllister MM, Blixt JA. Comparative ultrastructure of tachyzoites, bradyzoites, and tissue cysts of Neospora caninum and Toxoplasma gondii. *Int J Parasitol*. 1999;29(10):1509-1519. doi:10.1016/s0020-7519(99)00132-0
6. Ramaprasad A, Mourier T, Naeem R, et al. Comprehensive evaluation of toxoplasma gondii VEG and neospora caninum LIV genomes with tachyzoite stage transcriptome and proteome defines novel transcript features. *PLoS One*. 2015;10(4):e0124473. doi:10.1371/journal.pone.0124473
7. Reid AJ, Vermont SJ, Cotton JA, et al. Comparative genomics of the apicomplexan parasites Toxoplasma gondii and neospora caninum: coccidia differing in host range and transmission strategy. *PLoS Pathog*. 2012;8(3):e1002567. doi:10.1371/journal.ppat.1002567
8. Dubey JP, Barr BC, Barta JR, et al. Redescription of Neospora caninum and its differentiation from related coccidia. *Int J Parasitol*. 2002;32(8):929-946. doi:10.1016/s0020-7519(02)00094-2
9. Dubey JP, Schares G, Ortega-Mora LM. Epidemiology and control of neosporosis and Neospora caninum. *Clin Microbiol Rev*. 2007;20(2):323-367. doi:10.1128/cmr.00031-06
10. Reichel MP, Ayanegui-Alcerreca MA, Gondim LFP, Ellis JT. What is the global economic impact of Neospora caninum in cattle - The billion dollar question. Review. *Int J Parasitol*. 2013;43(2):133-142. doi:10.1016/j.ijpara.2012.10.022
11. Romand S, Thulliez P, Dubey JP. Direct agglutination test for serologic diagnosis of Neospora caninum infection. Article. *Parasitol Res*. 1998;84(1):50-53.
12. Bjorkman C, Holmdahl OJM, Uggla A. An indirect enzyme-linked immunoassay (ELISA) for demonstration of antibodies to Neospora caninum in serum and milk of cattle. *Vet Parasitol*. 1997;68(3):251-260. doi:10.1016/s0304-4017(96)01076-x
13. Bjorkman C, Lunden A, Holmdahl J, Barber J, Trees AJ, Uggla A. Neospora-caninum in dogs - detection of antibodies by ELISA using an iscom antigen. *Parasite Immunol*. 1994;16(12):643-648. doi:10.1111/j.1365-3024.1994.tb00320.x
14. Payne S, Ellis J. Detection of Neospora caninum DNA by the polymerase chain reaction. Article. *Int J Parasitol*. 1996;26(4):347-351. doi:10.1016/0020-7519(96)00030-6
15. Trees AJ, Williams DJL. Endogenous and exogenous transplacental infection in Neospora caninum and Toxoplasma gondii. *Trends Parasitol*. 2005;21(12):558-561. doi:10.1016/j.pt.2005.09.005
16. Davison HC, Otter A, Trees AJ. Estimation of vertical and horizontal transmission parameters of Neospora caninum infections in dairy cattle. *Int J Parasitol*. 1999;29(10):1683-1689. doi:10.1016/s0020-7519(99)00129-0
17. Silva RC, Machado GP. Canine neosporosis: perspectives on pathogenesis and management. Review. *Vet Med Res Rep*. 2016;7:59-70. doi:10.2147/vmrr.s76969
18. Bahrami S, Hamidinejat H, Fatemi-Tabatabaei SR, Sardarifar S. Effect of natural neosporosis on bull sperm quality. *Trop Anim Health Prod*. 2018;50(1):85-89. doi:10.1007/s11250-017-1403-8
19. Klauck V, Machado G, Pazinato R, et al. Relation between Neospora caninum and abortion in dairy cows: risk factors and pathogenesis of disease. *Microb Pathog*. 2016;92:46-49. doi:10.1016/j.micpath.2015.12.015
20. Dubey JP, Lindsay DS. A review of Neospora caninum and neosporosis. *Vet Parasitol*. 1996;67(1-2):1-59. doi:10.1016/s0304-4017(96)01035-7
21. Wilson DJ, Orsel K, Waddington J, et al. Neospora caninum is the leading cause of bovine fetal loss in British Columbia, Canada. *Vet Parasitol*. 2016;218:46-51. doi:10.1016/j.vetpar.2016.01.006
22. Weston JF, Heuer C, Williamson NB. Efficacy of a Neospora caninum killed tachyzoite vaccine in preventing abortion and vertical transmission in dairy cattle. *Prev Vet Med*. 2012;103(2-3):136-144. doi:10.1016/j.prevetmed.2011.08.010
23. Barr BC, Conrad PA, Sverlow KW, Tarantal AF, Hendrickx AG. Experimental fetal and transplacental neospora infection in the nonhuman primate. *Lab Invest*. 1994;71(2):236-242.
24. Robayo-Sanchez L, Gomez-Marin J, Cortes-Vecino J. Neospora caninum: biological relationship with toxoplasma gondii and its potential as zoonosis. Review. *Revista Mvz Cordoba*. 2017;22(3):6355-6365. doi:10.21897/rmvz.1139
25. Duarte PO, Oshiro LM, Zimmermann NP, et al. Serological and molecular detection of Neospora caninum and Toxoplasma gondii in human umbilical cord blood and placental tissue samples. *Sci Rep*. 2020;10(1):9043. doi:10.1038/s41598-020-65991-1
26. Oshiro LM, Motta-Castro ARC, Freitas SZ, et al. Neospora caninum and Toxoplasma gondii serodiagnosis in human immunodeficiency virus carriers. *Rev Soc Bras Med Trop*. 2015;48(5):568-572. doi:10.1590/0037-8682-0151-2015
27. Al-Bajalan MMM, Xia D, Armstrong S, Randle N, Wastling JM. Toxoplasma gondii and Neospora caninum induce different host cell responses at proteome-wide phosphorylation events; a step forward for uncovering the biological differences between these closely related parasites. *Parasitol Res*. 2017;116(10):2707-2719. doi:10.1007/s00436-017-5579-7
28. Spengler B. De novo sequencing, peptide composition analysis, and composition-based sequencing: a new strategy employing accurate mass determination by Fourier transform ion cyclotron resonance mass spectrometry. *J Am Soc Mass Spectrom*. 2004;15(5):703-714. doi:10.1016/j.jasms.2004.01.007
29. Spengler B. Accurate mass as a bioinformatic parameter in data-to-knowledge conversion: Fourier transform ion cyclotron resonance mass spectrometry for peptide de novo sequencing. *Eur J Mass Spectrom*. 2007;13(1):83-87. doi:10.1255/ejms.840

30. Spengler B, Hester A. Mass-based classification (MBC) of peptides: highly accurate precursor ion mass values can be used to directly recognize peptide phosphorylation. *J Am Soc Mass Spectrom*. 2008;19(12):1808-1812. doi:10.1016/j.jasms.2008.08.005
31. Kompauer M, Heiles S, Spengler B. Atmospheric pressure MALDI mass spectrometry imaging of tissues and cells at 1.4-mu m lateral resolution. *Nat Methods*. 2017;14(1):90-96. doi:10.1038/nmeth.4071
32. Spengler B, Hubert M, Kaufmann R. MALDI ion imaging and biological ion imaging with a new scanning UV-laser microprobe. In *Proceedings of the 42nd ASMS Conference on Mass Spectrometry and Allied Topics*. 1994.
33. Kadesch P, Hollubarsch T, Gerbig S, et al. Intracellular parasites toxoplasma gondii and besnoitia besnoiti, unveiled in single host cells using AP-SMALDI MS imaging. *J Am Soc Mass Spectrom*. 2020;31(9):1815-1824. doi:10.1021/jasms.0c00043
34. Hermosilla C, Zahner H, Taubert A. Eimeria bovis modulates adhesion molecule gene transcription in and PMN adhesion to infected bovine endothelial cells. *Int J Parasitol*. 2006;36(4):423-431. doi:10.1016/j.ijpara.2006.01.001
35. Matyash V, Liebisch G, Kurzchalia TV, Shevchenko A, Schwudke D. Lipid extraction by methyl-tert-butyl ether for high-throughput lipidomics. *J Lipid Res*. 2008;49(5):1137-1146. doi:10.1194/jlr.D700041-JLR200
36. Hu CX, van Dommelen J, van der Heijden R, et al. RPLC-ion-trap-FTMS method for lipid profiling of plasma: method validation and application to p53 mutant mouse model. *J Proteome Res*. 2008;7(11):4982-4991. doi:10.1021/pr800373m
37. Tyanova S, Temu T, Sinitcyn P, et al. The Perseus computational platform for comprehensive analysis of (prote)omics data. *Nat Methods*. 2016;13(9):731-740. doi:10.1038/nmeth.3901
38. Koelmel JP, Kroeger NM, Ulmer CZ, et al. LipidMatch: an automated workflow for rule-based lipid identification using untargeted high-resolution tandem mass spectrometry data. *BMC Bioinf*. 2017;18:331. doi:10.1186/s12859-017-1744-3
39. Kessner D, Chambers M, Burke R, Agusand D, Mallick P. ProteoWizard: open source software for rapid proteomics tools development. *Bioinformatics*. 2008;24(21):2534-2536. doi:10.1093/bioinformatics/btn323
40. Pluskal T, Castillo S, Villar-Briones A, Oresic M. MZmine 2: modular framework for processing, visualizing, and analyzing mass spectrometry-based molecular profile data. *BMC Bioinf*. 2010;11:395. doi:10.1186/1471-2105-11-395
41. Kaur G, Dufour JM. Cell lines valuable tools or useless artifacts. *Spermatogenesis*. 2012;2:1-5. doi:10.4161/spmg.19885
42. Taubert A, Wimmers K, Ponsuksili S, Jimenez CA, Zahner H, Hermosilla C. Microarray-based transcriptional profiling of Eimeria bovis-infected bovine endothelial host cells. *Vet Res*. 2010;41(5):70. doi:10.1051/vetres/2010041
43. Taubert A, Krull M, Zahner H, Hermosilla C. Toxoplasma gondii and Neospora caninum infections of bovine endothelial cells induce endothelial adhesion molecule gene transcription and subsequent PMN adhesion. *Vet Immunol Immunopathol*. 2006;112(3-4):272-283. doi:10.1016/j.vetinn.2006.03.017
44. Hermosilla C, Ruiz A, Taubert A. Eimeria bovis: an update on parasite-host cell interactions. Review. *Int J Med Microbiol*. 2012;302(4-5):210-215. doi:10.1016/j.ijmm.2012.07.002
45. Hermosilla C, Barbisch B, Heise A, Kowalik S, Zahner H. Development of Eimeria bovis in vitro: suitability of several bovine, human and porcine endothelial cell lines, bovine fetal gastrointestinal, Madin-Darby bovine kidney (MDBK) and African green monkey kidney (VERO) cells. *Parasitol Res*. 2002;88(4):301-307. doi:10.1007/s00436-001-0531-1
46. The LIPID MAPS® Lipidomics Gateway. 2020. https://www.lipidmaps.org/
47. Liu S, Sjovall J, Griffiths WJ. Analysis of oxosteroids by nano-electrospray mass spectrometry of their oximes. *Rapid Commun Mass Spectrom*. 2000;14(6):390-400. doi:10.1002/(sici)1097-0231(20000331)14:6(390::aid-rcm882)3.0.co;2-7
48. Jiang XT, Ory DS, Han XL. Characterization of oxysterols by electrospray ionization tandem mass spectrometry after one-step derivatization with dimethylglycine. *Rapid Commun Mass Spectrom*. 2007;21(2):141-152. doi:10.1002/rcm.2820
49. Honda A, Yamashita K, Hara T, et al. Highly sensitive quantification of key regulatory oxysterols in biological samples by LC-ESI-MS/MS. *J Lipid Res*. 2009;50(2):350-357. doi:10.1194/jlr.D800040-JLR200
50. Sidhu R, Jiang H, Farhat NY, et al. A validated LC-MS/MS assay for quantification of 24(S)-hydroxycholesterol in plasma and cerebrospinal fluid. *J Lipid Res*. 2015;56(6):1222-1233. doi:10.1194/jlr.D058487
51. Taubert A, Silva LMR, Velasquez ZD, Larrazabal C, Lutjohann D, Hermosilla C. Modulation of cholesterol-related sterols during Eimeria bovis macromeront formation and impact of selected oxysterols on parasite development. *Mol Biochem Parasitol*. 2018;223:1-12. doi:10.1016/j.molbiopara.2018.06.002
52. Maffucci T, Falasca M. Analysis, regulation, and roles of endosomal phosphoinositides. *Endosome Signaling Pt B*. 2014;535:75-91. doi:10.1016/b978-0-12-397925-4.00005-5
53. Besteiro S, Bertrand-Michel J, Lebrun M, Vial H, Dubremetz JF. Lipidomic analysis of Toxoplasma gondii tachyzoites rhoptries: further insights into the role of cholesterol. *Biochem J*. 2008;415:87-96. doi:10.1042/bj20080795
54. Birge RB, Boeltz S, Kumar S, et al. Phosphatidylserine is a global immunosuppressive signal in efferocytosis, infectious disease, and cancer. Review. *Cell Death Differ*. 2016;23(6):962-978. doi:10.1038/cdd.2016.11

SUPPORTING INFORMATION

Additional supporting information can be found online in the Supporting Information section at the end of this article.

How to cite this article: Anschütz NH, Gerbig S, Ventura AMP, et al. Atmospheric-pressure scanning microprobe matrix-assisted laser desorption/ionization mass spectrometry imaging of *Neospora caninum*-infected cell monolayers. *Anal Sci Adv*. 2022;1-11. https://doi.org/10.1002/ansa.202200016

Supplementary Information

Atmospheric-pressure scanning microprobe matrix-assisted laser desorption/ionization mass spectrometry imaging of *Neospora caninum*-infected cell monolayers

Anschütz, N.H., Gerbig, S., Peter Ventura, A., Silva, L.M.R., Larrazabal, C., Hermosilla, C., Taubert, A., Spengler, B., Analytical Science Advances 2022, 3, 244–254; https://doi.org/10.1002/ansa.202200016

https://chemistry-europe.onlinelibrary.wiley.com/action/downloadSupplement?doi=10.1002%2Fansa.202200016&file=ansa202200016-sup-0001-SuppMat.pdf

CHAPTER 3 – Publication 2

Mass Spectrometry Imaging of In Vitro *Cryptosporidium parvum*-Infected Cells and Host Tissue

Anschütz, N.H.; Gerbig, S.; Ghezellou, P.; Silva, L.M.R.; Vélez, J.D.; Hermosilla, C.R.; Taubert, A.; Spengler, B. Mass Spectrometry Imaging of In Vitro *Cryptosporidium parvum*-Infected Cells and Host Tissue. *Biomolecules* 2023, *13*, 1200.; https://doi.org/10.3390/biom13081200

biomolecules

MDPI

Article

Mass Spectrometry Imaging of In Vitro *Cryptosporidium parvum*-Infected Cells and Host Tissue

Nils H. Anschütz [1], Stefanie Gerbig [1], Parviz Ghezellou [1], Liliana M. R. Silva [2,3,4], Juan Diego Vélez [2], Carlos R. Hermosilla [2], Anja Taubert [2] and Bernhard Spengler [1,*]

[1] Institute of Inorganic and Analytical Chemistry, Justus Liebig University Giessen, 35392 Giessen, Germany; nils.h.anschuetz@anorg.chemie.uni-giessen.de (N.H.A.); stefanie.gerbig@transmit.de (S.G.); parviz.ghezellou@anorg.chemie.uni-giessen.de (P.G.)

[2] Institute of Parasitology, Biomedical Research Center Seltersberg, Justus Liebig University Giessen, 35392 Giessen, Germany; liliana.silva@vetmed.uni-giessen.de (L.M.R.S.); juan.velez@vetmed.uni-giessen.de (J.D.V.); carlos.r.hermosilla@vetmed.uni-giessen.de (C.R.H.); anja.taubert@vetmed.uni-giessen.de (A.T.)

[3] Egas Moniz Center for Interdisciplinary Research (CiiEM), Egas Moniz School of Health & Science, 2829-511 Caparica, Portugal

[4] MED—Mediterranean Institute for Agriculture, Environment and Development & CHANGE—Global Change and Sustainability Institute, Institute for Advanced Studies and Research, Universidade de Évora, 7006-554 Évora, Portugal

* Correspondence: bernhard.spengler@anorg.chemie.uni-giessen.de

Abstract: *Cryptosporidium parvum* is a zoonotic-relevant parasite belonging to the phylum Alveolata (subphylum Apicomplexa). One of the most zoonotic-relevant etiologies of cryptosporidiosis is the species *C. parvum*, infecting humans, cattle and wildlife. *C. parvum*-infected intestinal mucosa as well as host cells infected in vitro have not yet been the subject of extensive biochemical investigation. Efficient treatment options or vaccines against cryptosporidiosis are currently not available. Human cryptosporidiosis is currently known as a neglected poverty-related disease (PRD), being potentially fatal in young children or immunocompromised patients. In this study, we used a combination of atmospheric pressure scanning microprobe matrix-assisted laser desorption/ionization (AP-SMALDI) mass spectrometry imaging (MSI) and liquid chromatography-tandem mass spectrometry (HPLC-MS/MS) to determine and locate molecular biomarkers in in vitro *C. parvum*-infected host cells as well as parasitized neonatal calf intestines. Sections of *C. parvum*-infected and non-infected host cell pellets and infected intestines were examined to determine potential biomarkers. Human ileocecal adenocarcinoma cells (HCT-8) were used as a suitable in vitro host cell system. More than a thousand different molecular signals were found in both positive- and negative-ion mode, which were significantly increased in *C. parvum*-infected material. A database search in combination with HPLC-MS/MS experiments was employed for the structural verification of markers. Our results demonstrate some overlap between the identified markers and data obtained from earlier studies on other apicomplexan parasites. Statistically relevant biomarkers were imaged in cell layers of *C. parvum*-infected and non-infected host cells with 5 µm pixel size and in bovine intestinal tissue with 10 µm pixel size. This allowed us to substantiate their relevance once again. Taken together, the present approach delivers novel metabolic insights on neglected cryptosporidiosis affecting mainly children in developing countries.

Keywords: *Cryptosporidium parvum*; mass spectrometry imaging; AP-SMALDI

Citation: Anschütz, N.H.; Gerbig, S.; Ghezellou, P.; Silva, L.M.R.; Vélez, J.D.; Hermosilla, C.R.; Taubert, A.; Spengler, B. Mass Spectrometry Imaging of In Vitro *Cryptosporidium parvum*-Infected Cells and Host Tissue. *Biomolecules* **2023**, *13*, 1200. https://doi.org/10.3390/biom13081200

Academic Editors: Nicolas Cenac and Vladimir N. Uversky

Received: 13 June 2023
Revised: 21 July 2023
Accepted: 27 July 2023
Published: 31 July 2023

1. Introduction

Cryptosporidium parvum belongs to the phylum Alveolata (subphylum Apicomplexa) and is the most relevant zoonotic etiology of human cryptosporidiosis. Additionally to humans, this enteropathogenic parasite infects a wide range of vertebrate hosts, including

domestic as well as wild animals [1]. Oral infection with *C. parvum* oocysts occurs through contact with infected people/animals shedding at these infective stages or through drinking contaminated water or eating food washed with contaminated water [2]. *C. parvum* thick-walled oocysts are a highly resistant exogenous stage in the life cycle and are released through the feces of infected humans or animals, thereby leading to new infections upon subsequent ingestion by a new host. Ingested *C. parvum* thick-walled oocysts rupture in the gastrointestinal tract of vertebrate hosts. In this process, known as excystation, four sporozoites are released into the gut lumen. Free-released sporozoites must infect small intestinal epithelial cells (IECs) to achieve further parasite proliferation. In addition to thick-walled oocysts, a second type of thin-walled oocysts develops which hardly resists environmental effects. Nonetheless, these thin-walled oocysts might lead to endogenous autoinfections, probably being the main cause of persistent infection and disease in immunocompromised patients [1]. The epicytoplasmatic intracellular location of *C. parvum* sporozoites with their basal adhesive zones (feeding layers) is another peculiarity of this species when compared to other apicomplexans. Sporozoites within IECs will then undergo asexual merogony resulting in merozoites of the first generation, and these merozoites will again undergo a second merogony producing merozoites of the second merogony. Second-generation merozoites will conduct sexual gamogony, resulting in syngamy and final oocyst production. Afterwards, resistant thick-walled oocysts are excreted from the host through fecal material and the life cycle is completed.

Human cryptosporidiosis still represents a neglected poverty-related disease (PRD) [3]. The most common symptoms of human cryptosporidiosis are abdominal pain, nausea, anorexia, fever and profuse watery diarrhea [1]. The burden of this enteric PRD is currently considerably high in low-income countries [4]. It is a leading source of severe pediatric diarrhea [5]. In already weakened patients, especially young children, the course of the disease can be fatal [1,5]. Diarrheal diseases are responsible for 9% of global child morbidity and mortality [6]. Also, children's growth can be adversely affected after clinically manifested cryptosporidiosis [4]. Despite intense health consequences, no effective treatments or vaccines against cryptosporidiosis exist [7]. The well-tolerated antiparasitic agent nitazoxanide is the only FDA-approved drug for treating human cryptosporidiosis; nonetheless, it lacks efficacy in immunocompromised patients [7–9].

As an obligate fast-replicating parasite, *C. parvum* has reduced metabolic capacities due to a reductive evolutionary process. This minimal metabolic capability is further evidenced in its small genome comprising 9.1 Mb within eight chromosomes when compared to the *Plasmodium* genome of 23 Mb, contained in 14 chromosomes, or to other closely related apicomplexans such as *Toxoplasma*, *Neospora*, *Besnoitia* and *Eimeria* [10–12]. Consistently, *C. parvum* lacks a tricarboxylic acid cycle, oxidative phosphorylation, de novo pyrimidine and amino acid and cholesterol biosynthesis [10]. In this regard, it should be noted that the genus *Cryptosporidium* is an extreme example of reductive evolution among apicomplexans [11]. The metabolic possibilities of the parasite are therefore limited and it must use the IECs' metabolic abilities for successful fast intracellular replication. In this context, it was shown that *C. parvum*-infected host cells experience an upregulation of glycolysis and glutaminolysis [12,13]. Referring to in vitro culture systems, *C. parvum* withstands continuous cultivation and therefore many traditional biochemical methods as well as high-throughput drug screening are very limited [10]. Magnuson et al. used non-imaging MALDI-MS to fingerprint pure *C. parvum* oocysts [14]. The study by Snelling et al. is the first major proteomic study of *C. parvum*, later supplemented by Li et al. [15,16]. Mauzy et al. as well as Matos et al. provided a comprehensive transcriptome of the intracellular stages of *C. parvum* [17,18]. Mass spectrometry imaging (MSI), despite its well-known capabilities, has not yet played a predominant role in studying the metabolic signatures of *C. parvum*-infected host cells in vitro or in infected intestinal tissue. To the best of our knowledge, a comprehensive investigation of *C. parvum*-infected host cells and bovine intestine using MSI has not yet been performed in a biochemical context.

Since the beginning of the millennium, there have been significant improvements in MS instrumentation, and detailed mass analysis is now possible, allowing elemental formulae of compounds to be determined from highly accurate molecular mass values [19–21]. Annotations as well as subsequent identifications of analytes are possible. MSI provides the visualization of analyte distributions in tissues and cells. In this context, parasites can be visualized by MSI if infection markers are determined. The size of *C. parvum* oocysts and of the intracellular stages (i.e., sporozoites, trophozoites, meronts and gamonts) is approximately 4–5 µm in diameter [1], requiring MSI methodology with at least 5 µm lateral resolution. Due to improvements in MSI instrumentation, lateral resolutions (image pixel sizes) of 1–2 µm are now available, meaning that assembled or even single *C. parvum*-infected host cells can be examined with this method [22].

In this work, we applied MALDI-MSI and HPLC-MS/MS to investigate the metabolic alterations arising from an infection of *C. parvum* in human intestinal epithelial cells (HCT-8) as well as infected small intestines of neonatal calves to resemble an in vivo scenario as closely as possible. Our study provides the first molecular biomarkers of single *C. parvum*-infected human cells as well as bovine tissue, thereby improving the understanding of the metabolic alterations underlying pathophysiological mechanisms during cryptosporidiosis. Herein, analytes identified through combined MALDI-MSI/HPLC-MS will hopefully help to identify potential novel anti-cryptosporidial drug targets in the future.

2. Experimental Section

2.1. Parasites

The oocysts of *Cryptosporidium parvum* were obtained from experimentally infected neonatal calves kept at the Institute of Parasitology, Leipzig University, Germany, as previously reported [23]. *C. parvum* strain herein used belongs to the subtype 60-kDa glycoprotein (gp60) IIaA15G2RI and is the most common zoonotic subtype in Germany and in other industrialized countries. Preservation medium of oocysts was composed of sterile phosphate-buffered saline (PBS 1X, pH 7.4; Sigma-Aldrich, St. Louis, MI, USA) supplemented with 100 UI penicillin and 0.1 mg streptomycin/mL (Sigma-Aldrich) at 4 °C. Oocyst stocks were conserved for a maximum of three months to guarantee infectivity of sporulated oocysts. The *C. parvum* oocyst preservation medium was renewed monthly [12].

2.2. Cell Culture

Human ileocecal adenocarcinoma cells (HCT-8; ATCC CCL-244™) were maintained at 37 °C and 5% CO_2 using RPMI 1640 medium (Sigma-Aldrich, St. Louis, MI, USA) supplemented with 0.3 g/L L-glutamine (Sigma-Aldrich, St. Louis, MI, USA), 10% fetal bovine serum (FBS; Biochrom GmbH, Berlin, Germany), 100 UI penicillin and 0.1 mg streptomycin/mL (Sigma-Aldrich, St. Louis, MI, USA). The cell culture medium was changed every other day. Within one experiment, cells from the same passage were used for the infection assays.

2.3. Host Cell Infection

HCT-8 cells were seeded at a density of 1×10^5 cells/well on 10 mm round glass coverslips in 24-well plastic microtiter plates (Eppendorf, Hamburg, Germany). When cells reached 60–70% confluence, phase-contrast images were acquired with an inverted microscope (IX81, Olympus, Hamburg, Germany) equipped with a digital camera (XM10, Olympus, Hamburg, Germany) and the total cell number was determined to calculate the infection dose, applying an MOI (multiplicity of infection) of 0.5 (1 sporozoite per 2 host cells), as previously described [12]. Briefly, sporulated *C. parvum* oocysts were pelleted at 5000× *g* for 5 min at 4 °C. Thereafter, sporozoite excystation was induced by supplementation of acidified (pH 2.0) and sterile pre-warmed (37 °C) 1X Hank's balanced salt solution (HBSS; Sigma-Aldrich) for 10 min at 37 °C. Thereafter, excysted sporozoites were pelleted (5000× *g* for 5 min) and re-suspended in sterile RPMI 1640 cell medium supplemented with 0.3 g/L L-glutamine, 10% FBS, 100 UI penicillin and 0.1 mg streptomycin/mL (all Sigma-

Aldrich, St. Louis, MI, USA). Free-released sporozoites were added to HCT-8 monolayers for 3 h, and thereafter cell layers were washed thrice in order to remove free sporozoite and oocyst remnants, and fresh cell culture medium was added.

2.4. Preparation of Cell Monolayers and Parasite Pellets

HCT-8 cells were seeded on glass coverslips (10–15 mm, Thermo Fisher Scientific, Dreieich, Germany) and allowed to grow until 60–70% confluency. Cell layers were then infected as described above. At 24 hpi, cell culture medium was removed, and monolayers were washed with sterile PBS 1X before allowing them to dry and freeze at −80 °C until further use. For preparation of parasite pellets, 1×10^9 *C. parvum* oocysts were pelleted (5000× *g*, 5 min) in microcentrifuge tubes (1.5 mL, Eppendorf, Hamburg, Germany). After 2 washes in PBS 1X, the supernatant was removed and the pellet was frozen at −80 °C until further use.

2.5. Preparation of C. parvum-Infected Bovine Intestinal Cryo-Sections

Three sections were prepared from each intestinal tissue sample to serve as technical replicates. Both the naturally ($n = 1$) and experimentally ($n = 2$) *C. parvum*-infected intestinal samples were obtained from neonatal calves at the University of Leizig, Germany, as well as the associated control samples. Intestinal tissue samples were embedded in gelatine (8 vol.%) prior to sectioning. The section thickness of the naturally and artificially *C. parvum*-infected intestine sample was 30 µm. The sectioning was performed at −25 °C with a cutting angle of 11° using a Microm Sec35p® blade on a microcryotome (Microm HM 525, Microm International GmbH, part of Thermo Fisher Scientific, Walldorf, Germany). The quality of the sections was checked with an optical microscope (VHX-5000, Keyence, Japan). Subsequently, the sections were stored at −80 °C until AP-SMALDI MSI analysis.

2.6. MALDI-MS Sample Preparation

For MALDI measurements in positive-ion mode, 2,5-dihydroxybenzoic acid (DHB, Merck, Darmstadt, Germany) was used as a matrix. The matrix solution was produced by dissolving DHB (30 mg/mL) in 1:1 acetone/water with 0.1% trifluoroacetic acid (TFA, Sigma Aldrich, Steinheim, Germany). The host tissue as well as the cell pellet sections were covered with 100 µL of the matrix solution at a constant flow rate of 10 µL/min using a dedicated pneumatic sprayer (SMALDIPrep, TransMIT GmbH, Giessen, Germany).

2.7. Metabolite Extraction

The sample was mixed with 25 µL 0.1% ammonium acetate (Honeywell, Riedel-de Haen, LC-MS Chromasolv™). For cell lysis, the cell pellets were transferred to a potter homogenizer and the intestinal samples to a Mini-Mill PULVERISETTE 23 (Fritsch, Idar-Oberstein, Germany). Metabolites were extracted using methyl tert-butyl ether (MTBE) and methanol as described in the literature [24]. In summary, 100 µL methanol (Sigma Aldrich, St. Louis, MI, USA) and 400 µL MTBE (Sigma Aldrich, St. Louis, MI, USA) were added to this lysate. The mixture was incubated at 4 °C and 900 rpm for 1 h. Subsequently, 200 µL of ice-cold MS-grade water was added and the sample was centrifuged for 10 min at 1000× *g*. The lower aqueous phase was re-extracted, while the upper organic phase was collected. For re-extraction, 200 µL MTBE/methanol/water (4:1.2:1; *v*/*v*/*v*) was added to the aqueous phase. After 1 h of incubation at 4 °C and 900 rpm and centrifugation for 10 min at 1000× *g*, the organic phase was collected again. Organic phases were combined, dried under a nitrogen stream and resuspended in 500 µL acetonitrile/water (60:40; *v*/*v*).

2.8. UHPLC-MS/MS Analysis

The gradient settings in HPLC were modified from the literature [25]. Solvent A was acetonitrile/water (60:40) containing 0.1% formic acid and 10 mM ammonium formate (Sigma Aldrich, Germany) and solvent B was isopropanol/acetonitrile/water (90:8:2) containing 0.1% formic acid and 10 mM ammonium formate (Sigma Aldrich, Germany).

The elution was performed with a 32 min gradient. The initial condition was 32% of solvent B for 1.5 min. Over a period of 4 min, solvent B was increased to 45%. From 4 to 5 min, solvent B was increased to 52%, from 5 to 8 min to 58%, from 8 to 11 min to 66%, from 11 to 14 min to 70%, from 14 to 18 min to 75% and from 18 to 21 min to 97%. The gradient was kept constant between the 21st and 25th minute. Solvent B was then reduced to 32% and the gradient was held constant for 7 min. Throughout the measurement, the flow rate was maintained at 260 µL/min. Separation was performed on a Dionex UltiMate 3000 RSLC-System (Thermo Fisher Scientific, Dreieich, Germany), using Kinetex C18 (2.1 × 100 mm, 2.6 µm 100 Å particle size) column (Phenomenex, Torrance, CA, USA), coupled to a Q Exactive™ HF-X (Thermo Fisher Scientific, Dreieich, Germany) orbital trapping mass spectrometer.

2.9. MALDI-MS(I)

MALDI MS and MALDI MSI experiments were carried out using an AP-SMALDI^5 AF (TransMIT GmbH, Giessen, Germany) imaging system (pixel size: ≥5 µm) coupled to a Q Exactive™ HF (Thermo Fisher Scientific (Bremen) GmbH, Germany) orbital trapping mass spectrometer (mass resolution was set to R = 240,000 @ m/z 200). For internal calibration with DHB as a matrix, the lock mass m/z 716.12462 (corresponding to $[5DHB-4H_2O+NH_4]^+$) was set. In case of pNA, m/z 273.06238 (corresponding to $[2pNA-H_2-H]^-$) was used. In positive-ion mode the mass range was set to m/z 300–1200 and in negative-ion mode m/z 250–1000. In the case of the cell pellet sections, a pattern of 50 × 50 pixels was measured with a step size of 10 µm. Due to a larger (defocused) laser spot area at 10 µm step size, higher signal intensities were obtained. In addition, the Full Pixel mode of the ion source was used for ablation of the entire 10 µm × 10 µm area by a meandering movement [26].

2.10. Data Processing

The software Mirion (TransMIT GmbH, Giessen, Germany), together with the Perseus software platform (MPI of Biochemistry, Martinsried, Germany), was used to find potential biomarkers in the MS data of the cell pellets [27]. The utilized procedure was based on the published literature [28,29]. Using Mirion [30], all MALDI MS measurements of the cell pellets were merged and analyzed together. A list of all m/z values with a pixel coverage ≥ 0.5% was exported, the corresponding deviations (±5 ppm) were calculated and this modified list was compared to all single-cell measurements. The results were then loaded in Perseus, the datasets were classified into infected and non-infected host cells/intestinal tissues. Data were normalized by dividing the intensity values by their sum and afterwards by using the Z-score (median, for hierarchical clustering). Multiple-sample tests were carried out (ANOVA; permutation-based false discovery rate, FDR = 0.05, number of randomizations = 250). The invalid values were filtered out and post hoc tests were performed with the remaining values (visualized using hierarchical clusters). Annotations of the m/z values found by Perseus were provided by LipidMaps database. These accurate mass values and their deviations (±5 ppm) were used to create a mass list and utilized as an inclusion list for LC-MS/MS analysis. The MS raw files were renamed by the LipidMatch RenamingTool. Finally, lipids were identified using LipidMatch Flow [27].

3. Results and Discussion

C. parvum-infected HCT-8 as well as infected bovine neonatal intestinal mucosa were here used as model systems to be as close as possible to in vivo situation where exclusively IECs serve as suitable host cells. Figure 1 illustrates the general workflow. *C. parvum* oocysts were obtained from experimentally infected neonatal calves. Subsequently, oocysts were used to isolate sporozoites to generate cell pellets and infected monolayers. Additionally, *C. parvum*-infected intestine samples were obtained from diseased neonatal calves. Sections from infected and control cell pellets were used to determine statistically significant

biomarkers. These biomarkers were then visualized using MALDI-MSI in monolayers and sections of artificially and/or naturally infected small intestinal tissues.

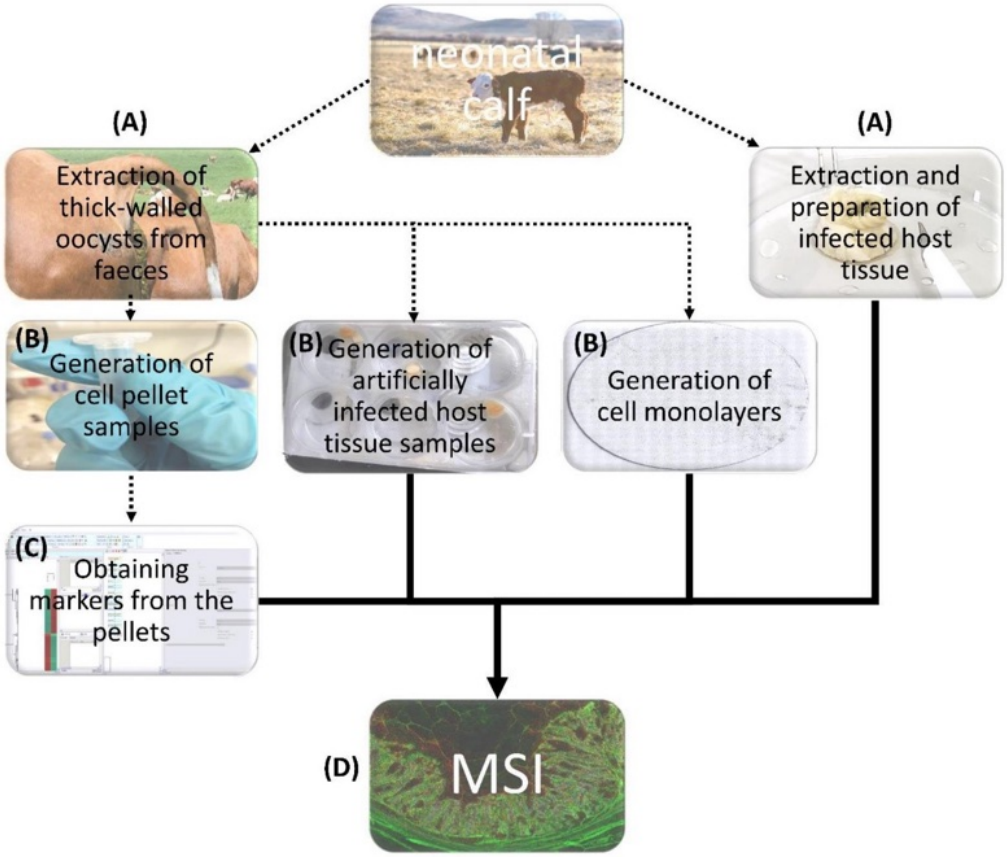

Figure 1. General workflow. Cryptosporidium parvum oocysts, infected intestine and non-infected intestine were obtained from neonatal calves (**A**). These thick-walled oocysts were then used to generate cell pellets, monolayers and artificially infected intestinal tissues (**B**). Sections from cell pellets were used to obtain statistically significant markers (**C**). Markers were visualized with the help of MALDI-MSI in monolayers and host intestinal tissues (**D**).

3.1. MALDI-MSI Measurements of Cell Pellets

The HCT-8 cell line is the most widely used in vitro system for *C. parvum*. studies. Cell pellets were sliced into consecutive thin sections to provide a homogeneous sample pattern for the MALDI-MS experiments and facilitate statistical evaluability. Figure 2 illustrates the chosen experimental approach. Different HCT-8 ($n = 3$) cell sections were measured, and the MS ion at m/z 530.3212 that was found to be a statistically relevant infection marker is displayed using the red color channel (Figure 2A,B). Figure 2A shows two images with a size of 50 × 50 pixels. Each analysis of the cell pellets was performed with a step size of 10 µm. The larger step sizes, along with a defocusing of the laser beam, led to larger spot sizes, resulting in a larger amount of sample material being ablated and ionized by the laser beam. Still, no satisfactory results could be achieved in standard "spot mode". Therefore,

measurements of the cell pellets were carried out with a signal-enhancing mode of the ion source, the Full Pixel mode. Here, a larger number of laser pulses are used to ablate the pixel area by a meandering movement [26], while in spot mode, laser pulses are applied only to a single spot in the center of the pixel. As a result, more material is removed from the area of the pixel as well as from the depth of the sample. The Full Pixel mode thus leads to an increase in signal intensities and an improved limit of detection. In contrast, a higher lateral resolution was required for the monolayers and the host tissue (step size and laser focus diameter 5 µm), due to the small size of *C. parvum* stages. Therefore, the spot mode with a higher number of pulses was used for this purpose.

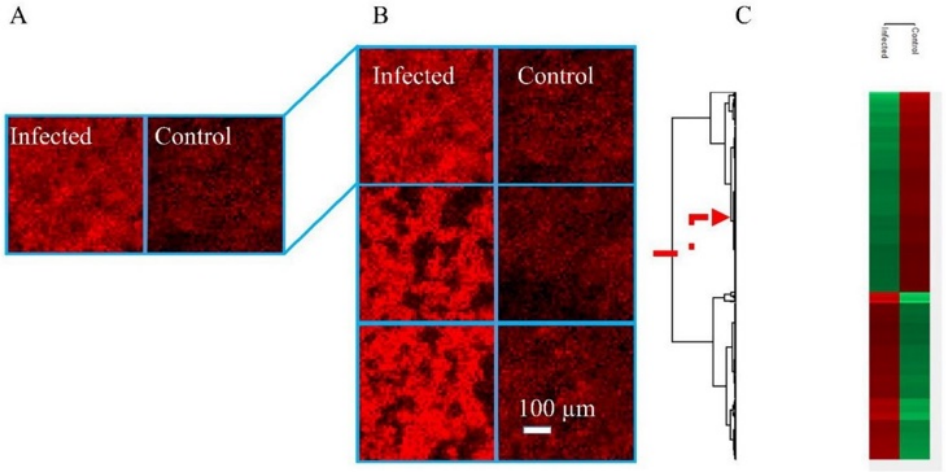

Figure 2. Workflow for determination of biomarkers: (**A**) The left part illustrates an infected section, and the right part the corresponding control sample. Upregulated infection marker LPE (22:4) as $[M+H]^+$, m/z 530.3212 ± 5 ppm, in red, each tile is 50 × 50 pixels with a step size of 10 µm. (**B**) Three technical replicates; LPE (22:4) as $[M+H]^+$, m/z 530.3212 ± 5 ppm, each tile is 50 × 50 pixels with a step size of 10 µm. (**C**) Segment of a heat map generated with Perseus. The color code of the column indicates whether it is a corresponding marker. Red means the signal is significantly increased compared to the other sample group. The red arrow indicates that the visualized marker is one of many markers within the heatmap.

The left part of Figure 2A illustrates an infected section, and the right part the corresponding control sample. The two samples were placed side by side on a sample holder, sprayed with matrix and measured subsequently. This ensured that the experimental conditions were identical. Signal intensities can therefore be interpreted as being quantitative on a relative scale. After that, another two infected and control pairs of technical replicates were measured in order to obtain triplicate measurements (Figure 2B). To exclude possible errors in sample preparation (e.g., sectioning) or possible heterogeneities within the cell pellets, technical replicates were measured. The same conditions were used for the preparation and storage of the samples. The Mirion [30] and Perseus [25] software platforms were used to determine potential biomarkers within the cell sections. The corresponding signals from the preceding step were filtered and non-fitting signals were rejected from the list. In the last step, post hoc tests were performed with the remaining signals (visualized using hierarchical clustering, see Figure 2C). The metabolism of *C. parvum* is known to be highly active [28], and a large number of differences in ion signals between control and infected samples are to be expected. For the in vitro HCT-8 model system, 1114 marker signals were found to be significantly upregulated in cases

of infection in positive-ion mode (see Supplementary Table S1) and 1118 marker signals in negative-ion mode (see Supplementary Table S2). In the case of downregulation, 1330 (see Supplementary Table S3) and 1386 marker signals (see Supplementary Table S4) were detected in positive- and negative-ion mode, respectively.

3.2. Annotation and Verification of Markers

The annotation of previously identified markers was performed using the LIPID MAPS database [31]. Lipids are basic components of the structural and functional categories of all cells. In cell membranes, they separate biofunctional areas and are involved in accomplishing various aspects of signal transmission. In the case of MALDI measurements of cell pellets and their following statistical evaluation, all m/z signals were taken into account. Due to this approach, the focus was exclusively on lipids. This is also reflected in the extraction process for the HPLC-MS/MS measurements and the database used. As a result, not every signal that was initially recognized by MALDI as a significant marker can subsequently be annotated or identified. In order to obtain meaningful annotations, the LIPID MAPS search criteria were selected to include appropriate ion adducts with the corresponding polarity. Only singly charged species were selected. In positive-ion mode, ions of types $[M+H]^+$, $[M+H\text{-}H_2O]^+$, $[M+Na]^+$, $[M+NH_4]^+$ and $[M+K]^+$, and $[M\text{-}H]^-$, $[M+Cl]^-$, $[M+HCOO]^-$, $[M+OAc]^-$ and $[M\text{-}CH_3]^-$ in negative-ion mode, were taken into account. In LIPID MAPS, a mass tolerance of m/z ± 0.05 was chosen and afterwards, values with a calculated deviation of more than 5 ppm between the theoretical and measured values were discarded. Annotations deviating from the m/z value by more than 1 ppm were discarded if several different annotations were found for the same m/z value. The corresponding results are illustrated in Figure 3. Because more than one annotation can meet the criteria described above, the number of annotations is larger than the number of m/z values. A total of 3221 annotations were determined for the positive-ion mode (for 880 different m/z values, see Supplementary Table S5) and 3059 annotations for the negative-ion mode (for 762 different m/z values, see Supplementary Table S6). In the case of downregulation, 2333 annotations (721 different m/z values, see Supplementary Table S7) were determined for the positive-ion mode and 1036 (380 different m/z values) annotations for the negative-ion mode (see Supplementary Table S8). Figure 3 shows the fractions of signal numbers (in [%]) of all annotated lipid categories (A1, B1, C1 and D1) as well as the various subclasses of the particularly prominent glycerophospholipids (A2, B2, C2 and D2). While parts A and B depict the results for the positive-ion mode, parts C and D show the results for the negative-ion mode. In the positive-ion mode, the proportions of lipid categories in the infected and control samples only minimally changed. Within the group of glycerophospholipids, the proportions of lipid classes slightly changed. The *C. parvum*-infected samples showed a larger number of phosphatidylserines (PSs) and phosphatidylinositols (PIs). The relative amount of phosphatidylcholines (PCs), phosphatidylethanolamines (PEs) and especially lysolipids (Lyso-) was found to be decreased in *C. parvum*-infected samples. In the negative-ion mode, the proportions of lipid classes changed significantly. The proportion of glycerophospholipids increased with parasitic infection. On the class level, the proportions of PC and PE decreased, while the ones of PI, PA and lysolipids increased.

Inclusion lists for the HPLC-MS/MS measurements were generated using the annotations obtained with LIPID MAPS. In addition, high-resolution full MS and MS/MS spectra were recorded. LipidMatch Flow in combination with ProteoWizard (MSConvertGUI) and Mzmine were used to identify the molecular markers already detected [32–34]. The corresponding settings for LipidMatch Flow can be found in Supplementary Table S9.

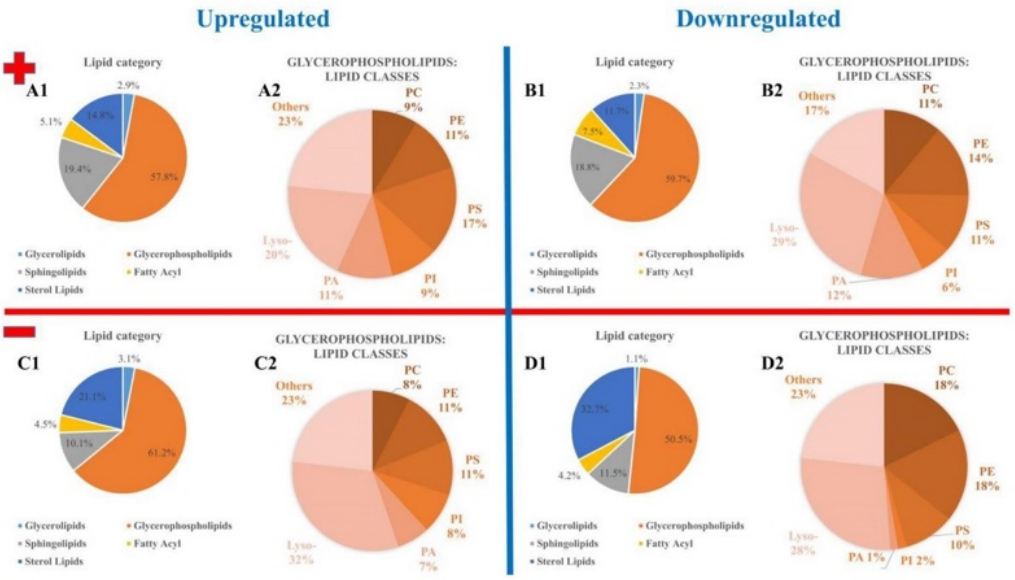

Figure 3. Overview of the annotated lipids, showing abundances of categories of detected HCT-8 markers (fractions of signal numbers (in [%])): (**A**,**B**) positive-ion mode; (**C**,**D**) negative-ion mode; (**A**,**C**) upregulated lipids; (**B**,**D**) downregulated lipids—(**1**) lipid categories, (**2**) detected lipid classes within the glycerophospholipids category.

In total, 37 of the annotations for upregulated lipids in *C. parvum*-infected samples in the positive-ion mode were confirmed by the MS/MS experiments (see Supplementary Table S10). The PC lipid class, a major structural component of membrane bilayers, was highly abundant. PC is known to be the dominant phospholipid class for *C. parvum* [35]. It is also significantly increased in infections with other apicomplexans, e.g., *Toxoplasma gondii* [36]. It is also known that PC is the most abundant phospholipid class in *T. gondii* and *Plasmodium falciparum* membranes [37,38]. PC synthesis is crucial for the replication of *T. gondii* tachyzoites and *P. falciparum* blood and liver stages [39–42]. In infected samples, 15 annotations of downregulated lipids were confirmed in positive-ion mode (see Supplementary Table S11). In negative-ion mode, 15 identifications were obtained from the previously annotated biomarkers in the case of upregulation (see Supplementary Table S12). In this context, 20 identifications could be obtained for downregulation (see Supplementary Table S13).

Irrespective of the ion mode, it has also been shown that this apicomplexan infection has an influence on the composition of the lysolipids. They are known for being ubiquitous intermediates in a variety of metabolic and signaling pathways in eukaryotic cells [43]. In the case of *P. falciparum*, there is evidence that the parasite lysophospholipase is used to generate phosphocholine for parasite PC synthesis from lysolipids already available in the parasitized host [44]. This is in agreement with our observation of a change in PC and lysolipid abundances in *C. parvum*-infected host cells and intestinal mucosa.

3.3. Mass Spectrometry Imaging of C. parvum-Infected Cell Layers and Intestinal Tissue at High Lateral Resolution

In positive-ion mode, 38 upregulated signals related to *C. parvum* infection and 16 downregulated signals were identified in both HCT-8 pellets and host tissue (see Supplementary Tables S10 and S11). Visualization of the small parasites (3–5 µm) attached

to the cells requires a lateral resolution of at least 5 µm for the MSI of monolayers and host tissue. In each panel of Figure 4, *C. parvum*-infected HCT-8 layers are shown at the bottom, and control samples at the top. Images were obtained in positive-ion mode. The green channel represents the total ion count (TIC) in the two images. The red channel shows the distribution of molecular markers obtained by LC-MS/MS analysis (mass tolerance of ±5 ppm) and identified as infection markers. As expected, these signals were found exclusively or with significantly higher signal intensity in *C. parvum*-infected cell layers (bottom side of each panel) than in the control samples. In Figure 4A, the distribution of an infection-specific signal at m/z 766.5720 assigned to [plasmanyl-PC(O-16:1/20:4)+H]$^+$ is shown, and Figure 4B displays the distribution of the signal at m/z 504.3036, assigned to [LPE(20:3)+H]$^+$. As mentioned earlier, the signal increase in the lipid class of the PC is typical of infection with apicomplexan parasites. LPE is part of cell membranes, which play an essential role in the activation of other enzymes and cell-mediated cell signaling [45].

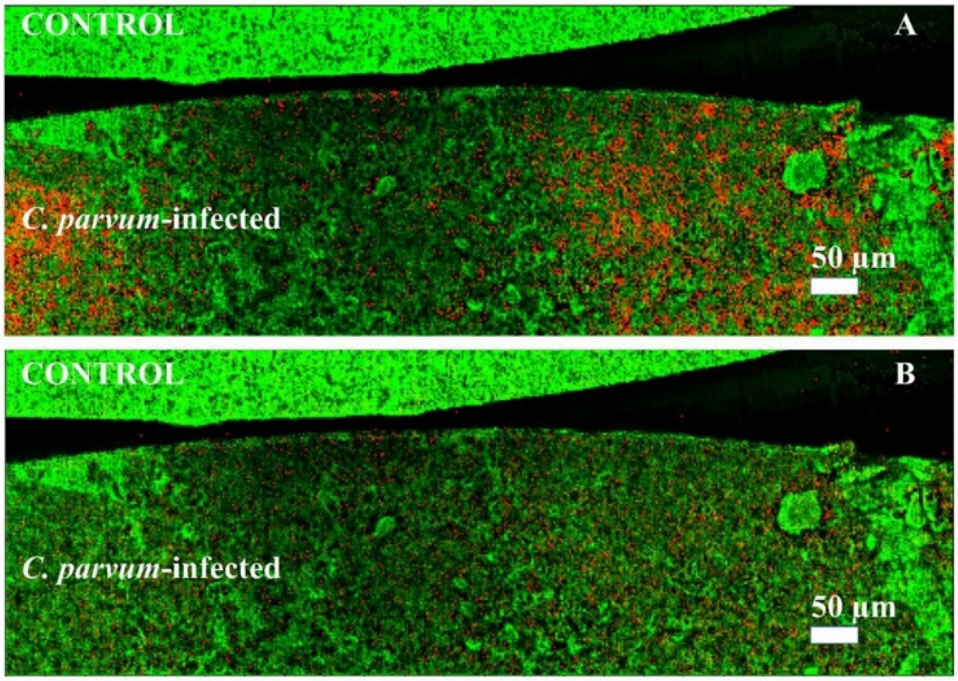

Figure 4. Visualization of biomarkers in cell monolayers: MALDI MSI measurements of cell monolayers in positive-ion mode, measured with 5 µm laser focus diameter and step size. The green channel in both images represents the TIC, used for visualization purposes only. The red channel shows the distribution of two different infection markers (±5 ppm mass tolerance) identified earlier by LC-MS/MS measurements of cell pellets or host tissue. (**A**) Infection marker signal at m/z 766.5720, identified as plasmanyl-PC(O-16:1/20:4) as [M+H]$^+$, (**B**) infection marker signal at m/z 504.3036, identified as LPE(20:3) as [M+H]$^+$.

In addition to cell monolayer measurements, cryo-sections of *C. parvum*-infected neonatal bovine intestinal tissue were analyzed. Figure 5A,B show MS images of a neonatal bovine intestine section. In Figure 5A, the green channel represents an ion channel at m/z 756.5513, used for visualization purposes only and indicating the complete intestine

section. The distribution of two infection-specific signals at m/z 504.3036, identified as $[LPE(20:3)+H]^+$, and m/z 530.3058, identified as $[LPE(22:4)+H]^+$, are shown in red and blue. It can be seen that the markers for the infection only occur in the inner or luminal area of the small intestine (outlined in white). This is the area where *C. parvum* replication takes place, resulting in trophozoite, meront, gamont and oocyst stages. To substantiate this fact, Figure 5B shows exclusively the infection biomarkers from Figure 5A. In Figure 5C, the corresponding optical image of the whole intestine section can be seen. The infected area is outlined in red.

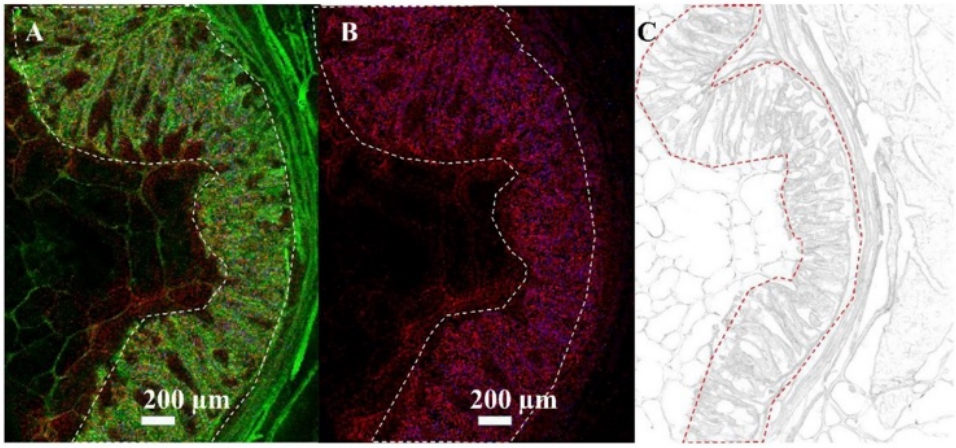

Figure 5. Visualization of infection biomarkers in host tissue: MALDI MSI measurements of *C. parvum*-infected neonatal bovine intestine in positive-ion mode, measured with 10 µm laser focus diameter and step size in Full Pixel mode. The red and blue channels show the distribution of two infection markers (±5 ppm mass tolerance) identified earlier by LC-MS/MS measurements of cell pellets or host tissue. (**A**) The green channel represents an ion signal at m/z 756.5513, used for visualization purposes only. Infection marker signal at m/z 504.3036, identified as LPE (20:3) as $[M+H]^+$ in red, and m/z 530.3058, identified as LPE (22:4) as $[M+H]^+$ in blue. (**B**) Infection marker signal at m/z 504.3036, identified as LPE (20:3) as $[M+H]^+$ in red and m/z 530.3058, identified as LPE (22:4) as $[M+H]^+$ in blue. (**C**) Optical image of the whole intestine section. The area of infection (wrinkles and villi) is outlined in red.

Finally, experimentally *C. parvum*-infected neonatal calf intestinal samples were examined by MS imaging. The samples were prepared in such a way that the inner part of the intestine, and therefore the site of infection, corresponded exclusively to the right part of the section. Figure 6A shows an MS image of the measured area, the corresponding optical images can be found in B (entire section) and C (measured area). It can be clearly seen that the biomarkers for the infection were exclusively detected in the right border of the section, which is where infective *C. parvum* sporozoites were applied. Panels A2 to A6 represent another 10 selected marker signals for infection.

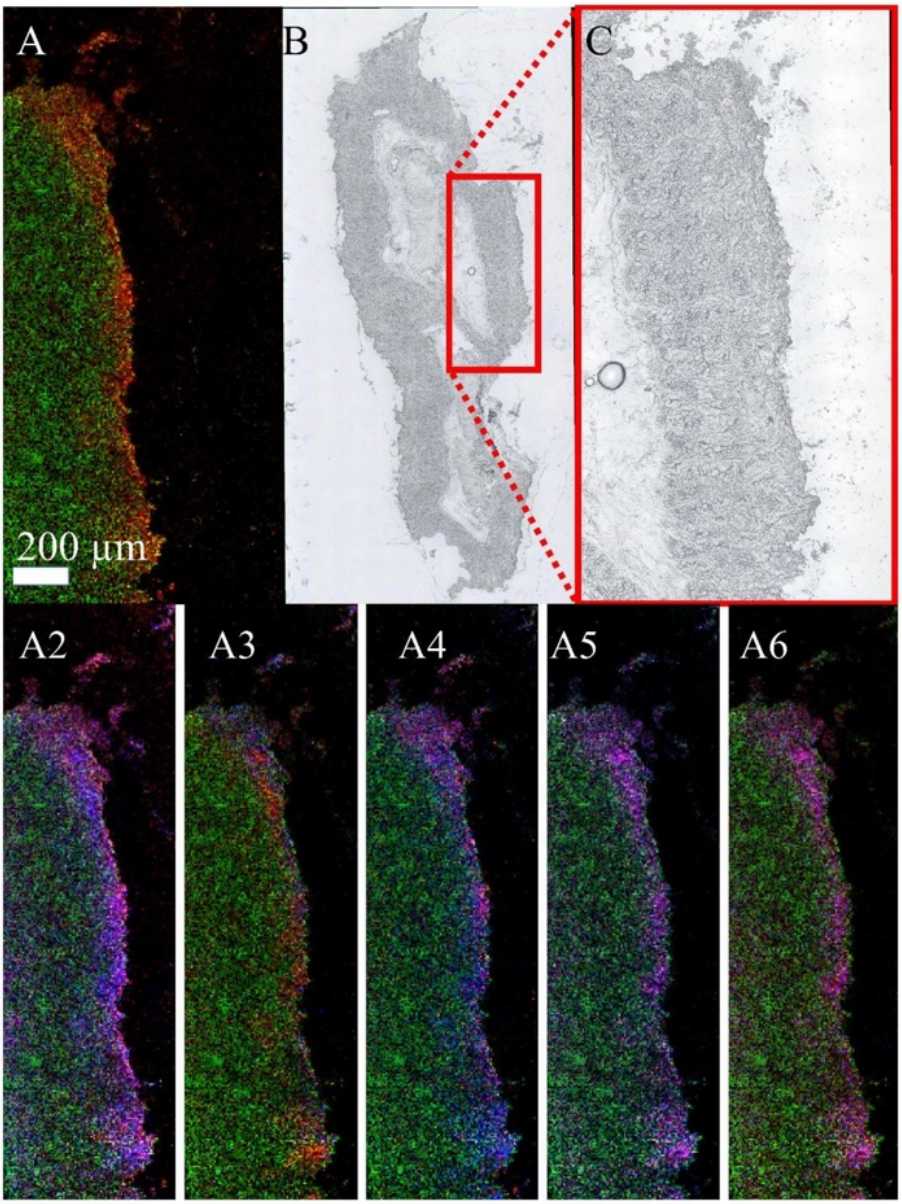

Figure 6. Visualization of biomarkers in experimentally *C. parvum*-infected neonatal bovine intestinal tissue: MALDI MSI measurements of bovine intestine in positive-ion mode, infected with *C. parvum* and measured with 12 µm laser focus diameter and step size. The green channel represents an ion signal at m/z 726.5603, used for visualization purposes only. The red and the blue channel show the

distribution of two infection markers (±5 ppm mass tolerance) identified earlier by LC-MS/MS measurements of cell pellets. (**A**) Infection marker signal at m/z 504.3057 (red), identified as LPE (20:3) as $[M+H]^+$, (**B**) optical image of the whole intestine section, (**C**) zoomed optical image of the measured area. (**A2**–**A6**) confirm the interpretation of A for another ten biomarkers. These ten biomarkers were always found in the same area and their distribution was congruent with A. (**A2**) Infection marker signals at m/z 532.3371 (red) and 558.2955 (blue), annotated by Lipid Maps as LPC (17:0) as $[M+Na]^+$ (further annotations possible) and LPC (18:2) as $[M+K]^+$ (further annotations possible); (**A3**) infection marker signals at m/z 540.3059 (red), annotated by Lipid Maps as LPC (18:3) as $[M+Na]^+$ (further annotations possible) and 576.3282 annotated by Lipid Maps as LPS (20:0) as $[M+Na]^+$ in blue (further annotations possible); (**A4**) infection marker signals at m/z 640.3220 (red) annotated by Lipid Maps as PS (24:3) as $[M+Na]^+$ (further annotations possible) and m/z 618.3399 (blue) annotated by Lipid Maps as PS (24:3) as $[M+H]^+$; (**A5**) infection marker signals at m/z 656.3557 (red) annotated by Lipid Maps as PS (27:5) as $[M+H]^+$ and m/z 657.3591 (blue) annotated by Lipid Maps as PI (21:0) as $[M+H]^+$; (**A6**) infection marker signals at m/z 521.3428 (red) annotated by Lipid Maps as DG (25:2;O2) as $[M+Na]^+$ and m/z 520.3394 (blue) annotated by Lipid Maps as LPC (18:2) as $[M+H]^+$.

The identified biomarkers as determined for *C. parvum* were compared to biomarkers of *T. gondii*-, *Besnoitia besnoiti*- and *Neospora caninum*-infected host cells, as previously published [28,29]. These parasites all belong to the taxonomic subphylum Apicomplexa and are thus suspected to show metabolic similarities to *C. parvum*. A comparison is shown in Supplementary Table S14. PI (36:1) as $[M-H]^-$ was identified as a marker for host cell infection by *C. parvum* as well as by *T. gondii*, *B. besnoiti* and *N. caninum*. Phosphatidylinositol is present in cell membranes, playing an important role in anchoring proteins to the membrane. For *T. gondii*, it has been shown that PIs play roles in the parasite's transition between its stages, i.e., tachyzoites and bradyzoites, and therefore are essential for establishing persistent infections in mammalian hosts, including humans [46]. To assess the metabolite profiles associated with infection, Hublin et al. performed a gas-chromatography-MS-based metabolomic analysis (mass range m/z 45–600) of fecal samples from experimentally infected mice. The seven lipids mentioned in the study, which were associated with a significant change in concentration, do not show any intersection with our results. In addition to different ionization techniques and the restriction to the positive-ion mode, the different selected mass ranges limit a possible intersection [47].

4. Conclusions

To the best of our knowledge, this is the first MSI study examining *C. parvum*-infected human host cells and bovine intestinal tissue at the molecular level to be as close as possible to an in vivo situation. By comparing technical triplicates of infected and non-infected sections of cell pellet samples, it was possible to find lipid biomarkers for infection with the parasite *C. parvum*, which belongs to the subphylum Apicomplexa. AP-SMALDI MS and MSI were used for describing obligate intracellular infections. The MS measurements were carried out in positive- and negative-ion modes, and the results were interpreted with software including statistical tools. With this method, 2232 ion signals were detected in *C. parvum*-infected samples, and were significantly different from those detected in the control ones. Using databases and structure elucidation based on MS/MS experiments, it was possible to structurally identify 54 biomarkers, while the others remained structurally undetermined. The obtained data were compared with already published data on other apicomplexan parasites (*T. gondii*, *B. besnoiti* and *N. caninum*). PI (36:1) was identified as a common marker for infection with all three mentioned parasites. For MSI experiments, cell layers as well as natural and experimentally infected host intestinal tissues were analyzed and previously found markers were imaged. This allowed infected cells or host intestinal tissue to be distinguished from uninfected cells and healthy host tissue. In this way, the parasitic infection could be made visible at a 5 to 10 µm lateral resolution. The presented research will be the basis for future detailed investigations on *C. parvum*'s modulation of

host cell metabolism. Such novel lipid data then will aid in uncovering alternative metabolic pathways, providing additional drug targets against *C. parvum* and other apicomplexan parasites of veterinary and public health importance.

Supplementary Materials: The following supporting information can be downloaded at: https://www.mdpi.com/article/10.3390/biom13081200/s1, Table S1: Posthoc test HCT 8 for infected cells in positive-ion mode; Table S2: Posthoc test HCT 8 for infected cells in negative-ion mode; Table S3: Posthoc test HCT 8 for control cells in positive-ion mode; Table S4: Posthoc test HCT 8 for control cells in negative-ion mode; Table S5: Annotations for upregulated ion signals in positive-ion mode; Table S6: Annotations for upregulated ion signals in negative-ion mode; Table S7: Annotations for downregulated ion signals in positive-ion mode; Table S8: Annotations for downregulated ion signals in negative-ion mode; Table S9: LipidMatch Flow settings; Table S10: Identified markers for upregulated ion signals in positive-ion mode; Table S11: Identified markers for downregulated ion signals in positive-ion mode; Table S12: Identified markers for upregulated ion signals in negative-ion mode; Table S13: Identified markers for downregulated ion signals in negative-ion mode; Table S14: Comparison of identified infection markers with literature.

Author Contributions: Conceptualization, N.H.A., S.G. and B.S.; Methodology, N.H.A.; Validation, S.G. and B.S.; Formal Analysis, N.H.A.; Investigation, N.H.A.; Resources, L.M.R.S., J.D.V., C.R.H., A.T. and B.S.; Data Curation, N.H.A.; Writing—Original Draft Preparation, N.H.A.; Writing—Review and Editing, N.H.A., S.G., P.G., L.M.R.S., C.R.H. and B.S.; Visualization, N.H.A.; Supervision, B.S.; Funding Acquisition, B.S., A.T. and C.R.H. All authors have read and agreed to the published version of the manuscript.

Funding: Financial support from the Federal State of Hesse, LOEWE Center DRUID (Novel Drug Targets against Poverty-Related and Neglected Tropical Diseases), the German 'Bundesministerium für Bildung und Forschung' (BMBF; DLR 01DG20023; CryptoNETs) and the Deutsche Forschungsgemeinschaft (DFG; Sp314/23-1) is gratefully acknowledged. We would like to thank the Hans-Böckler-Stiftung for granting Nils Anschütz a scholarship. Instrumental support from TransMIT GmbH and Thermo Fisher Scientific is gratefully acknowledged.

Institutional Review Board Statement: Not applicable.

Informed Consent Statement: Not applicable.

Data Availability Statement: The data presented in this study are available on request from the corresponding author.

Conflicts of Interest: B.S. is a consultant, S.G. an employee and N.H.A. is a part-time employee of TransMIT GmbH, Giessen, Germany. The other authors declare no conflict of interest.

References

1. Gerace, E.; Lo Presti, V.D.; Biondo, C. *Cryptosporidium* infection: Epidemiology, pathogenesis, and differential diagnosis. *Eur. J. Microbiol. Immunol.* **2019**, *9*, 119–123. [CrossRef] [PubMed]
2. Tzipori, S.; Ward, H. Cryptosporidiosis: Biology, pathogenesis and disease. *Microbes Infect.* **2002**, *4*, 1047–1058. [CrossRef]
3. Minghui, R.; WHO. *Ending the Neglect to Attain the Sustainable Development Goals: A Road Map for Neglected Tropical Diseases 2021–2030*; WHO: Geneva, Switzerland, 2020; 196p.
4. Khalil, I.A.; Troeger, C.; Rao, P.C.; Blacker, B.F.; Brown, A.; Brewer, T.G.; Colombara, D.V.; De Hostos, E.L.; Engmann, C.; Guerrant, R.L.; et al. Morbidity, mortality, and long-term consequences associated with diarrhoea from *Cryptosporidium* infection in children younger than 5 years: A meta-analyses study. *Lancet Glob. Health* **2018**, *6*, E758–E768. [CrossRef]
5. Kotloff, K.L.; Nataro, J.P.; Blackwelder, W.C.; Nasrin, D.; Farag, T.H.; Panchalingam, S.; Wu, Y.; Sow, S.O.; Sur, D.; Breiman, R.F.; et al. Burden and aetiology of diarrhoeal disease in infants and young children in developing countries (the Global Enteric Multicenter Study, GEMS): A prospective, case-control study. *Lancet* **2013**, *382*, 209–222. [CrossRef] [PubMed]
6. Liu, L.; Oza, S.; Hogan, D.; Chu, Y.; Perin, J.; Zhu, J.; Lawn, J.E.; Cousens, S.; Mathers, C.; Black, R.E. Global, regional, and national causes of under-5 mortality in 2000-15: An updated systematic analysis with implications for the sustainable development goals. *Lancet* **2016**, *388*, 3027–3035. [CrossRef] [PubMed]
7. Diptyanusa, A.; Sari, I.P. Treatment of human intestinal cryptosporidiosis: A review of published clinical trials. *Int. J. Parasitol.-Drugs Drug Resist.* **2021**, *17*, 128–138. [CrossRef]
8. Checkley, W.; White, A.C.; Jaganath, D.; Arrowood, M.J.; Chalmers, R.M.; Chen, X.M.; Fayer, R.; Griffiths, J.K.; Guerrant, R.L.; Hedstrom, L.; et al. A review of the global burden, novel diagnostics, therapeutics, and vaccine targets for *Cryptosporidium*. *Lancet Infect. Dis.* **2015**, *15*, 85–94. [CrossRef]

9. Fox, L.M.; Saravolatz, L.D. Nitazoxanide: A new thiazolide antiparasitic agent. *Clin. Infect. Dis.* **2005**, *40*, 1173–1180. [CrossRef]
10. Rider, S.D.; Zhu, G. Cryptosporidium: Genomic and biochemical features. *Exp. Parasitol.* **2010**, *124*, 2–9. [CrossRef]
11. Liu, S.Y.; Roellig, D.M.; Guo, Y.Q.; Li, N.; Frace, M.A.; Tang, K.; Zhang, L.X.; Feng, Y.Y.; Xiao, L.H. Evolution of mitosome metabolism and invasion-related proteins in *Cryptosporidium*. *BMC Genom.* **2016**, *17*, 1006. [CrossRef]
12. Velez, J.; Velasquez, Z.; Silva, L.M.R.; Gartner, U.; Failing, K.; Daugschies, A.; Mazurek, S.; Hermosilla, C.; Taubert, A. Metabolic Signatures of *Cryptosporidium* parvum-Infected HCT-8 cells and impact of selected metabolic inhibitors on *C. parvum* Infection under physioxia and hyperoxia. *Biology* **2021**, *10*, 60. [CrossRef]
13. Velez, J.; Silva, L.M.R.; Gaertner, U.; Daugschies, A.; Mazurek, S.; Hermosilla, C.; Taubert, A. First metabolic insights into ex vivo *Cryptosporidium parvum*-Infected bovine small intestinal xxplants studied under physioxic conditions. *Biology* **2021**, *10*, 963. [CrossRef] [PubMed]
14. Magnuson, M.L.; Owens, J.H.; Kelty, C.A. Characterization of *Cryptosporidium parvum* by matrix-assisted laser desorption ionization-time of flight mass spectrometry. *Appl. Environ. Microbiol.* **2000**, *66*, 4720–4724. [CrossRef] [PubMed]
15. Snelling, W.J.; Lin, Q.S.; Moore, J.E.; Millar, B.C.; Tosini, F.; Pozio, E.; Dooley, J.S.G.; Lowery, C.J. Proteomics analysis and protein expression during sporozoite excystation of *Cryptosporidium parvum* (Coccidia, Apicomplexa). *Mol. Cell. Proteom.* **2007**, *6*, 346–355. [CrossRef]
16. Li, D.F.; Cui, Z.H.; Wang, L.Y.; Zhang, K.H.; Cao, L.T.; Zheng, S.J.; Zhang, L.X. Tandem mass tag (TMT)-based proteomic analysis of *Cryptosporidium* andersoni oocysts before and after excystation. *Parasites Vectors* **2021**, *14*, 608. [CrossRef]
17. Mauzy, M.J.; Enomoto, S.; Lancto, C.A.; Abrahamsen, M.S.; Rutherford, M.S. The *Cryptosporidium parvum* transcriptome during in vitro development. *PLoS ONE* **2012**, *7*, e31715. [CrossRef]
18. Matos, L.V.S.; McEvoy, J.; Tzipori, S.; Bresciani, K.D.S.; Widmer, G. The transcriptome of *Cryptosporidium* oocysts and intracellular stages. *Sci. Rep.* **2019**, *9*, 7856. [CrossRef]
19. Spengler, B. De novo sequencing, peptide composition analysis, and composition-based sequencing: A new strategy employing accurate mass determination by Fourier transform ion cyclotron resonance mass spectrometry. *J. Am. Soc. Mass Spectrom.* **2004**, *15*, 703–714. [CrossRef]
20. Spengler, B. Accurate mass as a bioinformatic parameter in data-to-knowledge conversion: Fourier transform ion cyclotron resonance mass spectrometry for peptide de novo sequencing. *Eur. J. Mass Spectrom.* **2007**, *13*, 83–87. [CrossRef]
21. Spengler, B.; Hester, A. Mass-based classification (MBC) of peptides: Highly accurate precursor ion mass values can be used to directly recognize peptide phosphorylation. *J. Am. Soc. Mass Spectrom.* **2008**, *19*, 1808–1812. [CrossRef] [PubMed]
22. Kompauer, M.; Heiles, S.; Spengler, B. Atmospheric pressure MALDI mass spectrometry imaging of tissues and cells at 1.4-mu m lateral resolution. *Nat. Methods* **2017**, *14*, 90–96. [CrossRef]
23. Shahiduzzaman, M.; Dyachenko, V.; Obwaller, A.; Unglaube, S.; Daugschies, A. Combination of cell culture and quantitative PCR for screening of drugs against *Cryptosporidium parvum*. *Vet. Parasitol.* **2009**, *162*, 271–277. [CrossRef]
24. Matyash, V.; Liebisch, G.; Kurzchalia, T.V.; Shevchenko, A.; Schwudke, D. Lipid extraction by methyl-tert-butyl ether for high-throughput lipidomics. *J. Lipid Res.* **2008**, *49*, 1137–1146. [CrossRef]
25. Hu, C.X.; van Dommelen, J.; van der Heijden, R.; Spijksma, G.; Reijmers, T.H.; Wang, M.; Slee, E.; Lu, X.; Xu, G.W.; van der Greef, J.; et al. RPLC-Ion-Trap-FTMS method for lipid profiling of plasma: Method validation and application to p53 mutant mouse model. *J. Proteome Res.* **2008**, *7*, 4982–4991. [CrossRef] [PubMed]
26. Muller, M.A.; Kompauer, M.; Strupat, K.; Heiles, S.; Spengler, B. Implementation of a high-repetition-rate laser in an AP-SMALDI MSI system for enhanced measurement performance. *J. Am. Soc. Mass Spectrom.* **2021**, *32*, 465–472. [CrossRef]
27. Tyanova, S.; Temu, T.; Sinitcyn, P.; Carlson, A.; Hein, M.Y.; Geiger, T.; Mann, M.; Cox, J. The Perseus computational platform for comprehensive analysis of (prote)omics data. *Nat. Methods* **2016**, *13*, 731–740. [CrossRef]
28. Kadesch, P.; Hollubarsch, T.; Gerbig, S.; Schneider, L.; Silva, L.M.R.; Hermosilla, C.; Taubert, A.; Spengler, B. Intracellular parasites *Toxoplasma gondii* and *Besnoitia besnoiti*, unveiled in single host cells using AP-SMALDI MS imaging. *J. Am. Soc. Mass Spectrom.* **2020**, *31*, 1815–1824. [CrossRef]
29. Anschütz, N.H.; Gerbig, S.; Ventura, A.M.P.; Silva, L.M.R.; Larrazabal, C.; Hermosilla, C.; Taubert, A.; Spengler, B. Atmospheric-pressure scanning microprobe matrix-assisted laser desorption/ionization mass spectrometry imaging of *Neospora caninum*-infected cell monolayers. *Anal. Sci. Adv.* **2022**, *3*, 244–254. [CrossRef]
30. Paschke, C.; Leisner, A.; Hester, A.; Maass, K.; Guenther, S.; Bouschen, W.; Spengler, B. Mirion-A software package for automatic processing of mass spectrometric images. *J. Am. Soc. Mass Spectrom.* **2013**, *24*, 1296–1306. [CrossRef] [PubMed]
31. The LIPID MAPS®Lipidomics Gateway. Available online: https://www.lipidmaps.org/ (accessed on 7 July 2022).
32. Koelmel, J.P.; Kroeger, N.M.; Ulmer, C.Z.; Bowden, J.A.; Patterson, R.E.; Cochran, J.A.; Beecher, C.W.W.; Garrett, T.J.; Yost, R.A. LipidMatch: An automated workflow for rule-based lipid identification using untargeted high-resolution tandem mass spectrometry data. *BMC Bioinform.* **2017**, *18*, 331. [CrossRef] [PubMed]
33. Kessner, D.; Chambers, M.; Burke, R.; Agusand, D.; Mallick, P. Proteo Wizard: Open source software for rapid proteomics tools development. *Bioinformatics* **2008**, *24*, 2534–2536. [CrossRef] [PubMed]
34. Pluskal, T.; Castillo, S.; Villar-Briones, A.; Oresic, M. MZmine 2: Modular framework for processing, visualizing, and analyzing mass spectrometry-based molecular profile data. *BMC Bioinform.* **2010**, *11*, 395. [CrossRef]
35. Mitschler, R.R.; Welti, R.; Upton, S.J. A comparative-study of lipid compositions of *Cryptosporidium-parvum* (apicomplexa) and madin-darby bovine kidney-cells. *J. Eukaryot. Microbiol.* **1994**, *41*, 8–12. [CrossRef]

36. Besteiro, S.; Bertrand-Michel, J.; Lebrun, M.; Vial, H.; Dubremetz, J.F. Lipidomic analysis of *Toxoplasma gondii* tachyzoites rhoptries: Further insights into the role of cholesterol. *Biochem. J.* **2008**, *415*, 87–96. [CrossRef]
37. Welti, R.; Mui, E.; Sparks, A.; Wernimont, S.; Isaac, G.; Kirisits, M.; Roth, M.; Roberts, C.W.; Botte, C.; Marechal, E.; et al. Lipidomic analysis of *Toxoplasma gondii* reveals unusual polar lipids. *Biochemistry* **2007**, *46*, 13882–13890. [CrossRef]
38. Botte, C.Y.; Yamaryo-Botte, Y.; Rupasinghe, T.W.T.; Mullin, K.A.; MacRae, J.I.; Spurck, T.P.; Kalanon, M.; Shears, M.J.; Coppel, R.L.; Crellin, P.K.; et al. Atypical lipid composition in the purified relict plastid (apicoplast) of malaria parasites. *Proc. Natl. Acad. Sci. USA* **2013**, *110*, 7506–7511. [CrossRef] [PubMed]
39. Gupta, N.; Zahn, M.M.; Coppens, I.; Joiner, K.A.; Voelker, D.R. Selective disruption of phosphatidylcholine metabolism of the intracellular parasite *Toxoplasma gondii* arrests its growth. *J. Biol. Chem.* **2005**, *280*, 16345–16353. [CrossRef] [PubMed]
40. Caldarelli, S.A.; Duckert, J.F.; Wein, S.; Calas, M.; Perigaud, C.; Vial, H.; Peyrottes, S. Synthesis and evaluation of bis-thiazolium salts as potential antimalarial drugs. *Chemmedchem* **2010**, *5*, 1102–1109. [CrossRef]
41. Itoe, M.A.; Sampaio, J.L.; Cabal, G.G.; Real, E.; Zuzarte-Luis, V.; March, S.; Bhatia, S.N.; Frischknecht, F.; Thiele, C.; Shevchenko, A.; et al. Host cell phosphatidylcholine is a key mediator of malaria parasite survival during liver stage infection. *Cell Host Microbe* **2014**, *16*, 778–786. [CrossRef]
42. Bobenchik, A.M.; Witola, W.H.; Augagneur, Y.; Lochlainn, L.N.; Garg, A.; Pachikara, N.; Choi, J.Y.; Zhao, Y.O.; Usmani-Brown, S.; Lee, A.; et al. *Plasmodium falciparum* phosphoethanolamine methyltransferase is essential for malaria transmission. *Proc. Natl. Acad. Sci. USA* **2013**, *110*, 18262–18267. [CrossRef]
43. Richmond, G.S.; Smith, T.K. The role and characterization of phospholipase A(1) in mediating lysophosphatidylcholine synthesis in *Trypanosoma brucei*. *Biochem. J.* **2007**, *405*, 319–329. [CrossRef] [PubMed]
44. Sheokand, P.K.; Narwal, M.; Thakur, V.; Mohmmed, A. GlmS mediated knock-down of a phospholipase expedite alternate pathway to generate phosphocholine required for phosphatidylcholine synthesis in *Plasmodium falciparum*. *Biochem. J.* **2021**, *478*, 3429–3444. [CrossRef] [PubMed]
45. Ryu, S.B. Phospholipid-derived signaling mediated by phospholipase A in plants. *Trends Plant Sci.* **2004**, *9*, 229–235. [CrossRef]
46. Seron, K.; Dzierszinski, F.; Tomavo, S. Molecular cloning, functional complementation in *Saccharomyces cerevisiae* and enzymatic properties of phosphatidylinositol synthase from the protozoan parasite *Toxoplasma gondii*. *Eur. J. Biochem.* **2000**, *267*, 6571–6579. [CrossRef]
47. Hublin, J.; Ryan, U.; Trengove, R.; Maker, G. Metabolomic profiling of faecal extracts from *cryptosporidium parvum* infection in experimental mouse models. *PLoS ONE* **2013**, *8*, e77803. [CrossRef] [PubMed]

Supplementary information

Mass Spectrometry Imaging of In Vitro *Cryptosporidium parvum*-Infected Cells and Host Tissue

Anschütz, N.H.; Gerbig, S.; Ghezellou, P.; Silva, L.M.R.; Vélez, J.D.; Hermosilla, C.R.; Taubert, A.; Spengler, B. Mass Spectrometry Imaging of In Vitro *Cryptosporidium parvum*-Infected Cells and Host Tissue. *Biomolecules* 2023, *13*, 1200.; https://doi.org/10.3390/biom13081200

https://www.mdpi.com/2218-273X/13/8/1200/s1?version=1690877105

ACKNOWLEDGEMENT

First, I would like to thank Prof. Dr. Bernhard Spengler for giving me the opportunity to work in his research group, which enjoys a high prestige worldwide. Many thanks also for the created structures. The opportunity to work for TransMIT, the inclusion of my work in DRUID and the compulsory membership in the GGL are invaluable.

Of course, I would also like to thank the entire working group. It's not just about helpful tips, but also about motivating small talk.

My thanks also go to Prof. Taubert, Prof. Hermosilla and their entire working group for providing the samples.

I would like to thank the Hans Böckler Foundation for supporting me with a PhD scholarship.